P-N JUNCTION DIODE FABRICATED FROM ZnO NANOROD GROWN BY AQUEOUS SOLUTION METHOD

NGUYEN XUAN SANG

(B.Eng. (Hons), HUT)

A THESIS SUBMITTED

FOR THE DEGREE OF DOCTOR OF PHILOSOPHY

IN ADVANCED MATERIALS FOR MICRO- AND NANO-SYSTEMS (AMM&NS)

SINGAPORE-MIT ALLIANCE

NATIONAL UNIVERSITY OF SINGAPORE

2012

DECLARATION

I hereby declare that this thesis is my original work

and it has been written by me in its entirety.

I have duly acknowledged all the sources of

information which have been used in the thesis.

This thesis has also not been submitted for any

degree in any university previously

Nguyen Xuan Sang

15 August 2012

Acknowledgements

First of all, I would like to express my sincere appreciation to my supervisors, Prof. Chua Soo Jin and Prof. Eugene A. Fitzgerald for their guidance and support me throughout my PhD study. Their advices and supporting has been invaluable on both academic and personal level, for which I am extremely grateful.

I would like to express my thanks to Dr. Tay Chuan Beng for his helping and guiding me from first step of my research work. His important suggestions help me not only in my PhD research but also in my future work. I would like to thank Dr. Le Hong Quang and Dr. Soh Chew Beng from IMRE for their helps my research.

Great acknowledgment to Ms. Musni and Mr. Tan from Center for Optoelectronics, NUS, their experience and skill helped me in lab equipments and experiments. I would like to thanks Dr. Huang Xiaohu, Mr. Zhang Chen, and Ms. Tang Jie for their help in doing some of my research work. I also would like to give thanks to Ms. Doreen for SEM measurements, Mr. Eric TANG and Ms. TEO Siew Lang for photolithography, RIE and e-beam evaporator experiments in IMRE.

I would like to thank Prof. Choi wee Kiong, Ms. Hong Yanling, and Ms. Juliana Chai from Singapore – MIT Alliance program for their administrative support during my PhD. Great thanks to Singapore – MIT Alliance program for financial support.

Finally, I would like to give my special thanks to my parents, my wife, my son and my brothers, sister. Their support and love enable me to go through the hard time and complete this work.

TABLE OF CONTENTS

Acknowledgments……………………….………………………………i

Summary………………………………………………………...…vi

List of Tables…………………………………………………………..viii

List of Figures……………………………………………………...…ix

Chapter 1 Introduction……………………………………..…...………1

1.1 Background and basic properties of ZnO……………….………………1

1.1.1 Background……………………….……………………......…..1

1.1.2 Basic properties of ZnO………………………………….....….2

1.2 ZnO nanorods growth technique …………………………...…….…….5

1.2.1 Vapor phase methods……………………………….....….……5

1.2.2 Solution method……………………………………….....….…7

1.3 Doping ZnO nanorods ………………………….....…………………..9

1.3.1 Doping n-type ZnO……………………….…………………….9

1.3.2 Doping p-type ZnO………………………...…………….....…11

1.4 Application of ZnO in solid state lighting………………...……………...13

1.4.1 ZnO based heterojunction LED…………………….……..………13

1.4.2 ZnO based homojunction LED…………………….……….....16

1.5 Motivation of the thesis………………………………………….….…....19

1.6 Organization of the thesis…………………....………………….……...20

Chapter 2 Experiment setup and characterization methods....................22

2.1 Growth procedure………………………………………………...22

2.1.1 Aqueous solution growth procedure of ZnO nanorods ………..22

2.1.2 Reactions of the solution growth……………………………….23

2.1.3 Effect of pH on ZnO surface…………….…………………….26

2.1.4 Nucleation and growth………………….…………………...…28

2.2 LED fabrication equipments……………………….….………….30

2.2.1 RIE system...…………………………………………...30

2.2.2 Photolithography system……………………..………...31

2.2.3 E-beam evaporator…………………………...……32

2.3 Characterization equipments………………………..……....32

2.3.1 Microscopes……………………………………………33

2.3.2 Photoluminescence and electroluminescence…………..…...34

2.3.3 XPS and SIMS……………………………………..…...36

2.3.4 I-V and C-V……………………………………………38

2.4 Conclusions……………………………………………………38

Chapter 3 Optimization of the growth and post-treatment of n-ZnO nanorods……………………………………………………..….40

3.1. Morphology of n-type ZnO nanorods ……………………...…40

3.1.1 ZnO nanorods growth precursor……………………………40

3.1.2 Morphology of undoped ZnO nanorods…………………..…41

3.1.3 Morphology of ZnO nanorods doped with Ga and Al……....42

3.1.4 Discussion on growth habit of Ga and Al-doped nanorods…....47

3.2. Characterization of undoped ZnO Nanorods..…………….………50

3.2.1 X-Ray Diffraction analysis…………………………………..50

3.2.2 Transmission electron microscope (TEM) measurement………51

3.2.3 SIMS analysis…………………………………………………..52

3.2.4 Energy-dispersive X-ray spectroscopy (EDX)……….…...…53

3.2.5 XPS analysis…………………………………….…………...54

3. 3 Optical properties of ZnO nanorods……………………….………55

3.3.1 Photoluminescence of undoped ZnO nanorods ………………..56

3.3.2 Photoluminescence of Al and Ga doped ZnO nanorods……..…57

3.3.3 Photoluminescence of undoped ZnO nanorods after annealing..58

3.4 Conclusions ……………………………………………………......……...…59

Chapter 4 Optimization of p-type ZnO nanorods growth by doping with potassium using aqueous solution method………………......................….60

4.1 Principle of doping potassium for p-type ZnO ……………………..…...60

4.1.1 Motivation for use of potassium as p-type acceptor dopants in ZnO..……………………………………………………………………..…...60

4.1.2 Type and Nature of Potassium Defect in ZnO……………...….62

4.2 Properties of p-type ZnO nanorod ……………………………………….63

4.2.1 Morphology ……………………………………………………63

4.2.2 Lattice structure of p-type ZnO nanorods…………….........…64

4.2.3 Chemical composition of p-type ZnO nanorods……………….65

4.2.4 Electrical properties of p-type ZnO nanorods…………………71

4.2.5 Optical properties of p-type ZnO nanorods: Photoluminescenc.72

4.3 Improving the quality of p-type ZnO nanorods by of annealing……….. 73

4.3.1 Optical properties of p-type ZnO nanorods after heat-treatment………………………………………………………..73

4.3.2 Energy level of defects by low temperature PL of p-type ZnO nanorods……………………………………………….........74

4.4 Conclusions………………………………………………….........75

Chapter 5 Fabrication of p- type ZnO nanorods/n-GaN film hetero-junction ultraviolet light emitting diodes by aqueous solution method....77

5.1. Fabrication of p- type ZnO nanorods/n-GaN film hetero-junction LED..77

5.2 Electrical properties of the p-type ZnO nanorods/n-GaN film LED…….79

5.3 Optical properties of the p-type ZnO nanorods/n-GaN film LED……….81

5.3.1 Electroluminescence of the p-type ZnO nanorods/n-GaN film LED………………………………………………………………..81

5.3.2 Comparison of electroluminescence of the p-type ZnO nanorods/n-GaN film LED and p-ZnO film/n-GaN film LED………85

5.4 Conclusions…………………………………………………..……..…85

Chapter 6 Fabrication of ZnO coaxial nanorods homojunction on GaN substrates…………………………………………………………….......87

6.1 LED fabrication process……………………….………..….….…....87

6.2 Morphology of the ZnO homojunctions…………………….………..…88

6.3 Electrical properties of coaxial ZnO nanorods homojunction………..…89

6.3.1 Investigate the n- and p- contacts in the LED……………….....89

6.3.2 Electrical properties of coaxial ZnO nanorods homojunction…91

6.4 Optical properties of coaxial ZnO nanorods homojunction……………..94

6.5 Study the degradation of the ZnO homo-junction…………………..……96

6.6 Conclusion……………………………………........................…96

Chapter 7 Conclusions and recommendations…………….……..…98

7.1 Conclusions……………………………………..……..............98

7.2 Recommendations…………………………………...………........100

Bibliography…………………………………………….……...……...…103

Biography…………………………………………..………………113

Publication list…………………………………………….…….……... 114

Awards & Honors…………………………………………………......115

Summary

The growth of n- type and p-type ZnO nanorods using aqueous solution method is the first part of this work. n-type ZnO nanorods were obtained either by unintentional doped or doping with group III elements. p-type ZnO nanorods were obtained by doping with potassium. The ZnO nanorods were vertically aligned on GaN substrates. The undoped ZnO nanorods are n-type semiconductor that has the electron concentration of about $5x10^{17}cm^{-3}$. P-type ZnO doped at 0.07M KAc have hole concentration of about $2x10^{17}cm^{-3}$. Characterizations using X-ray photoelectron spectroscopy (XPS) and Secondary Ion Mass Spectroscopy (SIMS) show that the undoped ZnO nanorods are highly purity and have the Zn/O ratio of about 50:50. The similar characterization of p-type ZnO shows the existence of potassium along the p-type ZnO nanorods. Photoluminescence (PL) measurements of n-type and p-type ZnO nanorods were conducted to show the near band-edge emission at 370nm and impurity centers emission in visible range. Heat-treatment at 450°C was applied to improve the near band-edge PL emission of the n-type and p-type ZnO nanorods by three orders of magnitudes.

Using p-type ZnO nanorods growth technique, we fabricated a p-type ZnO nanorod/n-GaN film heterojunction ultraviolet LED. The LED demonstrates a rectifying I-V characteristic with a turn-on voltage of 2.7 V and a reverse bias leakage current of 10^{-6} A at 5V. Ideality factor, which was calculated from ln(I)-V characteristic, is 6.5. The existence of interface charges in the ZnO/GaN interface is the main cause for the low turn-on voltage and high ideality factor of the heterojunction. Electroluminescence

(EL) spectra of the LED were obtained at room temperature consists of an ultraviolet peak at 378 nm and a broad yellow emission centered at 560nm. Fitting and comparing EL of the LED with PL of p-ZnO and n-GaN show that p-ZnO contributes more to the EL than n-GaN.

Finally, we have demonstrated the fabrication of a ZnO nanorod core-shell homojunction UV LED. The ZnO homojunction demonstrates a rectifying I-V characteristic with a turn-on voltage of 3.35V and an ideality factor of 22.1 in the voltage range of 3.5 to 5.0 V. The p-doped and undoped nanorods have hole and electron concentrations of 2 x 10^{17} and 5 x $10^{17}cm^{-3}$ respectively as determined from a good fit of the I-V characteristics with the simulation results obtained by TMA MEDICI. These values agree well with those obtained from Hall measurement of similarly doped films. Room temperature EL spectra consist of an ultraviolet peak at 372nm and a broad visible peak centered at 560nm. A red shift was observed in the UV EL peak at higher applied currents. Comparison between the EL and PL spectra of the ZnO homojunction and GaN substrate confirms that the light is emitted from the ZnO homojunction. The stability of the LED was demonstrated for duration of three weeks after storage in normal ambient conditions.

LIST OF TABLES

Table 1.1 Summary of electron concentration levels of unintentional doped ZnO grown using various methods……………………………..………..….10

Table 1.2 Summary of various group III elements as well as their corresponding growth methods and levels of n-doping…..………………..…11

Table 1.3 Calculated nearest-neighbor bond lengths and the defect energy levels for negatively charged substitution impurities…...……………………11

Table 1.4 Summary of p-type ZnO using group V elements dopants……….12

Table 1.5 Survey of structure, method, and emission color of ZnO based heterojunction LEDs…………………………………………..…..…14

Table 1.6 Structure, the growth method and the emission peak position of ZnO nanostructures based hererojunction LEDs…………………………......15

Table 1.7 Structure, the growth method and the emission peak position of ZnO homojunction LEDs…………………………………………...........18

Table 4.1 Calculated nearest-neighbor bond lengths and the defect energy levels for negatively charged substitution impurities……………………..….61

Table 4.2 Quantitative calculation of all elements in p-type ZnO nanorods at 500°C……………………………………………..…………………..68

Table 4.3 Summary of measured Hall effect carrier concentrations for undoped and potassium doped ZnO films. A positive and negative sign indicates hole and electron concentration per cm^{-3} respectively…………….…72

Table 5.1 Turn-on voltage and ideality factor of p-ZnO nanorods/n-GaN film I-V characteristics at different ammonia concentration ……….…………..…80

Table 6.1 Summary of reported values of turn-on voltages and ideality factors for ZnO and GaN homojunctions……………………………………….....93

LIST OF FIGURES

Figure 1.1: Unit cell of the crystal structure of ZnO……….……………….03

Figure 1.2 Scanning electron microscopy (SEM) images of ZnO combs formed by evaporating ZnO powder at 1400°C for 2 hours. (a) Low-magnification SEM image of ZnO combs. (b) High-magnification SEM image of a comb made of an array of rectangular ZnO nanobelts ~400 nm wide at a spacing of ~700 nm. (c) Array of nanobelts ~280 nm wide at a spacing of ~250 nm. Upper right inset shows the growth front of one rectangular nanobelt. Scale bar = 500 nm. Lower left inset is an SEM image of the stem of a comb. Scale bar = 10 µm. (d) Aligned nanobelts ~500 nm wide at a spacing of ~300 nm. Inset is the growth front of a nanobelt. Scale bar = 500 nm…………………...……………...…………………...…………………04

Figure 1.3 A few examples of ZnO nanorods and tetrapods. From Sauer and Thonke (a), Waag (b), Grund- mann (c), and Wissinger (d)…………………05

Figure 1.4 Schematic showing the free energy of the precursors in gaseous and hydrated states and the final ZnO product……..………………….……..09

Figure 1.5 Zinc oxide homostructural p–i–n junction shows electroluminescence (EL) in forward bias at room-temperature. Electroluminescence spectrum from the p–i–n junction (blue) and photoluminescence (PL) spectrum of a p-type ZnO fi lm measured at 300 K. The p–i–n junction was operated by feeding in a direct current of 20 mA…………………………………………………………..……..….17

Figure 2.1 Schematic of ZnO growth by aqueous solution method…………23

Figure 2.2 Hydrolysis of hydrated Zn^{2+} metal ions in aqueous solution. The circle labeled M is Zn ………………………………………………......…24

Figure 2.3 The ionic equilibrium of Zn^{2+} in aqueous solution at 90°C ……..25

Figure 2.4 A model for adsorption of Zn^{2+} on ZnO surface…………………27

Figure 2.5 The dependence of adsorption of Zn^{2+} ions on the pH of the growth solution……………………………………………………………………27

Figure 2.6 Processes involved in heterogeneous nucleation on a substrate surface……………………………………………………………………..28

Figure 2.7 (a) A diagram of a RIE setup. An RIE consists of two electrodes (1 and 4) that create an electric field (3) meant to accelerate ions (2) toward the surface of the samples (5). (b)The front view of the Oxford Plasma 80 RIE system…………………………………………………………...……30

Figure 2.8 An example of pattern sample using AZ 5214 (a) and front view of the SUSS Mask Aligner system (b)…………………………………..…….31

Figure 2.9 Typical Process Recipe of the SUSS Mask aligner…………..…31

Figure 2.10 Electron beam source and Edwards Auto306 E-beam evaporation system……………………………..……………...……...……………32

Figure 2.11 (a) Electron beam in SEM and (b) the JEOL FESEM 6700 system in IMRE……………………………………..…………..…………33

Figure 2.12 Front view of JEOL 2000V TEM system. …………………..…….34

Figure 2.13 Renishaw 2000 Raman/PL microscope set up………………….35

Figure 2.14 The electroluminescence measurement by probe under photo-detector…………………………………………………………………….36

Figure 2.15 Principle of XPS analysis system…………………………………37

Figure 2.16 Schematic diagram of the SIMS process……………………..………38

Figure 2.17 Set up of I-V and C-V measurement system………………...…38

Figure 3.1 SEM images of ZnO nanorods grown at (a) 0.18, (b) 0.36 M and (c) 0.54 M NH_4OH. The concentration of $ZnAc_2$, growth temperature and duration were kept constant at 0.01 M, 90°C and 1 h respectively …………41

Figure 3.2 SEM images showing the morphology and area density of ZnO nanorods for (a) 0.01, (b) 0.02 and (c) 0.03 M of $ZnAc_2$. The concentration of NH_4OH, growth temperature and duration were kept constant at 0.37 M respectively...……………………………………………………………......42

Figure 3.3 Morphology of ZnO:Ga using (a) 0, (b) 0.02, (c) 0.08 and (d) 0.20 mM $Ga(NO_3)_3$. The concentration of $ZnAc_2$, NH_4OH, growth temperature and duration are kept constant at 0.01 M, 0.37 M, 90°C and 1h. Cross-sectional SEM images of corresponding ZnO:Ga using (e) 0.02 mM and (f) 0.20mM..44

Figure 3.4 Effect of doping $Ga(NO_3)_3$ on the morphology of ZnO grown on GaN substrate with (a) 0.18 M NH_4OH, (b) 0.37 M NH_4OH, and (c) 0.54 M NH_4OH...…………………………………………………………………..45

Figure 3.5 Morphology of ZnO:Al nanorods grown with (a) 0, (b) 5 and (c) 10 mM $AlCl_3$. The concentrations of $ZnAc_2$, NH_4OH, growth temperatures and durations were kept constant at 0.1 M, 0.37 M, 90°C and 1 h respectively..………………………………………………………………...46

Figure 3.6 Cross-sectional SEM images of ZnO nanorods grown with (a) 0.18 M, (b) 0.37 M and (c) 0.55 M NH_4OH. The concentrations of $ZnAc_2$, $AlCl_3$, growth temperatures and durations were kept constant at 0.01M, 5 mM, 90°C and 1 h………………………………………………………………………47

Figure 3.7 Schematic diagram summarizing the changes in ZnO growth habit in the presence of varying concentrations of $Ga(NO_3)_3$ and $AlCl_3$ dopant salts…………………………………………………………………..47

Figure 3.8 Schematic diagram summarizing the factors affecting the growth habit of ZnO in the presence of $Ga(NO_3)_3$ and $AlCl_3$ dopant salts.…………48

Figure 3.9 XRD of ZnO nanorods growth on GaN substrate. The growth condition is 0.01M ZnAc, 0.37 M NH_4OH. The red lines are standard position of ZnO bulk…….. 51

Figure 3.10 The (a) low and (b) high resolution TEM images of ZnO nanorods grown in the solution consisting of 0.01 M $ZnAc_2$, 0.37 M NH_4OH at 90°C for 1 h……..52

Figure 3.11 SIMS depth profile of of ZnO nanorods grown on GaN substrate using 0.01 M $ZnAc_2$ and 0.37 M NH_4OH at 90°C for 1 h. …………………53

Figure 3.12 EDX spectrum of ZnO nanorods grown on Si substrate using 0.01 M $ZnAc_2$ and 0.37 M NH_4OH at 90°C for 1 h……………………………..…53

Figure 3.13 XPS spectrum of ZnO nanorods grown on GaN substrate, the growth condition is 0.2g $ZnAc_2$, 1.2ml NH_3, 1 hour and 90°C. …………..…54

Figure 3.14 The XPS spectrum of Zn $2p_{1/2}$ and Zn $2p_{3/2}$ peaks from ZnO nanorods grown on GaN substrate in 0.02 M $ZnAc_2$ and 0.37 M NH_4OH at 90°C for 1 h………………………………………………………..…55

Figure 3.15 The XPS spectrum of O 1s peak from ZnO nanorods grown on GaN substrate in 0.02 M $ZnAc_2$ and 0.37 M NH_4OH at 90°C for 1 h……..…55

Figure 3.16 Photoluminescence of ZnO nanorods grown at (a) 0.54 M (b) 0.37 M, and (c) 0.18 M NH_4OH. The other growth parameters are concentration of $ZnAc_2$, growth temperature and duration were kept constant at 0.01 M, 90°C and 1 h…………………………………………………..….57

Figure 3.17 Photoluminescence of (a) un-doped, (b) 10 mM $AlCl_3$ and (c) 0.08 mM $Ga(NO_3)_3$ doped ZnO nanorods. The other growth parameters are concentration of $ZnAc_2$, NH_4OH, growth temperature and duration were kept constant at 0.01 M, 0.37M, 90°C and 1 h………………………………....58

Figure 3.18 Photoluminescence of un-doped ZnO nanorods annealed at different temperatures, varying from 200°C to 600°C. The anneal time is 30 minutes. The growth parameters are concentration of $ZnAc_2$, NH_4OH, growth temperature and duration were kept constant at 0.01 M, 0.37M, 90°C and 1h………………………………………………………………………..59

Figure 4.1 Schematic diagram showing the simulated lattice structure of ZnO (a) without any complexes, (b) with K_{Zn}-H_i and (c) K_{Zn}-K_i complexes.….…63

Figure 4.2 The SEM images of ZnO:K nanorods grown at (a) 0.00, (b) 0.07, and (c) 0.15 M KAc. Concentration of $ZnAc_2$, NH_4OH, growth temperature and duration are kept constant at 0.01 M, 0.37 M respectively at 90°C for 1 h……………………………………………………………………....64

Figure 4.3 (a) HRTEM of ZnO nanorods grown in 0.01 M $ZnAc_2$, 0.15M NH_4OH and 0.07 M KAc. The white spot represent the oxygen atoms. (b) SAED image of the same ZnO nanorod. ……………………………………65

Figure 4.4 ToF-SIMS of ZnO:K nanorods on n-GaN substrate showing incorporation of K ……………………………..………….………….……66

Figure 4.5 ToF-SIMS mapping image of p-type ZnO nanorods…………..…67

Figure 4.6 XPS spectra of the ZnO nanorods growth in aqueous solution includes: 0.01 M $ZnAc_2$, 0.07MKAc and 0.37 M NH_4OH. The measured temperatures are (a) 25 and (b) 500°C……………………………….....67

Figure 4.7 XPS spectra of the K 2p peaks of ZnO nanorods growth in aqueous solution includes: 0.01 M $ZnAc_2$, 0.07MKAc and 0.37 M NH_4OH. The measured temperatures are (a) 25 and (b) 500°C……………………………68

Figure 4.8 XPS spectra of the O 1s peaks of ZnO nanorods growth in aqueous solution includes: 0.01 M $ZnAc_2$, 0.07MKAc and 0.37 M NH_4OH. The measured temperatures are (a) 25 and (b) 500°C……………………………69

Figure 4.9 XPS spectra of the Zn 2p peaks of ZnO nanorods growth in aqueous solution includes: 0.01 M $ZnAc_2$, 0.07MKAc and 0.37 M NH_4OH. The measured temperatures are (a) 25 and (b) 500°C………………………..70

Figure 4.10 (a) Raman scattering spectra of p-type ZnO nanorods at room temperature and (b) plot of peak positions of A_1-LO against the concentration of KAc for as-grown samples A, B, C, D and E which are grown in 0, 0.03, 0.08, 0.13 and 0.18 M KAc respectively. The inset of (b) shows the fitted components consisting of the A_1-LO peak and its surface mode for sample C…………………………………………………………………………...71

Figure 4.11 Room temperature photoluminescence of potassium doped ZnO at different doping concentration vary from 0.00 to 0.13M KAc. The other parameters are $ZnAc_2$, NH_4OH concentration; growth temperature and duration are 0.01M, 0.37M, 90°C and 1 h, respectively……………………..73

Figure 4.12 Low-temperature (16K) photoluminescence of potassium doped ZnO annealed at different temperature. The ZnO: K nanorods were grown in aqueous solution contain 0.01 M $ZnAc_2$, 0.07 M KAc, 0.18 M NH_4OH at 90°C for 1 h…………...74

Figure 4.13 Normalized low temperature (16K) photoluminescence of potassium doped ZnO annealed 700°C for 30 minutes, inset is band diagram of potassium doped ZnO……..………………………………..……………..75

Figure 5.1 Fabrication process of p-ZnO nanorods/ n-GaN film heterojunction LED…...…………………………………………………….….………78

Figure 5.2 Comparison of the experiment and simulated I-V characteristic of p-ZnO nanorods/n-GaN films heterojunction, the simulation was performed

by using TMA MEDICI software with the hole and electron concentration of 3×10^{17} and 5×10^{17} cm^{-3}, respectively. The inset shows I–V characteristic of (a) n-metal/n-GaN contact, (b) p-ZnO/p-metal contact…………………….....79

Figure 5.3 Electroluminescence spectra of p-ZnO nanorods/n-GaN film LED at difference applied current………………………….……….………….82

Figure 5.4 Fitting of electroluminescence spectra of p-ZnO nanorods/n-GaN film LED at difference applied current to investigate effect of thermal heating on peak position. Temperatures of the device are estimated…………………83

Figure 5.5 Normalized PL spectra of p-type ZnO nanorods, n-GaN film and EL spectrum of p-ZnO nanorods/n-GaN film hererojunction LED.…………84

Figure 6.1 Fabrication process of coaxial ZnO nanorod homojunction LED……………………………………………………………………..88

Figure 6.2 (a) SEM images showing the exposed tips of the un-doped ZnO nanorods covered in photo-resist (0.02 $ZnAc_2$ with 0.37M NH_4OH, 1h, 90°C) after dry etching in O_2 plasma (100W) for 11 minutes and (b) corresponding ZnO core-shell homonjunction grown in solution containing 0.02 M $ZnAc_2$ and 0.37M NH_4OH for the core layer while the shell layer nanorod is grown with 0.02 M $ZnAc_2$, 0.370 M NH_4OH and 0.07 M KAc. The photoresist has been removed..…………………………………………….…………....89

Figure 6.3 I-V characteristic of (a) n-metal/n-GaN contact, (b) n-GaN/n-ZnO junction and (c) p-ZnO/p-metal contact.………………………….….…90

Figure 6.4 (a) SEM cross-sectional image of p-type ZnO grown on unintentionally doped GaN epi-layer. The p-ZnO was grown using two growth cycles, where each growth cycle consists of an aqueous solution of 0.02 M $ZnAc_2$, 0.37 M NH_4OH and 0.07 M KAc maintained at 90°C in a water bath for 1h. (b) Schematic of the structure to measure the I-V across the In/Zn dots for line (b) in the Fig 6.3. …….…………………...…………………90

Figure 6.5 Schematic diagram of the structure to obtain the I-V characteristic between the n-ZnO nanorod and the n-GaN epilayer, Ohmic contacts to n-ZnO nanorods and n-GaN epilayer were achieved using an indium dot and Ti (10 nm) / Au (50 nm) respectively…………………………………………….91

Figure 6.6 Comparison of the experiment and simulated I-V characteristic of ZnO coaxial homojunction LED. The simulated I-V was obtained using TMA MEDICI software with the hole and electron concentration of $2x10^{17}$ and $5x10^{17}$ cm^{-3}, respectively.…………………………………………………92

Figure 6.7 Electroluminescent spectra of ZnO coaxial homojunction LED at different applied currents; insert are photos of electroluminescence of ZnO coaxial nanorods homojunction LED at 20mA and 30mA.………………..…94

Figure 6.8 UV peak intensity increases linearly with applied current and UV peak position red shifts linearly with the applied current.…………………...95

Figure 6.9 Comparison of the EL of ZnO homojunction with the PL of GaN and ZnO..95

Figure 6.10 The electroluminescence of ZnO coaxial homojunction at 20 mA after 1 day and 3 weeks……………………………………………………96

Chapter 1 Introduction

This chapter introduces the background of ZnO which including its unique properties, historical and current research status, and ZnO nanostructures. The chapter also reviews the fabrication methods of ZnO film, nanostructure, and doping of ZnO. Application of ZnO in solid-state lighting will be reviewed. This chapter includes 7 sections. Section 1.1 introduces the background of research and properties of ZnO. Section 1.2 describes the methods for growing ZnO nanorods while section 1.3 focuses on doping of ZnO nanorods. Section 1.4 presents a literature review of ZnO homo-junction light emitting diode (LED). Section 1.5 presents the motivation and objectives of this thesis. Finally, section 1.6 outlines the organization of this thesis.

1.1 Background and basic properties of ZnO

1.1.1 Background

Artificial lighting consumes a significant part of all electrical energy consumption worldwide. 20 and 50 percent of the energy consumed in homes and offices, respectively, is due to lighting [1]. Thus, demand for energy saving lighting source is rising in recent years. Efficient solid-state light sources such as LEDs provide the best solution. However, LED technology which uses GaN material is limited by the high cost of GaN fabrication. As a result, ZnO, with its promising properties, has been considered a good candidate to replace GaN in solid state lighting.

Zinc oxide (ZnO), a IIb-VI compound semiconductor, has a wide bandgap of 3.34 eV and a large exciton binding energy of 60meV at room temperature. Therefore, ZnO, like GaN, will be important for blue and ultra-

violet optical devices. The most important advantages of ZnO over GaN are its larger exciton binding energy and the availability of single crystal substrates. Other favorable aspects of ZnO include its low power threshold for optical pumping, radiation hardness and biocompatibility. Together, these properties of ZnO make it an ideal candidate for a variety of devices ranging from sensors to ultra-violet laser diodes and devices such as displays. [2]

ZnO is not a new material despite the recent surge in research work, as ZnO has been widely studied since 1930 and its studies peaked around the end of the 1970s and the early 1980s [3]. Subsequently, the interest faded away, partly because of difficulty in doping p-type, which is essential for optoelectronics application. A revival in ZnO research began in the mid-1990s based on its possibility to grow epitaxial layers, quantum wells, nanorods or quantum dots and its possible applications in blue/UV optoelectronics, radiation hard electronic devices, visible-blind electronic circuits, semiconductor spintronics and transparent conducting oxides [3-5]. The present renaissance on ZnO research started in the mid-1990s and has been documented by numerous conferences, workshops, and symposia and by more than 2000 ZnO-related papers in the year 2005 and an even higher number for 2006, compared to about 100 in 1970 (sources: INSPEC, Web of Science).

1.1.2 Basic properties of ZnO

Zinc oxide crystallizes in the hexagonal wurtzite-type structure, as shown in Fig 1.1. It has a polar hexagonal axis, the c-axis, chosen to be parallel to z. The primitive translation vectors a and b lying in the x–y plane, are of equal length, and include an angle of 120°, while vector c is parallel to the z-axis. One zinc ion is surrounded tetrahedrally by four oxygen ions and

vice versa. The primitive unit cell contains two formula units of ZnO. The values of the primitive translation vectors at room temperature are: a =b ≈ 0.3249 nm and c ≈ 0.5206 nm [3].

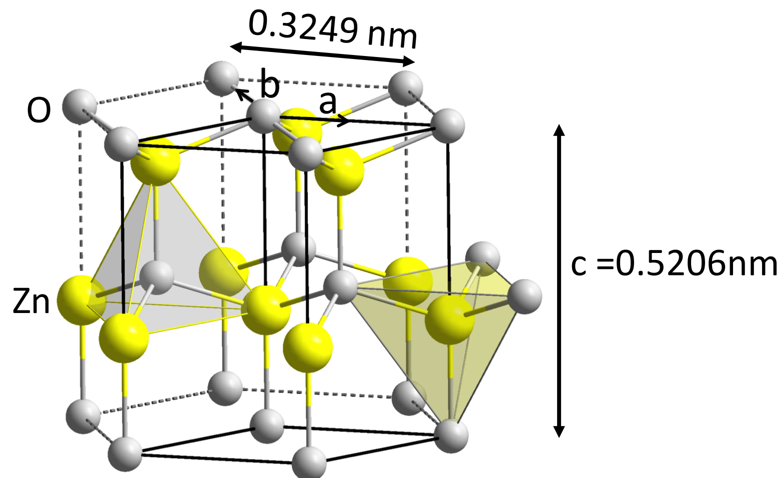

Fig 1.1: Unit cell of the crystal structure of ZnO. Taken form Wikipedia.

In contrast to other II –VI semiconductors, which exist both in the cubic zincblende and the hexagonal wurtzite-type structures, ZnO crystallizes with great preference in the wurtzite-type structure. The cubic zincblende-type structure can be stabilized to some extent by epitaxial growth of ZnO on suitable cubic substrates [3].

ZnO has probably the richest variety of different nanostructures. Its range includes highly ordered nanowire arrays, tower-like structures, nanorods, nanobelts, nanosprings, nanocombs, and nanorings. An example of ZnO nanostructure is shown in Fig 1.2. In this figure, ZnO nanocombs have been synthesized by thermal evaporation of ZnO powder in a tube furnace [6].

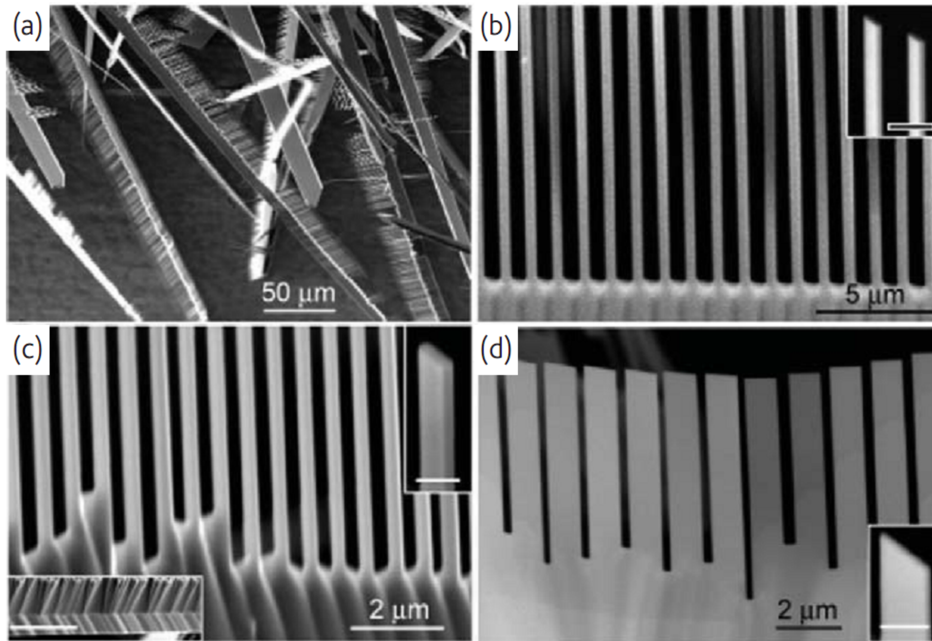

Fig 1.2 Scanning electron microscopy (SEM) images of ZnO combs formed by evaporating ZnO powder at 1400°C for 2 hours. (a) Low-magnification SEM image of ZnO combs. (b) High-magnification SEM image of a comb made of an array of rectangular ZnO nanobelts ~400 nm wide at a spacing of ~700 nm. (c) Array of nanobelts ~280 nm wide at a spacing of ~250 nm. Upper right inset shows the growth front of one rectangular nanobelt. Scale bar = 500 nm. Lower left inset is an SEM image of the stem of a comb. Scale bar = 10 µm. (d) Aligned nanobelts ~500 nm wide at a spacing of ~300 nm. Inset is the growth front of a nanobelt. Scale bar = 500 nm. [6]

Another example of ZnO nanostructure is the growth of whisker-like ZnO nanorods. These are needle-like crystals with diameters in the range of a few tens to a few hundred nm and lengths of several µm. In Fig 1.3 a–d, we give a few recent examples by Sauer and Thonke, Waag, Grund- mann, and Wissinger [3].

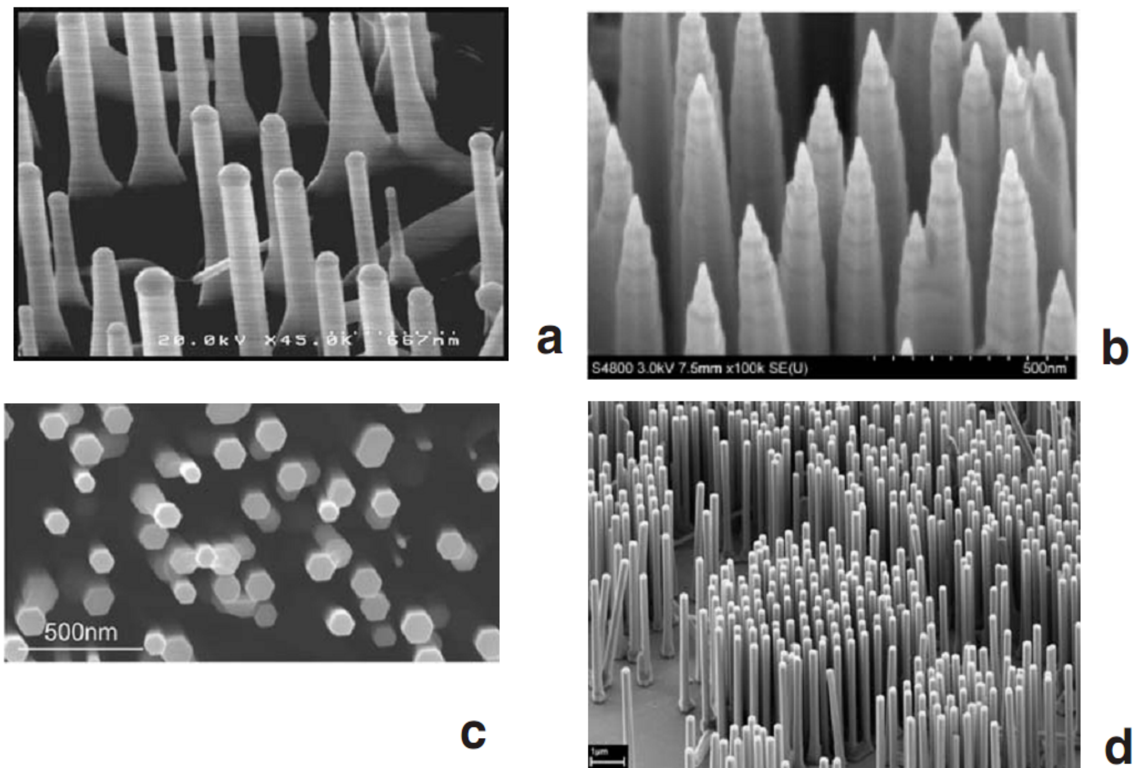

Fig 1.3 A few examples of ZnO nanorods and tetrapods: From Sauer and Thonke (a), Waag (b), Grund- mann (c), and Wissinger (d) [3]

1.2 ZnO nanorods growth techniques

1.2.1. Vapor phase methods

a) Vapor phase transport

In vapor phase transport, the ZnO material is vaporized from a solid source, typically in powder form, and transported onto a substrate where it condenses and deposits. Thermal evaporation, laser ablation, sputtering, or electron beam can be used to vaporize the ZnO powder source. ZnO powder is heated to close to its melting point, which is about 1975°C for vaporization. For example, in thermal evaporation method, the temperature at which ZnO powders are heated is in the range from 1100 to 1400°C. In this method, a carrier gas is needed to direct the ZnO vapors to deposit on a substrate placed downstream of the carrier gas [3].

In order to reduce the growth temperatures, sub-oxides of zinc (ZnO_x, $0 \leq x < 1$) can be used instead which have a melting point of about 419°C. ZnO_x can be obtained by reduction of ZnO using graphite [7, 8] as shown in the reactions (1.1) and (1.2) below:

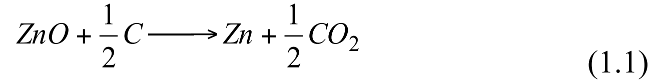

$$ZnO + \frac{1}{2}C \longrightarrow Zn + \frac{1}{2}CO_2 \quad (1.1)$$

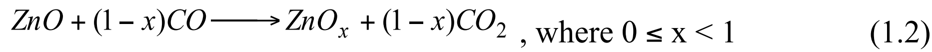

$$ZnO + (1-x)CO \longrightarrow ZnO_x + (1-x)CO_2 \text{, where } 0 \leq x < 1 \quad (1.2)$$

Reduction can also be achieved using hydrogen [8, 9], or reduction of zinc salts such as ZnS [10].

b) Chemical vapor deposition (CVD) and metal-organic chemical vapor deposition (MOCVD)

The use of volatile Zn sources in CVD and MOCVD methods allows even lower vaporization temperatures to be applied. In CVD, zinc acetylacetonate hydrate (hereon denoted as $Zn(acac)_2$), with vaporization temperatures between 130°C and 140°C, is typically used as a source. Upon vaporization, Zn^{2+} vapor is transported by nitrogen for reaction with oxgen at temperatures ranging from 500 to 600°C.

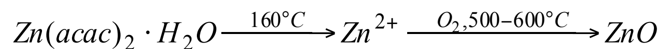

$$Zn(acac)_2 \cdot H_2O \xrightarrow{160°C} Zn^{2+} \xrightarrow{O_2, 500-600°C} ZnO$$

In MOCVD, a metal-organic source, typically dimethyl zinc or diethyl zinc with vaporization temperatures ranging from 117°C to 130°C, is used. The metal-organic source is decomposed to form Zn vapor and then transported using inert gas argon into the reaction chamber where it reacts with oxygen to form ZnO. This reaction typically takes place at temperatures ranging from 300 to 500°C [11].

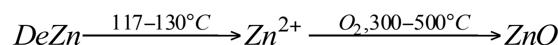

$$DeZn \xrightarrow{117-130°C} Zn^{2+} \xrightarrow{O_2, 300-500°C} ZnO$$

c) Molecular beam epitaxy (MBE)

In MBE method, high purity Zn metal (melting point 420°C) is thermally evaporated in a Knudsen effusion cell. Under ultrahigh vacuum conditions (< 10^{-8} Pa), Zn vapor is directed onto the substrate which typically has a thin layer of Ag as a catalyst. In the presence of O_2 and a growth temperature of 300 to 500°C, growth of ZnO on the substrate can be achieved [12, 13].

1.2.2 Solution phase method

a) Review of solution phase method

In general, oxides are particularly suited for growth in solution. Literature is rich with reports of nanostructures fabricated in chemical solutions. The ease of ZnO growth in solution is reflected in the low growth temperatures of 60 to 90°C. Growth precursors in aqueous solution generally consists of a zinc salt, such as zinc acetate, zinc nitrate or zinc chloride, and a base such as sodium hydroxide and aqueous ammonia. Growth of ZnO in aqueous solution is an attractive alternative to MOCVD because it is a simple, cheap, non-toxic and low temperature method. Large-scale processing has also been demonstrated [14].

Andres-Verges et al. [15] first introduced aqueous solution method for growth of ZnO in 1990. In his report, ZnO rods were formed in aqueous solutions which contain of zinc nitrate, zinc chloride and hexamethylenetetramine. An improvement of this method using a seed layer was introduced by Vayssieres et al. [16] ten years later. Using a seed layer, ZnO nanorods can be grown on large lattice mismatch material such as glass and Si substrates. In our group, Le et al. studied the growth of ZnO nanorods

on GaN substrates using zinc acetate ($ZnAc_2$) and ammonium hydroxide (NH_4OH) [17]. In addition, Tay et al. focused on the growth ZnO nanorods and film using a growth solution consisting of $ZnAc_2$ and NH_4OH on various substrates [18, 19]. He reported the effect of concentration, supersaturation, pH, solubility and complexes on morphology, density, structural and optical properties of ZnO nanorods.

b) Difference between gas phase and solution phase growth methods

Since growth of ZnO by solution phase method is carried out at low temperatures compared to that of gas phase methods, the gaseous phase methods have a large driving force and a lower activation energy barrier as shown in Fig 1.4. Growth of ZnO is more readily achieved with precursors in gaseous state than in solution state. Since the growth needs a sufficient energy for diffusion, nucleation and growth, growth in gaseous phase can be achieved over a wider range of precursor concentrations, as a result of the large driving force.

Aqueous solution methods have a small driving force and high activation energy barrier as shown in Fig 1.4. The formation of ZnO is obtained by shifting the chemical equilibrium to favor hydrolysis and condensation of ZnO. By control of precursor concentrations and zinc solubility, growth of ZnO is obtained.

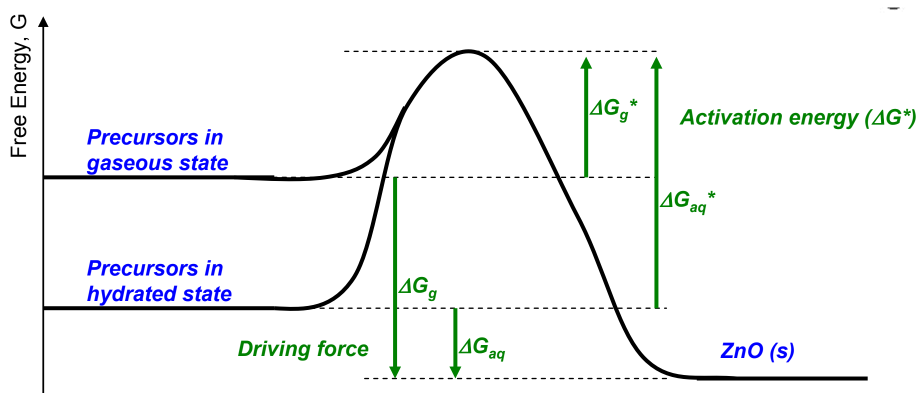

Fig 1.4 Schematic showing the free energy of the precursors in gaseous and hydrated states and the final ZnO product. Taken form reference [20]

c) Advantage of solution base-method against gas phase method

In terms of energy and material saving, aqueous solution methods have clear advantages over gas phase methods. In addition, aqueous solution methods can give high homogeneity and faster growth rates because the growth precursors in solution have higher concentrations than those of the gas phase. Finally, aqueous solution method is a low cost, safe and simple process. The equipment used is only a growth vessel, water bath or microwave oven. In comparison, gas phase methods need a more sophisticated set-up to operate in high temperatures and at low vacuum ambient.

1.3 Doping ZnO nanorods

1.3.1 Doping n-type ZnO

The growth of ZnO results in defects. Defects in ZnO can be oxygen vacancies, zinc interstitials and hydrogen interstitial. All of these defects are donor impurities. These donor defects result in unintentional doping of n-type ZnO.

However, unintentionally doped n-type ZnO is difficult in controlling the electron concentration. First, the defect density is not a stable factor; it strongly depends on the temperature of ZnO. For example, the concentration of hydrogen in ZnO varies when ZnO is heated to 200°C [21]. Second, it is difficult to control the electron concentration of ZnO. The Table 1.1 below shows the electron concentration of unintentionally doped ZnO grown by different methods.

Table 1.1 Summary of electron concentration levels of unintentional doped ZnO grown using various methods. Taken from reference [20].

Type of film	Growth method	Electron conc. (cm^{-3})	Substrate	Ref.
Polycrystalline	PLD	10^{18} - 10^{20}	Si	[22]
Polycrystalline	Magnetron sputtering	10^{19}	Glass & Sapphire	[23]
Polycrystalline	MOCVD	10^{17} - 10^{18}	Sapphire	[24]
Polycrystalline	Aqueous solution	10^{19}	$MgAl_2O_4$ (111)	[25]
Single crystal	Hydrothermal at 300-400°C	10^{13} to 10^{14}	ZnO seed	[26]
Single crystal	vapor phase transport	10^{14}-10^{15}	n.r.	[27]

Polycrystalline ZnO films which have high intrinsic defects have the highest electron concentration. Single crystalline ZnO films have much lower defects and have lower intrinsic electron concentration. The Table 1.1 shows that solution phase growth methods seem to result in lower electron concentration for the single crystalline ZnO film than those obtained by gas phase methods.

To obtain a high quality and controllable n-type ZnO, we first fabricate ZnO with low intrinsic defect level and then dope the ZnO to obtain a stable and controllable n-type ZnO. The suitable dopants for n-type ZnO are group-III elements such as Ga, Al and In. These dopants substitute the Zn sites to

obtain high levels of electron concentration beyond 10^{20} cm^{-3}. Success in n-doping has been achieved by both solution phase and gas phase methods. Table 1.2 summarizes the various dopants and methods that have been reported.

Table 1.2 Summary of various group III elements as well as their corresponding growth methods and levels of n-doping. Taken from reference [20].

Dopant	Electron conc. (cm^{-3})	Growth method	Substrate	Ref.
Ga	10^{18} - 10^{20}	MBE	AlMgO4	[28]
	> 10^{20}	PLD	Glass	[29]
Al	> 10^{21}	Filtered cathodic vacuum arc	p-doped 4H-SiC	[30]
	> 10^{21}	Aqueous Solution	Glass	[31]
In	> 10^{20}	Mag. Sputtering	Glass	[32]
	10^{19}	Hydrothermal	ZnO seed	[33, 34]

1.3.2 Doping p-type ZnO

Doping p-type ZnO is difficult to obtain with high quality and in a stable form. This difficulty is due to the high densities of donor impurities, low solubility of the acceptor dopants and deep energy levels of the dopants [28]. The possible dopants for p-type ZnO can be group IA elements such as K, Na and Li or group V elements such as P, N and As. Group V elements tend to replace O while group IA elements replace Zn in ZnO structure. Theoretical calculation of all possible dopants by Park et al. [35] are shown in the Table 1.3.

Table 1.3 Calculated nearest-neighbor bond lengths and the defect energy levels for negatively charged substitutional impurities. Taken from reference [35].

Element	Bond lengths (Å)	Strain (%)	Defect energy level (eV)
Li	2.03	5	0.09
Na	2.10	9	0.17
K	2.42	25	0.32

N	1.88	-3	0.40
P	2.18	13	0.93
As	2.23	16	1.15

The bond length of Zn-O is 1.93 Å [35], close to bond length of Li-O and Na-O. Therefore, Li and Na dopants have the lowest strain energy in ZnO. In terms of thermodynamic consideration, Li and Na are the best candidates for p-type ZnO. However, Li and Na, which have smaller atom radii than Zn, tend to occupy the interstitial sites. The interstitial Li and Na form donor impurities and compensate the acceptor contributions. This results in n-type ZnO obtained by doping with these dopants.

Group V dopants are not potential dopants because they have deeper acceptor energy levels. However, experiments show that group V elements can have lower acceptor energy levels than those predicted by simulation which results are presented in Table 1.3. Some groups have reported their successful growth of p-ZnO by doping with group V elements such as N or P [36-38] . Table 1.4 summarizes the p-type doping concentrations that have been achieved using various dopants from group V elements.

Table 1.4 Summary of p-type ZnO using group V elements dopants. Taken from reference [20]

Dopant	Hole concentration (cm^{-3})	Method	Substrate	References
N	2×10^{16}	MBE	ScAlMgO4	[39, 40]
P	$1.9 \times 10^{16} – 3.8 \times 10^{19}$	RF sputtering	Glass, n-Si	[41]
As	$2.5 \times 10^{17} – 1.2 \times 10^{18}$	PLD	c-sapphire	[42]
Sb	1×10^{16}	MBE	p-Si (111)	[43]

Despite the success of p-type ZnO growth presented in Table 1.4, controversy on the quality of p-type ZnO still remained [6]. The problems needed to be solved are improving carrier mobility and the stability of p-type

ZnO. An alternative to obtain more stable p-type ZnO is by using co-doping. Co-doping can increase the solubility of the dopant and lower its ionization energy [44]. This approach has been successfully demonstrated in Al-N [45], In-N [46] and Ga-N [47] combinations using magnetron sputtering. The hole concentrations are reported in the range from 10^{17} to 10^{18} cm^{-3}. This co-doping approach is also successfully used for group I elements such as Li co-doped with N [48]. This combination has achieved very reproducible and stable hole concentrations of about 10^{19} cm^{-3}. However, the mechanism leading to the enhanced p-type stability is still unclear [49].

Among the group I element dopants, potassium (K) does not seem to be potential candidate and it was forgotten. The challenges for p-type ZnO doping with K are low solubility of K and large atomic radius of K lead to increase oxygen vacancy. However, ZnO dope with K can address the challenges to obtain p-type conductivity. K can co-dope with hydrogen to reduce the chance of forming oxygen vacancy and improve its solubility. Reports on the success of fabrication of p-type ZnO by doping K by our group [50, 51] show that potassium is a potential dopant to study.

1.4 Application of ZnO in solid-state lighting

ZnO-based light emitters have been considered as a potential candidate for the next generation of high efficiency blue/near-UV light sources, due to the direct wide band gap energy of 3.37 eV, a large exciton binding energy of 60 meV at room temperature, and several other manufacturing advantages of ZnO. ZnO is a low cost of raw and processed material, which can set a new cost-point for LED.

1.4.1 ZnO based heterojunction LED

a) Heterojunction LEDs with ZnO film

Due to difficulty in fabrication p-type ZnO, in LED application, heterojunctions of n-ZnO and other p-type materials have been reported in the published literature. Among these p-type materials, p-GaN is of particular interest considering that it has similar crystallographic and electronic properties to ZnO [36, 52, 53]. In addition, it has been suggested that the ZnO nanowire/GaN heterojunction has higher carrier injection efficiency and recombination rate than other junctions. The other p-type material for ZnO heterojunction LED is AlGaN, p-Si, and conducting oxides. Table 1.5 reviews the structure, method, and emission color of ZnO based heterojunction LEDs. To improve optical characteristics with ZnO-based heterojunction LEDs, double and triple heterostructure LEDs were demonstrated [54, 55]. Heterojunction LEDs have been constructed mostly by depositing n-type ZnO or n-type MgZnO on various p-type semiconductor layers. However, there have been several attempts to fabricate the heterojunction LEDs constructed by depositing p-type ZnO on various n-type semiconductor layers [36, 56].

Table 1.5 Survey of structure, method, and emission color of ZnO based heterojunction LEDs. Taken form reference [57].

Structure	Growth method	Emission Color	Ref.
n-ZnO/p-GaN	PLD	UV (375)	[58]
n-ZnO/p-GaN	MOCVD	Blue-violet (415)	[59]
n-ZnO/p-AlGaN	CVD	UV (385)	[60]
n-ZnO/n-MgZnO/n-CdZnO/p-GaN	MOCVD	Blue, red	[54]
n-MgZnO/n-ZnO/p-AlGaN/p-GaN	MBE	UV(390)	[55]
n-MgZnO/CdZnO/p-GaN	MBE	UV(390,410)	[61]
p-ZnO/n-Si	MBE	UV (381) Visible (485,612,671)	[56]
p-ZnO/n-GaN	RF-megnetron	Blue-violet (409)	[36]

	sputtering		
n-ZnO/p-GaN, n-ZnO.n-MgZnO/n-ZnO/p-GaN	MBE	UV (375) Visible (415,525)	[62]
n-ZnO/p-Si	MOCVD	Visible (580)	[63]
n-ZnO/u-ZnOp-Si	Magnetron Sputtering	Visible (500-650)	[64]
p-SrCu2O2/n-ZnO/ITO/YSZ	PLD	UV (382)	[65], [66]
n-ZnO/p-GaN/Al_2O_3	CVD	Blue (430)	[67]
n-ZnO/u-ZnO/p-$CuGaS_2$/n-GaP	Helicon-wave excited plasma sputtering	Greenish white	[68]

b) Heterojunction LEDs with ZnO nanostructures

The ZnO nanostructures have attracted much attention for fabrication of optical device due to their optical properties arising from quantum confinement such as enhanced radiative recombination of carriers. The research for application to LEDs using the ZnO nanostructures has focused on 1-D nanostructure due to the crystal orientation of ZnO. However, the difficulties in obtaining stable and reliable p-doping method still remains with ZnO nanostructures. Therefore, most of heterojunction devices using n-type ZnO nanostructure use p-type made from materials such as p-type GaN, Si, NiO, and polymers. The properties of heterojunction LEDs with ZnO nanostructures are summarized in Table 1.6 together with the LED structure, the growth method of ZnO nanostructures, and the emission peak position.

Table 1.6 Structure, the growth method and the emission peak wavelength of ZnO nanostructures based hererojunction LEDs. Taken form reference [57].

Structure	Growth method	Emission color (nm)	Ref.
n-ZnO nanorods/p-GaN film	MOCVD	UV (370), Blue (440), Yellow (560)	[69]
n-ZnO films/n-ZnO nanowire/p-GaN film	MOCVD	Blue (425-440)	[52]

n-ZnO nanorod/p-GaN fim	MOCVD	Blue (440-560)	[70]
n-ZnO nanowire in polystyrene/PEDOT:PSS	CVD	UV (380)	[71]
n-ZnO nanorod/p-Si substrate	Solution method	UV (387), Green (535)	[72]
n-ZnO nanorod/p-NiO film	Solution method	UV-violet, broad visible (500-800)	[73]
n-ZnO nanowire in PMMA/NPB	Solution method	UV (342)	[74]
n-ZnO nanowire/PEDOT:PSS	Electrodeposition	Broad visible (500-1100)	[75]
n-ZnO nanowire/p-GaN film	PLD	UV (380)	[76]
n-ZnO nanorod/p-$CuAlO_2$ film/p-Si film	Vapor phase transport	UV (378), Green (492)	[77]

1.4.2 ZnO based homojunctions LED

The first important work on ZnO homojunction was conducted in 2004 by Tsukazaki et al. [38]. His report introduced the repeating temperature modulation technique to fabricate reliable and reproducible p-type ZnO in order to fabricate the p-i-n ZnO homojunction. Laser MBE and doping with nitrogen was used to fabricate p-type ZnO films. The fabricated p-i-n homojunction LED has a rectifying I–V characteristic with a threshold voltage of about 7 V which is much higher than the bandgap of ZnO (3.34 eV). This large value attributed to high resistivity of the p-type ZnO layer. In addition, they also obtained EL spectra of the LED with multireflection interference fringes. The EL spectra show a red-shift compared to the exciton emission of undoped ZnO layer at 3.2 eV. This is partly due to the low hole concentration in the p-type ZnO. The PL spectrum (black) of a p-type ZnO film is also shown in Fig 1.5. The higher energy EL peak located at around 2.95 eV matches well with the PL spectrum. Although the quality of this ZnO homo-junction LED is relatively high, the growth method is too complicated.

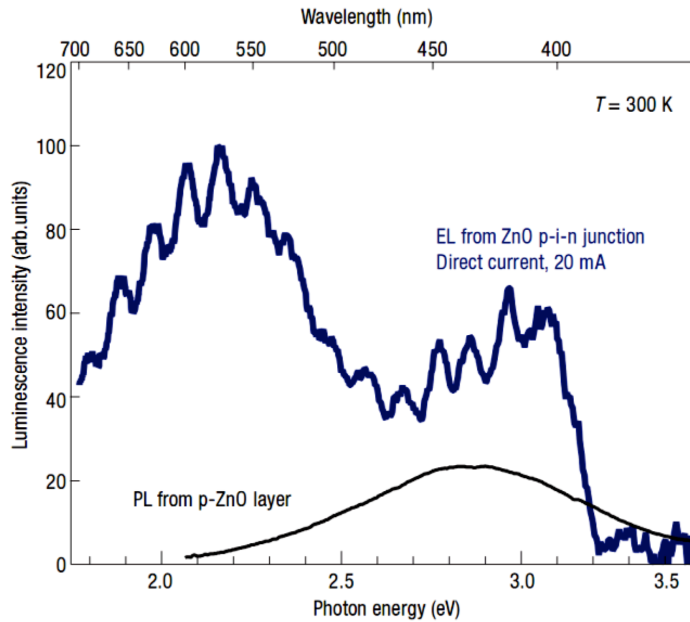

Fig 1.5 ZnO homostructural p–i–n junction shows electroluminescence (EL) in forward bias at room-temperature. Electroluminescence spectrum from the p–i–n junction (blue) and photoluminescence (PL) spectrum of a p-type ZnO film measured at 300 K. The p–i–n junction was operated by feeding in a direct current of 20 mA. Taken from reference [38]

More studies on ZnO homojunction LED were published in 2007 and 2008. For example, Ryu et al. [37, 78, 79] was able to obtain ZnO LED structure by adding $Be_{0.3}Zn_{0.7}O$ layer and a BeZnO/ZnO active layer comprising of MQWs between n-type and p-type ZnO. They also introduced ultraviolet light emitting diodes, and excitonic ultraviolet lasing in ZnO-based emitting devices. There have been several attempts to reduce hydrogen incorporation at or near the surface and mesa sidewall that was introduced when the LED structure was fabricated by wet etching and photolithography. In 2008, Kim et al. [80] reported that annealing at 350°C for 5 min in O_2 ambient can improve the I–V characteristics and the EL intensity of ZnO homojunction LED. Annealing can reduce hydrogen incorporation at or near the surface and mesa sidewall of the LED structure. Wang et al. [81] studied the passivation effects of dielectric materials (SiO_2 and SiN_x) on ZnO LEDs.

The study of ZnO homojunction LED has been developed for the last 5 years. The properties of ZnO-based homojunction LEDs are summarized in Table 1.7, together with the structure, growth method, and emission peak position.

Table 1.7 Structure, the growth method and the emission peak position of ZnO homojunction LEDs. Taken from reference [57].

Structure	Growth method	Emission color (nm)	Ref.
n-ZnO/u-ZnO/p-ZnO	MBE	Blue (430)	[38]
p-ZnO/n-ZnO, p-ZnO/MgZnO/ZnO:Ga/MgZnO/n-ZnO	Rf-magnetron sputtering	UV (380)	[82]
n-ZnO/n-$Be_{0.3}Zn_{0.7}O$/BeZnO-ZnO MQW/p-$Be_{0.3}Zn_{0.7}O$/p-ZnO	Hybrid beam deposition	UV (388), Green (550)	[78]
n-ZnO/p-ZnO	MOCVD	UV (375), Visible (430-600)	[83]
n-ZnO/p-ZnO	MBE	Blue-violet (420-440)	[84]
n-ZnO/p-ZnO	MBE	UV (388)	[85]
n-ZnO/p-ZnO	MBE	UV (383), Visible (420-605)	[86]
n-ZnO/p-ZnO	MOCVD	UV (410) Visible (536,710)	[87]
p-ZnO/MgZnO/ZnO/MgZnO/n-ZnO	PLD	UV (385), Visible (500-1000)	[80]
n-MgZnO/p-MgZnO	MOCVD	Blue-green	[88]
n-ZnO/p-ZnO	MOCVD	UV (379)	[89]
p-ZnO/n-ZnO substrate	Excimer laser doping	UV (370-380)	[90]
n-ZnO/p-ZnO	PLD	Blue white	[91]
p-ZnO/n-ZnO/Si	React. Sputtering	None	[92]
n-ZnO/p-ZNO/GaAs substrate	Hybrid beam deposition	none	[93]
p-ZnO/n-ZnO/n-SiC	Hybrid beam deposition	none	[37]
N_2O implanted ZnO/n-ZnO/Al_2O_3	CVD	UV (388)	[94]
p-ZnO/n-ZnO/ZnO	MOCVD	UV (384)	[95]
p-ZnO/n-ZnO/Al_2O_3	RF Sputtering	none	[96]

p-ZnO/n-ZnO/a-Al2O3	MBE	Blue (430)	[97]
n-ZnO/p-ZnO/Al2O3	MBE	Visible (423-523)	[98]
n-ZnO/p-ZnO/p-GaAs	MOCVD	UV (387), Visible (496)	[99]
n-ZnO/p-ZnO/n^+-GaAs	PLD	Visible (496)	[100]
p-ZnO/n-ZnO/i-ZnO/n-Si	DC Sputtering	UV (389), Blue (480)	[101]

1.5 Motivation of the thesis

As explained in the previous sections, LED technology which uses GaN as its major material is limited by the high cost of GaN fabrication. As a result, ZnO, a cheaper material with its promising properties, have been considered as a good candidate to replace GaN in LED fabrication. In order to commercialize ZnO LED, aqueous solution method is used as it can fabricate cheap, large scale ZnO nanostructures for LED application. In this thesis, we report on the successful of fabrication ZnO homojunction light emitting diode (LED) using chemical solution route method. Solution methods offer an alternative processing route that is environmentally-friendly, low cost, non-toxic, and suitable for large scale processing.

In order to obtain ZnO homojunction, n- type and p-type doped ZnO must be obtained. n-type ZnO is easily grown by unintentionally doped ZnO while p- type doping is not easy to obtain. Current achievements in p-type doping have mainly focused on group V elements as well as co-doping using group I and V elements by gas phase methods. Thus another objective of this thesis is to investigate p-doping of ZnO using group I elements with aqueous chemical growth methods. In this thesis, potassium (K) was selected to dope p-type ZnO.

This is the first study on ZnO nanorod homojunction LED which fully used the solution method. We obtained the LEDs with rectified I-V characteristics. This experimental I-V characteristic fit well with MEDICI simulation of ZnO homojunction device. Besides I-V, light emission of the LED was observed and taken at different applied currents. A strong UV electroluminescence from the LED shows the good quality of this ZnO nanorod material. This relatively high quality ZnO homojunction LED presents a potential for fabricating reliable LED.

1.6 Organization of the thesis

This thesis comprises 7 Chapters which are organized as follows:

Chapter 1 briefly introduces the material properties of ZnO, its growth methods and doping. It also contains the literature review of ZnO based LEDs and motivation of the thesis.

Chapter 2 introduces the experimental setup and characterization methods of ZnO nanorods and the homojunctions.

Chapters 3 to 6 provide the experimental detail. Chapter 3 focuses on the growth of n-type ZnO nanorods on GaN substrates and post-treatment to improve electrical and optical properties of n-type ZnO nanorods.

Chapter 4 reports the successful growth of p-type ZnO by doping with potassium. The electrical and optical properties are also presented.

Chapter 5 introduces the growth of p-ZnO nanorods/n-GaN film LED by aqueous solution method. Electrical and optical properties of the heretojunction were studied and explained in this chapter.

Chapter 6 describes the fabrication of ZnO coaxial homojunction LED. The electrical and optical properties of this device are revealed. The degradation of ZnO homo-junction LEDs is also investigated.

Finally, chapter 7 summarizes and concludes the result and presents the directions for further work.

Chapter 2 Experimental setup and characterization methods

This chapter describes the experimental procedures and characterization methods of ZnO nanorods and ZnO LEDs that are fabricated in this research. This chapter comprises of four sections. In section 2.1, growth process, reactions and nucleation of ZnO nanorods in aqueous solution are introduced. In section 2.2, fabrication equipments used for fabrication of LED are described. LED fabrication equipments used are photolithography, e-beam evaporator and reactive ion etching (RIE). Section 2.3 describes characterization equipments used such are scanning electron microscopy (SEM), Raman, photoluminescence (PL) spectroscopy and I-V, C-V measurement devices. Finally, section 2.4 concludes the entire chapter.

2.1 Growth procedure

2.1.1 Aqueous solution growth procedure of ZnO nanorods

The experimental procedure for undoped ZnO nanorod growth is described in 3 steps. In the first step, aqueous growth solution was prepare as follows: A certain amount of zinc acetate $ZnCH_3COO_2$, here after denoted as $ZnAc_2$ was first dissolved in deionized water at room temperature. This is followed by the addition of a specific amount of ammonium hydroxide (NH_4OH), to give a pH 8 – 10. The resulting suspension was transferred into a glass bottle. In the second step, substrates are prepared. GaN substrate was cleaned with acetone, IPA and deionized water. For Si substrate, atfter cleaning, Si wafer was coated with ZnO nanoparticles by spin-coating method. In the third step, substrate was immersed in the solution. The substrate was suspended facing downward, away from the bottom of the bottle. The bottle

was sealed and put into the water bath which was kept at 90°C for one hour. Then, the sample was taken out, rinsed in DI water and dried to get ZnO nanorods formed on substrate [18, 51]. The water bath and bottle system used are as shown in Fig 2.1.

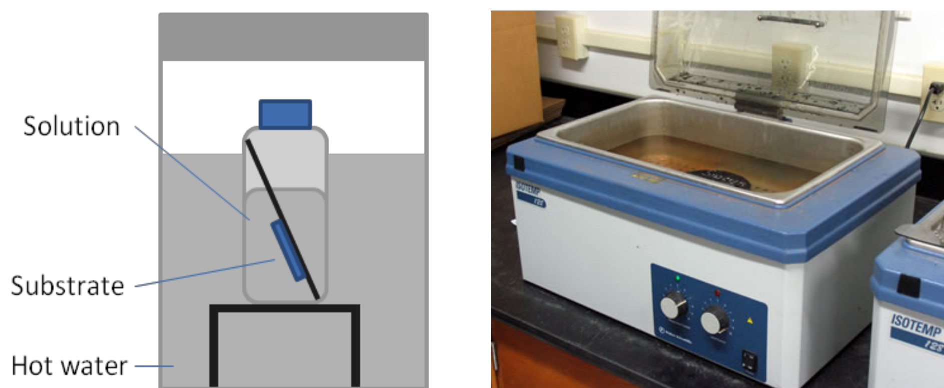

Fig 2.1 Schematic of ZnO growth by aqueous solution method

The process for doping ZnO nanorods on substrate is the similar to that described for growing undoped ZnO nanorods. To achive n-type doping ZnO, Ga and Al was doped. The growth solution was prepared with addition of $Ga(NO_3)_3$, and $AlCl_3$ respectively. To achieve p-type doping, an amount of potassium acetate (KAc) was added into growth solution. The concentration of doping was varied by changing concentration of doping salts.

2.1.2 Reactions of the solution growth

The growth of ZnO nanorods comprises of 2 steps. The first is hydrolysis of Zn^{2+} ions in aqueous solution. Second is condensation of the hydrolyzed zinc ions to form ZnO.

a) Hydrolysis of Zn^{2+} ions in aqueous solution

When $ZnAc_2$ and NH_4OH are mixed in an aqueous solution, the hydrolysis of $ZnAc_2$ and NH_4OH take place. Hydrolysis means the cleavage of chemical bonds by the addition of water. Generally, hydrolysis is a step in the degradation of a substance (source: Wikipedia).

In aqueous solution, Zn^{2+} ions are formed and solvated in solution:

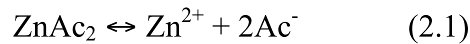

$$ZnAc_2 \leftrightarrow Zn^{2+} + 2Ac^- \qquad (2.1)$$

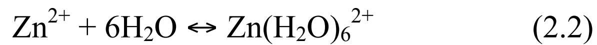

$$Zn^{2+} + 6H_2O \leftrightarrow Zn(H_2O)_6^{2+} \qquad (2.2)$$

In the hydrated Zn^{2+} ion, electrons from the oxygen of water molecules are drawn to the positive ions. The electron deficient oxygen in turn attracts electrons from the O-H bonds. This weakens the O-H bonds and makes it easier to break. In other word, the positively charged metal ion attracts the electrons away from the O-H bond, leading to the breakage of the O-H bond and release of the H^+ ion into the solution. This process is called hydrolysis of the hydrated Zn^{2+} ion and is schematically shown in Fig 2.2. In this figure, the cirle labeled M is Zn.

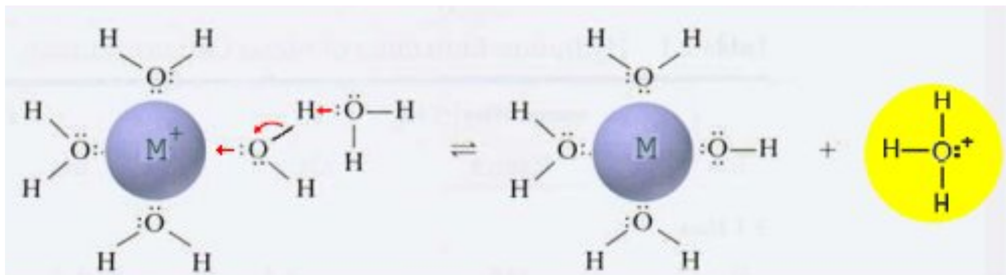

Fig 2.2 Hydrolysis of hydrated Zn^{2+} metal ions in aqueous solution. The circle labeled M is Zn. Taken form reference [20].

Hydrolysis of the hydrated zinc ion gives zinc hydroxide complexes:

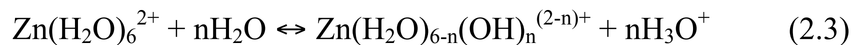

$$Zn(H_2O)_6^{2+} + nH_2O \leftrightarrow Zn(H_2O)_{6-n}(OH)_n^{(2-n)+} + nH_3O^+ \qquad (2.3)$$

Omit the water, we have the hydrolysis equations:

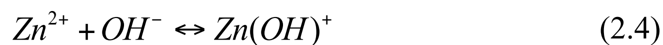

$$Zn^{2+} + OH^- \leftrightarrow Zn(OH)^+ \qquad (2.4)$$

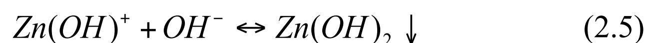

$$Zn(OH)^+ + OH^- \leftrightarrow Zn(OH)_2 \downarrow \qquad (2.5)$$

$$Zn(OH)_2 \downarrow \leftrightarrow Zn(OH)_2 \qquad (2.6)$$

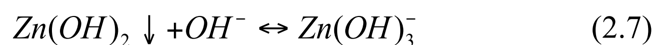

$$Zn(OH)_2 \downarrow + OH^- \leftrightarrow Zn(OH)_3^- \qquad (2.7)$$

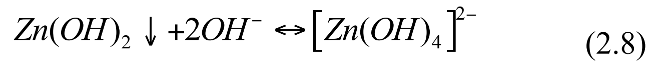

$$Zn(OH)_2 \downarrow +2OH^- \leftrightarrow \left[Zn(OH)_4\right]^{2-} \quad (2.8)$$

The species of zinc hydroxide complexes depend on pH of the aqueous solution. In order to determine the type and amount of species in the aqueous solution, the ionic equilibrium of the solution is computed. Fig 2.3 gives an example of the ionic equilibrium of the solution for Zn^{2+} in aqueous solution at 90°C [20]. In growth of ZnO nanorods, the pH of aqueous solution is in the range of 9 – 10. The dominant zinc hydroxide complex is $Zn(OH)_3^-$.

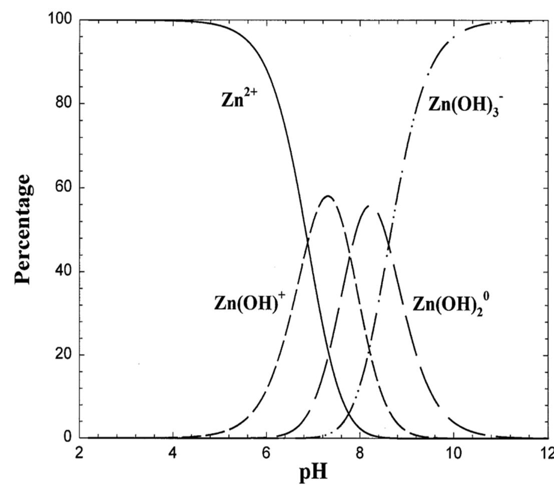

Fig 2.3 The ionic equilibrium of Zn^{2+} in aqueous solution at 90℃. Taken form reference [18].

b) Condensation of ZnO

The growth of ZnO after hydrolysis is the condensation of the hydrolyzed zinc ions [102]. The condensation reactions of ZnO can be olation and oxolation. In olation, an "ol" bridge is formed by a condensation reaction between a hydroxo- and aquo-species,

$$\text{Zn-OH} + \text{Zn-OH}_2 \rightarrow \text{Zn-OH-Zn} + H_2O \quad (2.9)$$

In oxolation, an "oxo" bridge is formed by the condensation reaction between two hydroxo-species:

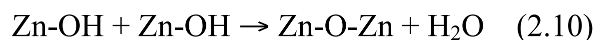

$$\text{Zn-OH} + \text{Zn-OH} \rightarrow \text{Zn-O-Zn} + H_2O \quad (2.10)$$

Equation (2.1 – 2.10) represents the typical hydrolysis and condensation reactions that lead to the growth of ZnO.

2.1.3 Effect of pH on ZnO surface

Fig 2.4 illustrates a typical model for adsorption on a hydrated ZnO surface [103]. In ZnO surface, the Zn^{2+} ion attracts H_2O molecule lead to adsorption of H_2O. Then, the Zn2+ ion weakens and breaks the O-H bond, leading to dissociation of H_2O molecule. Once water molecule loses its H^+ ion, another hydrated Zn^{2+} ion from the solution can be absorbed onto site OH^- that has dissociated, as shown in Fig 2.4. The pH of aqueous solution or concentration of H^+ ions controls the dissociation rate of H_2O molecules and OH^-. Therefore, the surface of ZnO, the overall charge can be net negative (OH^- is dominant), neutral or positive (Zn^{2+} is dominant), depending on pH of the growth solution. In acidic medium, the surface charge is positive while in basic medium, it is negative. There is a pH point where the ZnO surface is neutral. That point was called zero charge (PZC). The PZC for ZnO is in the pH range about 8.7 [104, 105].

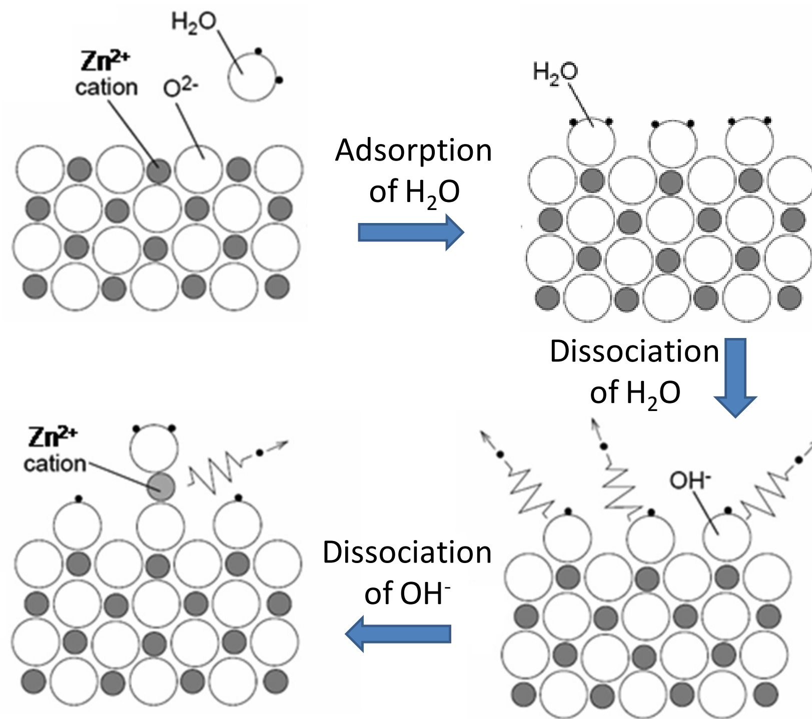

Fig 2.4 Model for adsorption of Zn^{2+} on ZnO surface. Taken form reference [20].

Effects of the pH of growth solution on adsorption of Zn^{2+} in the growth of ZnO are shown in Fig 2.5. It is clearly seen that, at high pH, ZnO grows fastest because there are more ready sites for adsorption due to ready dissociation of the OH^- ion than that of lower pH. The adsorption rate of Zn^{2+} is higher when the pH is higher than the PZC of ZnO. Therefore, higher pH of solution also results in higher growth rate of ZnO nanorods.

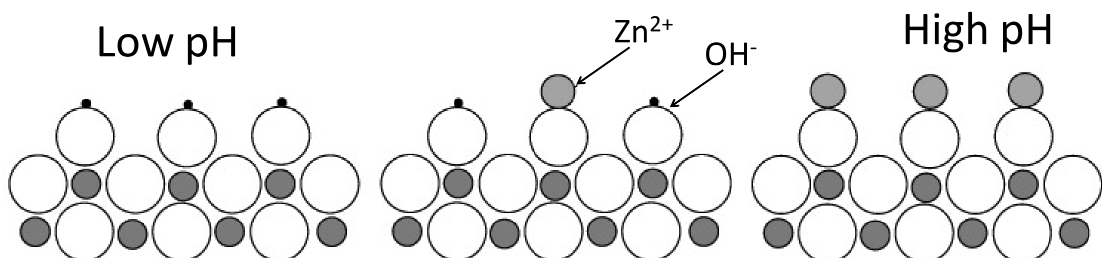

Fig 2.5 The dependence of adsorption of Zn^{2+} ions on the pH of the growth solution [20]

2.1.4 Nucleation and growth

The growth of ZnO nanorods on substrates includes: nucleation on the substrate and crystal growth.

a) Nucleation

The first stage of the growth of ZnO on substrates is nucleation when ions absorb in the substrates. Nucleation normally occurs at nucleation sites on surfaces contacting the aqueous solution. This is called heterogeneous nucleation (from Wikipedia). Upon adsorption, the contact area between the ions cluster and the solution is reduced. Smaller contact area reduces the surface energy between ions cluster and solution. However, there is interface energy between the ions and the substrate surface. Fortunately, the interface energy is usually less than surface energy between the ion cluster and the solution. As a result, surface adsorption reduces the critical energy for nucleation. Due to a lower energy barrier, heterogeneous nucleation can occur near equilibrium saturation conditions. Fig 2.6 shows the model of heterogeneous nucleation on a substrate surface.

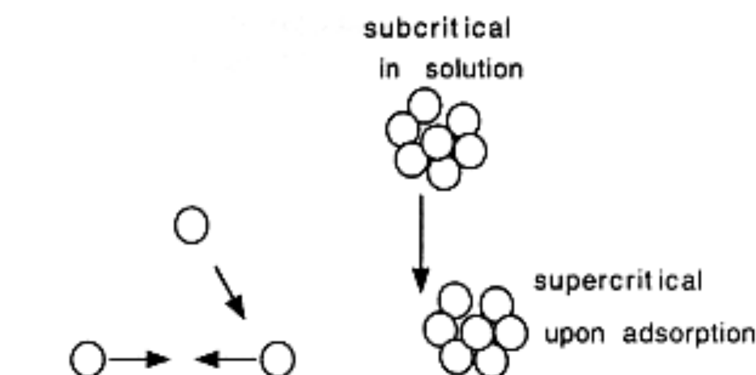

Fig 2.6 Processes involved in heterogeneous nucleation on a substrate surface. Taken from reference [20].

The interface energy between the ion cluster and the substrate surface depends on the morphology and material of the substrates. The rough surface of the substrate allows higher nucleation rate. Therefore, ZnO nanostructures tend to grow in the defect area of the substrates surface. In some cases, the density of ZnO nanostructures corresponds closely to defect density on the surface of the substrates.

Another factor affecting nucleation is the material of the substrates. Interface energy depends on lattice mismatch of ZnO and the substrate. In the case of GaN substrate, the lattice mismatch is 1.9%, which is relatively small. It is possible for ZnO to grow heterogeneously on GaN substrate. In case of ZnO growth on Si <100> substrate, the lattice mismatch is about -67%. The large tensile strain in ZnO leads to a high interface energy at the ZnO – Si interface. Therefore, the nucleation rates on Si <100> substrate are limited.

In 2001, Vayssieres et al. have overcome the difficulty in lattice mismatch to grown ZnO nanorods on high lattice mismatch substrates by applying a pre-coat of ZnO nanoparticles on the substrate surface [106]. The ZnO particles provide nucleation sites for ZnO to grow. Therefore, ZnO nanostructure can grow on various substrates such as Si, glass, plastic and sapphire. However, the ZnO particles layer is not in the same lattice direction with substrate. As a result, ZnO nanostructures grown on this substrate are not well aligning.

b) Crystal growth

For the growth of ZnO nanostructure or film in substrates, another energy we need to consider is strain energy that forming when ZnO growth thicker. The strain energy is depending on lattice mismatch between the

substrate and ZnO crystal. For example, the lattice mismatch between gallium nitride (GaN) and ZnO are 1.9%, which indicates that the ZnO film is slightly tensile on the GaN substrate. Due to the small mismatch, it is not surprising that ZnO can nucleate readily on GaN substrates in solution. However, ZnO are preferred grown in Volmer-Weber model in GaN substrate to form ZnO nanorods.

2.2 LED fabrication equipments

2.2.1 Dry ion etching (RIE)

In the LED fabrication process, we need to etch down the photo-resist with a controllable etching rate. The Oxford Plasma 80 RIE, a dry ion etching system was selected because it is an anisotropic etching method. The front view and principle of reactive-Ion Etching (RIE) was showed in Fig 2.7. RIE is an etching technology, which uses chemically reactive plasma to remove material deposited on wafers. The plasma is generated under low pressure by an electromagnetic field. High-energy ions from the plasma attack the surface and remove it.

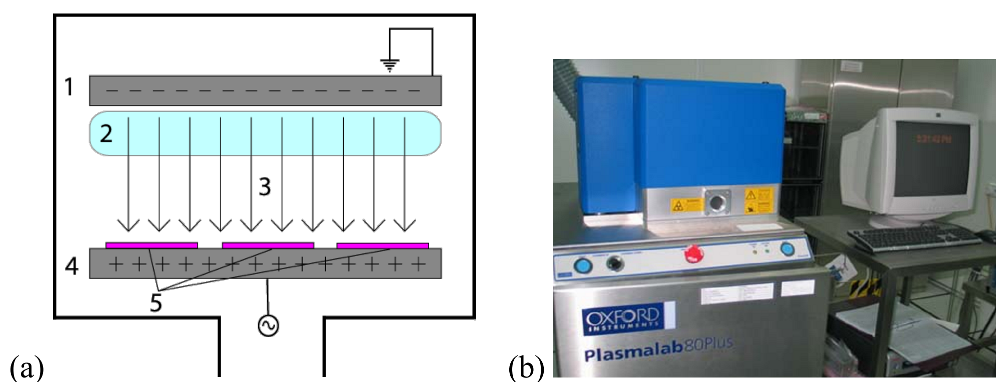

Fig 2.7 (a) A diagram of a RIE setup. An RIE consists of two electrodes (1 and 4) that create an electric field (3) meant to accelerate ions (2) toward the surface of the samples (5). (b)The front view of the Oxford Plasma 80 RIE system

The Oxford Plasma 80 RIE system consists of a cylindrical vacuum chamber, which use corrosion-resistant turbo-molecular pump to reach the expected vacuum. The lower electrode in the bottom portion of the chamber is graphite electrode using He cooling. The wafer platter is electrically isolated from the rest of the chamber, which is usually grounded. In the etching process of photoresist, oxygen was used to generate oxygen plasma.

2.2.2 *Photolithography*

Photolithography is a process used in LED fabrication process. It uses light to transfer a geometric pattern from a photo-resist on the substrate. The system we used in this thesis is SUSS Mask Aligner MA 10. Fig 2.8 shows an example of sample patterned by photolithography and front view of the SUSS MA 10.

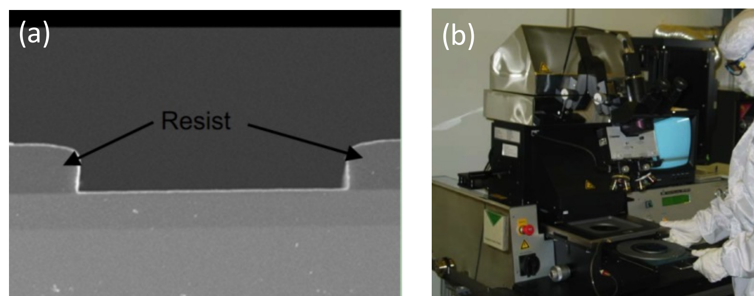

Fig 2.8 an example of pattern sample using AZ 5214 (a) and front view of the SUSS Mask Aligner system (b).

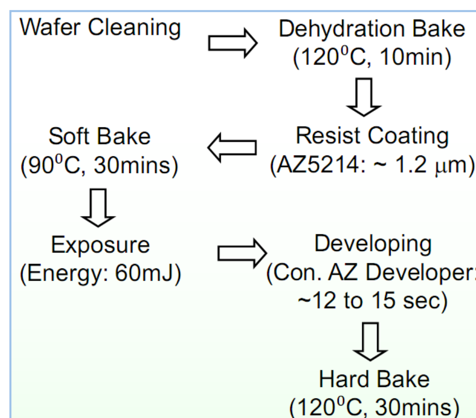

Fig 2.9 Typical Process Recipe of the SUSS Mask aligner

The process of photolithography combines six steps in sequence as shown in Fig 2.9.

2.2.3 E-beam evaporators

In the LED fabrication process, we need evaporate thin metal layers such as Au, Ti for forming n- and p- contacts. The equipment used is Auto306 E-beam Evaporation System, which is shown in Fig 2.10. The principle of method is followed: An electrical current is passed through a tungsten filament, which emits electrons. Then, electron beam is bent and focused into the crucible by magnetic forces (Fig 2.10). Under the heat of the electron beam, metal in crucible is melted and vaporized. Then, metal vapor travel in all direction and condenses on the substrate. In the process, the pressure of chamber is remained under $3.0\text{x}10^{-6}$ mbar and substrate temperature during evaporation is under 100°C.

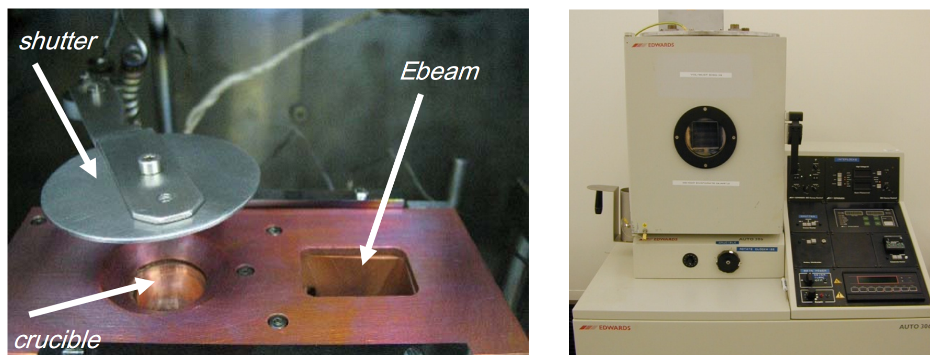

Fig 2.10 Electron beam source and Edwards Auto306 E-beam evaporation system

2.3 Characterization techniques

The growth method described earlier was used to grow ZnO nanostructures. In this work, the structural, optical and electrons transport properties of the resulting structures are examined using field-emission scanning electron microscopy, micro-photoluminescence spectroscopy, micro-

Raman spectroscopy and Hall measurement. In the following sections, some background theory on the characterization method as well as relevant ZnO-related characterization results will be presented. This information will serve as the foundation for understanding the experimental results that will be discussed in Chapters 3 through 6 of the thesis.

2.3.1 Microscope

a) Scan electron microscope (SEM)

The scan electron microscope was used to investigate the morphology of ZnO nanorods. The system used is JEOL FESEM 6700 which can obtain high resolution image of the samples. The resolution of the JEOL 6700 can be 2.2 nm and magnification can vary from 25 to 650,000. Fig 2.11 shows the picture of the JEOL FESEM 6700 system. The information about the sample obtained by SEM includes morphology, crystalline structure and orientation of materials making up the sample.

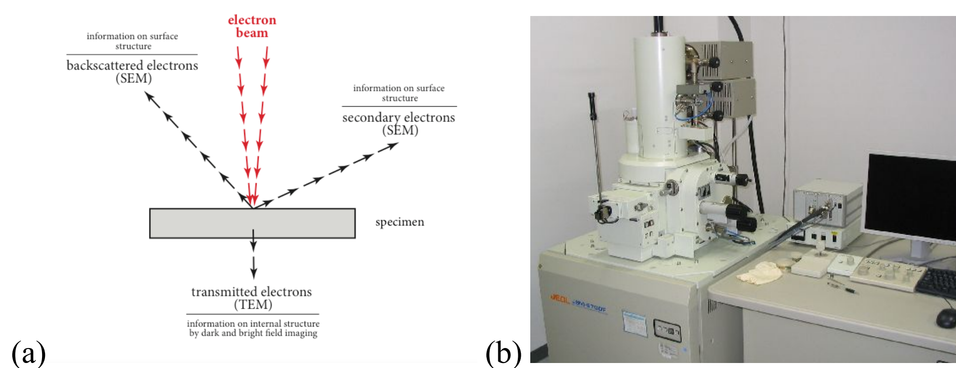

Fig 2.11 (a) Electron beam in SEM and (b) the *JEOL FESEM 6700 system in IMRE*

b) Transmission electron microscope (TEM)

In order to investigate the crystal structure of ZnO nanorods, we used a HR-TEM system model JEOL 2000V as shown in Fig 2.12. In this system, the based pressure is ultra-high to investigate the sample while eliminating

contamination effects. The electron acceleration voltage: 200 KeV and lattice resolution is 0.21 nm. In principle, the transmission electron microscope uses a high-energy electron beam transmitted through a very thin sample to image and analyze the microstructure of materials with atomic scale resolution. The electrons are focused with electromagnetic lenses. TEM measurement gives the information about the morphology, crystal phases, and defects in a material.

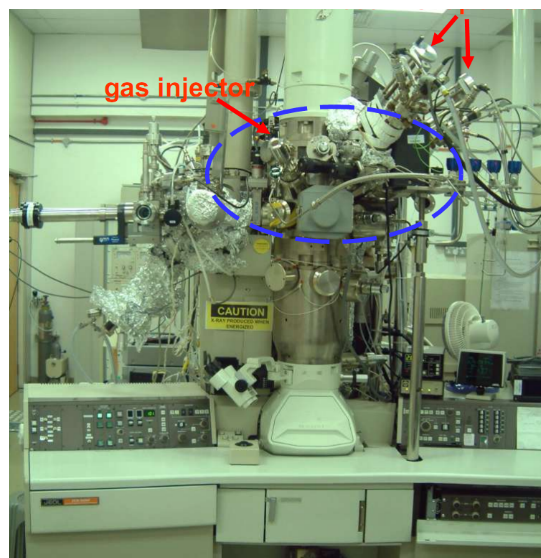

Fig 2.12 Front view of JEOL 2000V TEM system

2.3.2 Photoluminescence (PL) and electroluminescence (EL)

a) Photoluminescence

Photoluminescence is an important technique for measuring the purity and crystalline quality of semiconductors. In this thesis, we used the Renishaw 2000 Raman/PL microscope system to measure the PL of ZnO. The front view of the PL system is in Fig 2.13. PL is a process in which a substance absorbs photons (electromagnetic radiation) and then re-radiates photons. Quantum mechanically, this can be described as an excitation to a higher energy state and then a return to a lower energy state accompanied by the emission of a

photon. This is one of many forms of luminescence (light emission) and is distinguished by photo-excitation. The period between absorption and emission is typically extremely short, in the order of 10 nanoseconds.

In order to measure the photoluminescence of ZnO at low temperature, we set up a cooling system to tune the temperature from 15K to 300K. The cooling system can put below the microscope of the Renishaw 2000 to measure samples at low temperature.

Fig 2.13 Renishaw 2000 Raman/PL microscope set up

b) Electroluminescence (EL) system

Electroluminescence (EL) is a key factor to measure operation of LED. EL is obtained by measure the light emitted from a p-n junction under an electric current. The set up using in this work is shown in Fig 2.14. In principle, electroluminescence is the result of radiative recombination of electrons and holes in a semiconductor. The excited electrons release their energy as photons - light. The semiconductor material device to form a p-n junction device can be LEDs or laser.

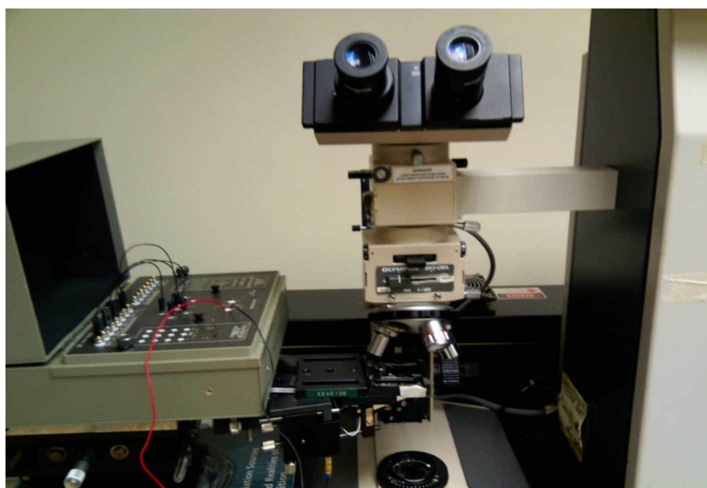

Fig 2.14 the electroluminescence measurement by probe under photo-detector

2.3.3 X-ray photo-electron spectroscopy (XPS) and Secondary Ion Mass Spectrometry (SIMS)

a) *X-ray photo-electron spectroscopy (XPS)*

To investigate the composition and electronic state of ZnO, XPS measurement was conducted. The system used is ESCALab 250i-XL & Thetaprobe A1333 in Institute of Material Research and Engineering (IMRE). Principle of XPS was shown in Fig 2.15. In this system, the temperature of sample can vary from 30°C to 600°C. This XPS is able to achieve high-energy resolution. Spectroscopy provides quantitative information on composition, chemical states and functional groups over a range of analysis areas (~20 μm to several mm).

In principle, XPS uses soft x-rays to examine core-levels of material. In XPS, the photon is absorbed by an atom in a molecule or solid, leading to ionization and the emission of a core (inner shell) electron. These electrons were called photoelectrons. The kinetic energy distribution of the emitted photoelectrons can be measured using an electron energy analyser and a photoelectron spectrum can thus be recorded. From energy of these

photoelectrons, binding energies (BE) of energy levels in solids is calculated to have information about the materials.

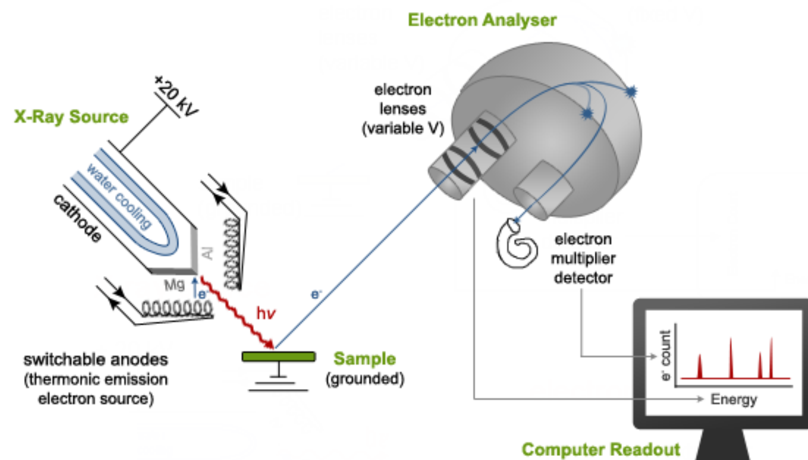

Fig 2.15 Principle of XPS analysis system

b) Time-of-Flight Secondary Ion Mass Spectrometry (TOF-SIMS)

Chemical composition of ZnO can be analysed by SIMS to compare against that of XPS. In addition, SIMS is a more sensitive method than XPS. SIMS can do a depth profile and determine the distribution of chemical species of ZnO. SIMS uses a pulsed primary ion beam to desorbs and ionize atoms and molecules from the surface of a sample. The resulting secondary ions are accelerated into a mass spectrometer, which measures their “time-of-flight” from the sample to the detector to determine the mass of the ions. Because each element has its own mass, analysis of the mass spectrum allows us to determine what elements are in the sample. The schematic diagram of the SIMS process was shown in Fig 2.16.

Depth Profiling of SIMS is conducted using the dual beam technique - one high current beam for sputtering and the other pulsed beam for mass analysis - allows measurement of depth profiles. Depth resolution around 1

nm can be obtained. Analysis beam is Ga^+ ion beam and sputtering beam is Ar^+ ion beam.

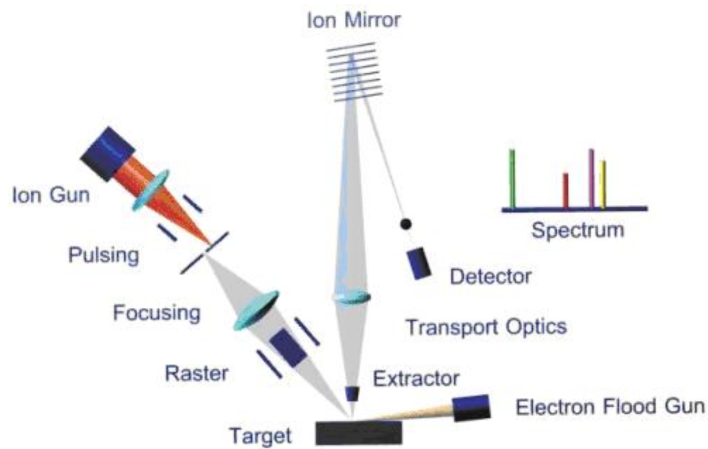

Fig 2.16 Schematic diagram of the SIMS process

2.3.4 Current – voltage (I-V) and capacitance-voltage (C-V) measurement

The I-V and C-V measurements are conducted on probe station using HP 4156A to measure I-V and C-V, shown in Fig 2.17.

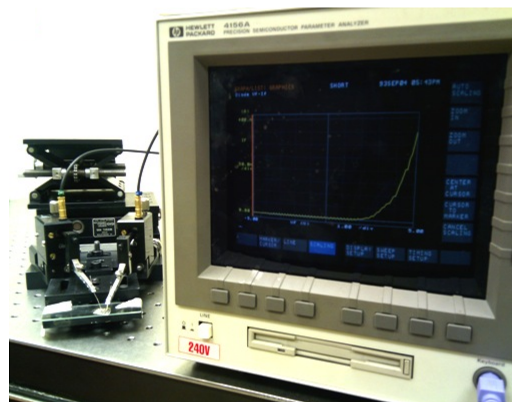

Fig 2.17 set up of I-V and C-V measurement system

2.4 Conclusions

This chapter describes the experimental procedures of ZnO nanorods and characterization equipment of ZnO nanorod and ZnO LED. The growth process of ZnO in solution, which includes hydrolysis and condensation, are shown. The reactions in the solution, effect of pH on growth of ZnO are part

of this chapter. The nucleation and growth of ZnO nanorods are also explained. Another main part of the chapter is introducing LED fabrication equipments and characterization equipments. The principle and set up of RIE, photolithography and e-beam evaporator are introduced. Characterization techniques used are SEM, TEM, XPS, and SIMS. The background and set up of these equipments as well as its relevant ZnO-related characterization results are presented.

Chapter 3 Optimization of the growth and post-treatment of n-ZnO nanorods

Unintentionally doped ZnO typically display n-type conductivity because of the defects which act as donors. These donors consist of zinc vacancies, oxygen interstitials or hydrogen interstitials. However, incorporation of extrinsic donors through intentional doping is still needed to achieve stable and high concentrations of free electrons in n-type ZnO. Donor dopants can be group III elements such as Al and Ga. This chapter describes the growth, optimization and post-treatment of two types of ZnO nanorods that were grown in aqueous solution. The first type of ZnO nanorods was unintentionally-doped, while the second type had been intentionally doped with group III element dopants such as Ga and Al. The morphology, crystal structure and photoluminescence of these nanorods were measured and analysed.

3.1. Morphology of n-type ZnO nanorods

3.1.1 n-type ZnO nanorods growth precursor

The growth process of the undoped ZnO nanorods has been described in Chapter 2. The growth parameters are the solution chemistry, growth temperature and growth duration. The effects of growth temperature and duration on morphology of ZnO nanorods have been reported [18, 19, 107]. In this work, we set the growth temperature duration at 90°C and 1 hour, the optimized value in the references. The solution chemistry was varied by changing relative concentrations of $ZnAc_2$, NH_4OH and dopant salt such as $Ga(NO_3)_3$ and $AlCl_3$ in the aqueous solution. The concentration of $ZnAc_2$ and NH_4OH was varied in the range 0.1 ~ 0.3 M and 0.16 ~ 0.54 M respectively.

The dopant salts $Ga(NO_3)_3$ and $AlCl_3$ were varied from 0.02 ~ 0.20 mM and 5 ~ 10 mM respectively.

3.1.2 Morphology of undoped ZnO nanorods

a) Morphology of undoped ZnO nanorods at difference pH of the growth precursor

As described in Chapter 2, the solubility of ZnO in the growth solution depends on the pH of the solution, and determines the morphology and density of ZnO nanorods. Higher NH_4OH concentrations increases the pH and solubility leading to nanorods with larger diameters, longer lengths and lower rod density [18]. SEM images of ZnO nanorods grown at different concentrations of NH_4OH, namely 0.18, 0.36 and 0.54 M, are shown in Figs 3.1 (a), (b) and (c) respectively. Generally, the nanorods were vertically-oriented relative to the GaN substrate with a preferential growth direction along the c-axis. Furthermore, they were single crystalline with hexagonal cross-sections.

As predicted, Figs 3.1 (a - c) show that the increasing concentration of NH_4OH from 0.18 to 0.54 M led to the increase of average nanorod length and diameter from 1.0 to 3.0 μm, and from 120 to 150 nm respectively while the area density decreases from 2.5×10^9 to 1.1×10^9 cm^{-2}.

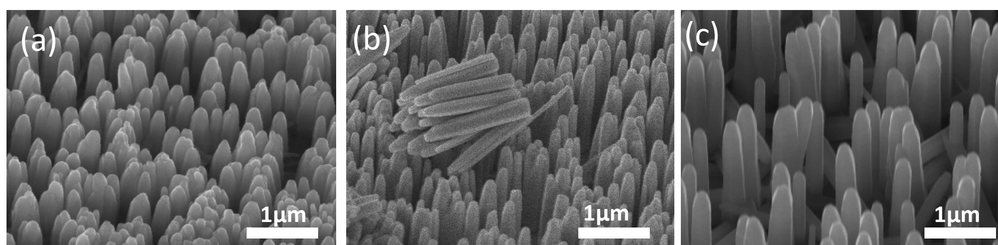

Fig 3.1. SEM images of undoped ZnO nanorods grown at (a) 0.18, (b) 0.36 M and (c) 0.54 M NH_4OH. The concentration of $ZnAc_2$, growth temperature and duration were kept constant at 0.01 M, 90°C and 1 h respectively.

b) Morphology of undoped ZnO nanorods at different Zn^{2+} concentration

The SEM images of ZnO nanorods grown in the solution with $ZnAc_2$ concentrations of 0.01, 0.02 and 0.03 M are shown in Figs 3.2 (a), (b) and (c) respectively. As the concentration of $ZnAc_2$ increases from 0.01 to 0.03 M, the diameters of the nanorods remains relatively unchanged while the density increases, leading a transition from isolated nanorods in Fig 3.2 (a) to merged columnar films in Fig 3.2 (c). This can be understood through the effect of $ZnAc_2$ on the solubility of Zn. As more $ZnAc_2$ is added into the solution, the solubility of Zn decreases leading to a higher driving force for nucleation and thus a higher density of nanorods. In fact, continuous columnar ZnO films has been grown using this approach by using a high concentration of $ZnAc_2$ and a longer growth duration by means of multiple growth cycles as shown in our earlier work [50].

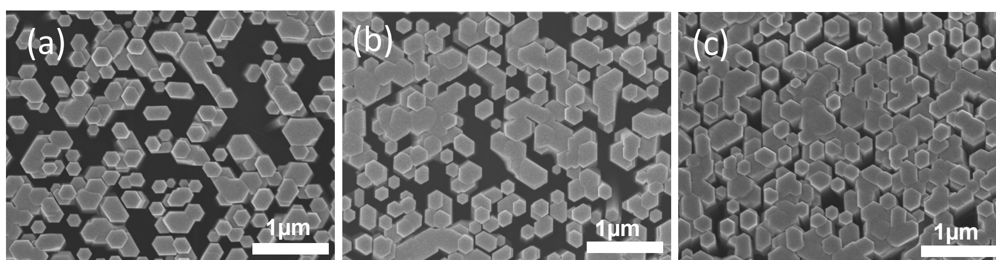

Fig 3.2 SEM images showing the morphology and area density of undoped ZnO nanorods for (a) 0.01, (b) 0.02 and (c) 0.03 M of $ZnAc_2$. The concentration of NH_4OH, growth temperature and duration were kept constant at 0.37 M respectively.

3.1.3 Morphology of ZnO nanorods doped with Ga and Al

Extrinsic doping using group III elements are important for achieving stable and high levels of electron concentration in n-type ZnO. The introduction of dopant salts in the growth solution will lead to the competition of surface adsorption between the primary growth cation Zn^{2+} and the secondary dopant cations such as Ga^{3+} and Al^{3+}. As such, the concentration of

dopant salts is expected to affect the growth rates and morphology of ZnO nanorods.

a) Morphology of Ga doped ZnO nanorods

In this work, the $Ga(NO_3)_3$ salt was used as the Ga dopant source. In order to investigate the effect of $Ga(NO_3)_3$, three different concentrations were used: 0, 0.02, 0.08 and 0.20 mM $Ga(NO_3)_3$. The concentration of $ZnAc_2$, NH_4OH, growth temperature and duration was kept constant at 0.01 M, 0.37 M, 90°C and 1 h respectively. Growth was carried out using Si substrates that were precoated with a layer of ZnO nanoparticles.

Figs 3.3 (a-f) show the SEM images of the morphology of ZnO nanorods under doping with Ga. The SEM images show that $Ga(NO_3)_3$ has a strong effect on the morphology of ZnO. With 0.02 mM of $Ga(NO_3)_3$, the morphology of ZnO nanorods do not change in comparison with undoped ZnO. At higher concentrations of $Ga(NO_3)_3$, significant change in the morphology of ZnO was observed. Above 0.08 mM $Ga(NO_3)_3$, the nanorods merged to form a continuous film with grain boundaries clearly visible. At 0.20 mM $Ga(NO_3)_3$, hexagonal plates were observed covering the top surface of the film. These figures highlight the importance of keeping the concentration of $Ga(NO_3)_3$ needs to be kept below 0.08mM $Ga(NO_3)_3$ to avoid coalescence and formation of continuous films. Also apparent from the cross-sectional SEM images shown in the Figs 3.3 (e-f) are the reduction in the thickness of the films and the relatively constant rod diameters with increasing amount of $Ga(NO_3)_3$.

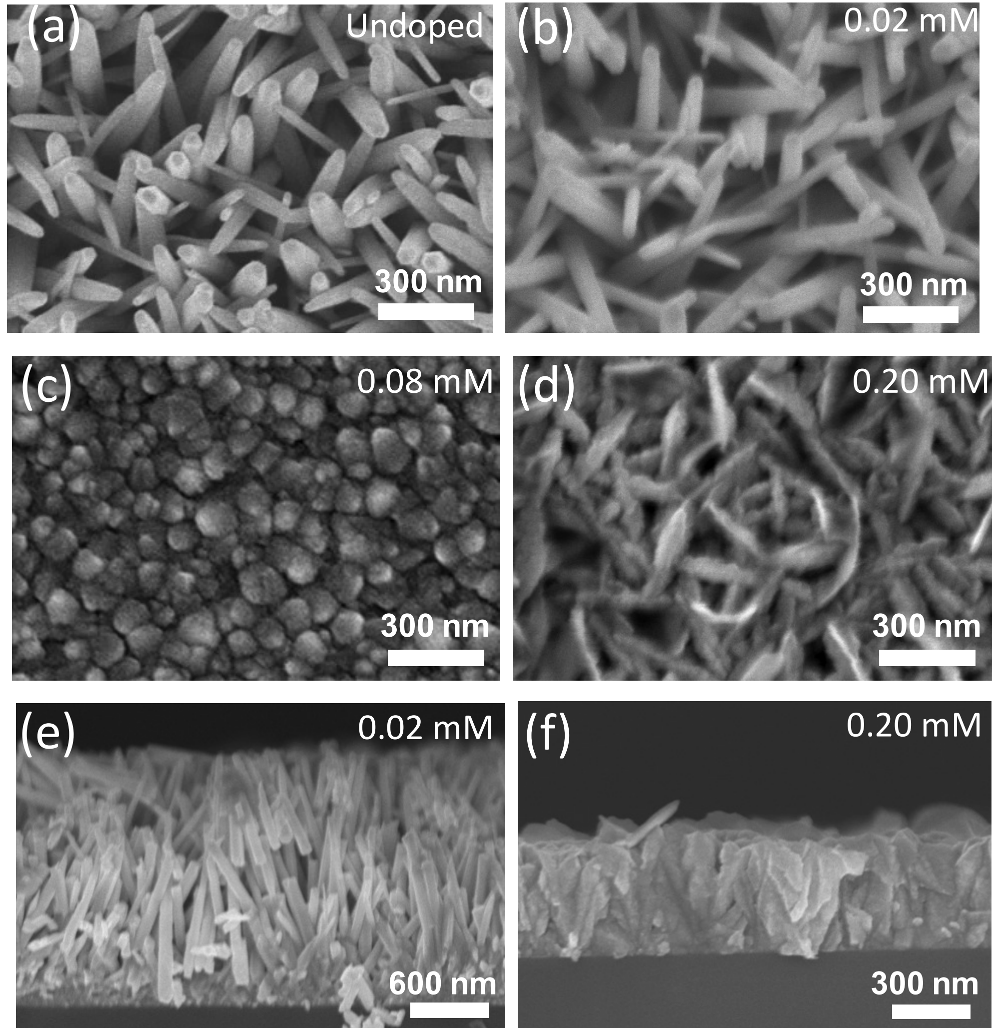

Fig 3.3 Morphology of ZnO:Ga using (a) 0, (b) 0.02, (c) 0.08 and (d) 0.20 mM $Ga(NO_3)_3$. The concentration of $ZnAc_2$, NH_4OH, growth temperature and duration are kept constant at 0.01 M, 0.37 M, 90℃ and 1h. Cross-sectional SEM images of corresponding ZnO:Ga using (e) 0.02 mM and (f) 0.20mM.

To further understand the role of $Ga(NO_3)_3$ in determining the morphology of nanorods, the concentration of NH_4OH was varied from 0.18 to 0.55 M while the concentration of $Ga(NO_3)_3$ was kept constant at 0.08 mM to ensure no formation of films. Other growth parameters such as the concentration of $ZnAc_2$, growth temperature and duration were kept constant 0.01 M, 90°C and 1 h respectively. In order to study the effect of $Ga(NO_3)_3$ concentration on the density of nanorods, a lattice-matched GaN epilayer on sapphire was chosen. By using a lattice-matched GaN as a growth template, a

well-aligned array of nanorods can be obtained. Compared to the randomly oriented nanorods on Si substrates as shown in Fig 3.3 (a), the well-aligned array of nanorods on GaN allows more accurate evaluation of the area density. Fig 3.4 shows the SEM images of the ZnO:Ga nanorods that were grown in (a) 0.18, (b) 0.37 and (c) 0.55 M NH_4OH. As the concentration of NH_4OH increases, the diameter and length of nanorods increases. This is in agreement with our understanding of the effect of solubility of Zn on the diameter and lengths of nanorods. However, it is observed the area density increases from 0.18 to 0.37 M and then decreases at 0.54 M NH_4OH. It is unclear at this moment why the area density increases before decreasing.

Furthermore, in Fig 3.4 (a-c), layer-by-layer growth was clearly seen as indicated by black arrows in the figures. It appears that the addition of $Ga(NO_3)_3$ salt encourages lateral growth which implies that it may be naturally easy to obtain smooth n-type ZnO films by doping with Ga.

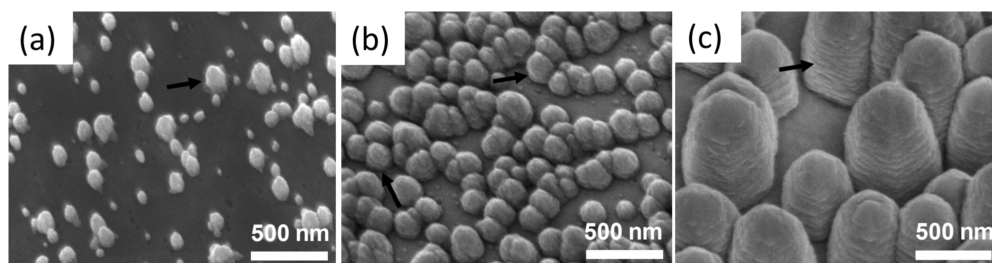

Fig 3.4 Effect of doping $Ga(NO_3)_3$ on the morphology of ZnO grown on GaN substrate with (a) 0.18 M NH_4OH, (b) 0.37 M NH_4OH, and (c) 0.54 M NH_4OH.

b) Morphology of Al doped ZnO nanorods

Another important n-type dopant is aluminum (Al). To study the effect of Al doping in ZnO, $AlCl_3$ salt was used as the dopant source. Two different concentrations of $AlCl_3$ were used: 5 and 10 mM. Growth was carried out on pre-coated silicon substrates at 90°C for 1 h with $ZnAc_2$ and NH_4OH

concentrations maintained at 0.01 M and 0.37 M respectively. Figs 3.5 (a-c) show the cross-sectional SEM images of the samples grown in 0, 5 and 10 mM of $AlCl_3$, respectively. These figures show the same trend for rod lengths as observed in the case of $Ga(NO_3)_3$ whereby higher concentrations of dopant salts, either $Ga(NO_3)_3$ or $AlCl_3$, lead to shorter rod lengths from 3.2 µm for un-doped ZnO nanorods to 2.0 µm at 0.10 M $AlCl_3$. However, in the case of $AlCl_3$, the rod diameters showed a clear reduction with increasing concentrations of $AlCl_3$. The reduction in diameter is larger than the reduction in length, leading to sharply higher aspect ratios of the nanorods.

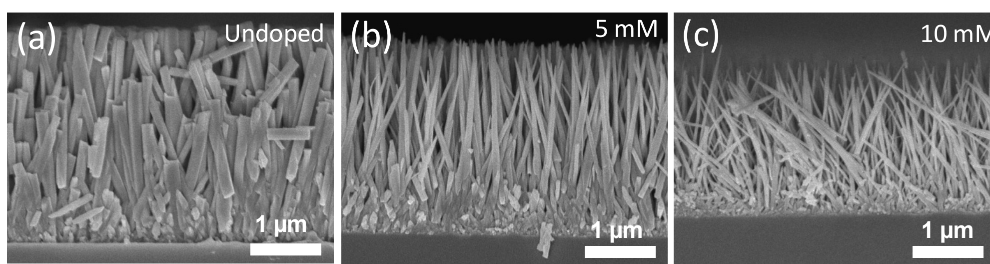

Fig 3.5 Morphology of ZnO:Al nanorods grown with (a) 0, (b) 5 and (c) 10 mM $AlCl_3$. The concentrations of $ZnAc_2$, NH_4OH, growth temperatures and durations were kept constant at 0.1 M, 0.37 M, 90°C and 1 h respectively.

To study the effect of pH variation, the concentration of NH_4OH was increased from 0.18 to 0.55 M, while the other parameters were kept constant at 0.01 M $ZnAc_2$, 5mM $AlCl_3$, 90°C and 1 h. Fig 3.6 (a-c) shows the cross-sectional view of the nanorods grown with 0.18, 0.37 and 0.55 M NH_4OH respectively. In general, the length and radius of ZnO:Al nanorods increased with the pH of the solution, in agreement with the solubility of Zn as the main driver of growth.

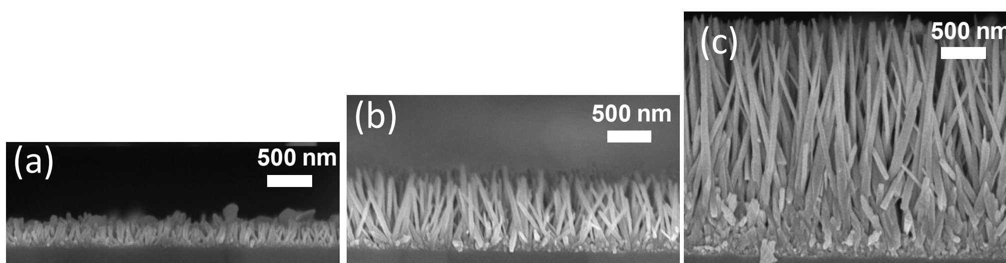

Fig 3.6 Cross-sectional SEM images of ZnO nanorods grown with (a) 0.18 M, (b) 0.37 M and (c) 0.55 M NH_4OH. The concentrations of $ZnAc_2$, $AlCl_3$, growth temperatures and durations were kept constant at 0.01M, 5 mM, 90°C and 1 h.

3.1.4 Discussion on Growth Habit of Ga and Al-doped ZnO Nanorods

In the presence of dopant salts, a clear change in the nanorod morphology was observed. In general, higher dopant salt concentrations lead to shorter rod lengths. Two different behaviour was observed for lateral growth: higher $AlCl_3$ concentrations produced narrower rods while $Ga(NO_3)_3$ did not produce any significant change in the nanorod diameters. These observations are summarized in the schematic shown in Fig 3.7.

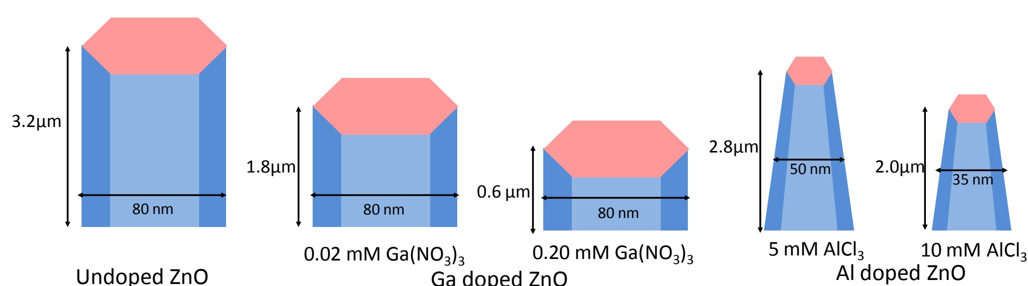

Fig 3.7 Schematic diagram summarizing the changes in ZnO growth habit in the presence of varying concentrations of $Ga(NO_3)_3$ and $AlCl_3$ dopant salts.

These changes in the growth habit can be easily understood by the competitive adsorption of the various ionic species onto the growth surfaces. The following discussion on the changes in the growth habit will be carried out with the aid of the schematic diagram shown in Fig 3.8. Adsorption is determined by two factors: the charges on the hydrated ZnO surface as well as the population of charged species in the solution.

In pH range where growth was carried out, the hydrated surfaces of ZnO are expected to carry a net negative charge because the adsorped water molecules readily hydrolyze when the pH is greater than the PZC of ZnO, as explained earlier in Chapter 2. However, for the top surface of the nanorods, the larger positive charge contribution from polar c-face of ZnO leads to an overall positive charge.

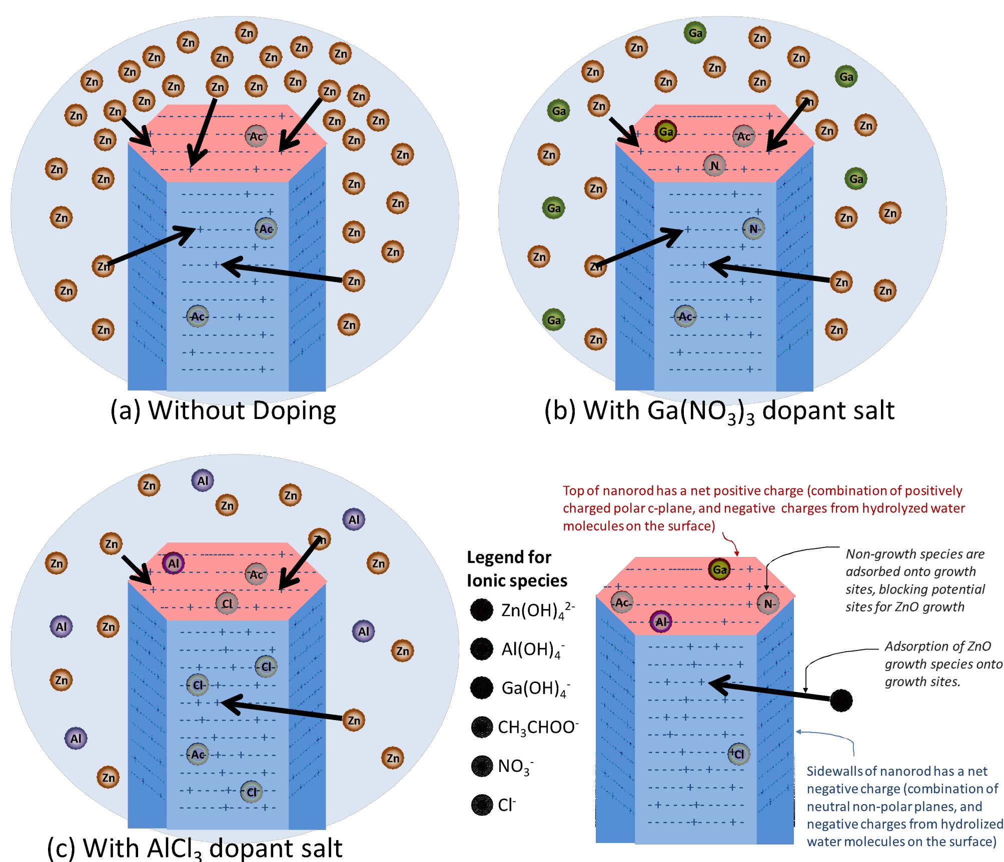

Fig 3.8 Schematic diagram summarizing the factors affecting the growth habit of ZnO in the presence of $Ga(NO_3)_3$ and $AlCl_3$ dopant salts.

The major species in this pH range were $Zn(OH)_4^{2-}$ for the growth solution without any dopant salts. The negatively charged $Zn(OH)_4^{2-}$ were attracted to the positively charged top surface and led to the formation of nanorods in the c-axis direction. Upon addition and ionization of dopant salts such as $Ga(NO_3)_3$, thermodynamics dictate that the dominant Ga ionic species will be the negatively charged $Ga(OH)_4^-$ and NO_3^- [108]. Implicitly, charge

balance of ionic species in the solution will require a reduction in the concentration of $Zn(OH)_4^{2-}$. As a result, two main implications on the growth rate occured with the addition of dopant salts:

- Firstly, the reduced concentration of $Zn(OH)_4^{2-}$ led to a lower driving force of nucleation, and thus a slower growth rate.
- Secondly, the negatively charged dopant species, $Ga(OH)_4^-$ and NO_3^-, preferentially adsorbed onto the positively charged top surface of the nanorods. This impeded the adsorption of $Zn(OH)_4^{2-}$ and further reduced the growth rate in the c-axis direction.

Using this understanding, it is easy to see that higher concentations of $Ga(NO_3)_3$ led to further reduction of growth species $Zn(OH)_4^{2-}$ and increased adsorption of dopant species onto the top c-plane which produced even shorter rod lengths. On the other hand, the negatively charged $Ga(OH)_4^-$ and NO_3^- species, regardless of their concentrations, are not expected to adsorp onto the negatively charged sidewalls, and as such, the diameters of the nanorods appear unaffected by increasing concentrations of dopant salts.

Although this model explains the reduction the possible reason for narrower ZnO nanorods under effects of $AlCl_3$ is due to effect of Cl^- ions on the growth of ZnO nanorods in solution. In the growth of ZnO nanorods, the surface charges effect the growth of ZnO nanorods. In undoped ZnO nanorods growth, surface charges are Zn^+ which control the growth of ZnO in sideway or front-way. In this case, Cl^- is an anion which block the growth of ZnO in side-way which result in narrower the tip of the ZnO nanorods. This

phenomenon is also block the growth of ZnO, which shorten the ZnO nanorods as shown in Fig 3.5.

3.2. Characterization of undoped ZnO nanorods

In the section 3.1, morphology of n-type ZnO nanorods were studied to show that the ZnO nanorods doped with Ga are coalesced to form a film structure while the ZnO nanorods doped with Al are short and small at the tip. In term of morphology, un-doped ZnO nanorods are the best choice for nanorod LED fabrication. Moreover, electron concentration of undoped ZnO measured using Hall effect is $5x10^{17}cm^{-3}$. Therefore, undoped ZnO nanorods will be used for ZnO nanorods core-shell homojunction LED in the Chapter 6. This section characterizes the undoped ZnO nanorods to see their structural, composition and optical properties.

3.2.1 X-Ray Diffraction analysis

Fig 3.9 shows the XRD spectrum from ZnO nanorods grown on GaN epilayers in aqueous solution consisting of 0.01 M $ZnAc_2$ and 0.37 M NH_4OH at 90°C for 1 h. The corresponding SEM image of the nanorods can be seen in Fig 3.2 (a). The XRD spectrum in Fig 3.9 is typical of nanorods grown on GaN epilayers, whereby three main peaks are located at 34.34°, 42.56° and 72.56°. The peaks at 34.34° and 72.56° can be indexed to the (002) and (004) surfaces of ZnO while the final peak at 42.56° belongs to the underlying sapphire substrate. The (002) peak position is close to that of the standard bulk ZnO peak at 34.36°, suggesting that the nanorods have little, or no strain, in their structure. This is not surprising because interface area between ZnO and GaN is very small, and strain is able to relax along the direction of the rod.

The FMHM of the (002) ZnO peak is 0.3°, which confirms the high crystallinity of the nanorods. These results suggest that high quality single crystal ZnO nanorods can be produced at very low cost using aqueous solution routes for high performance applications.

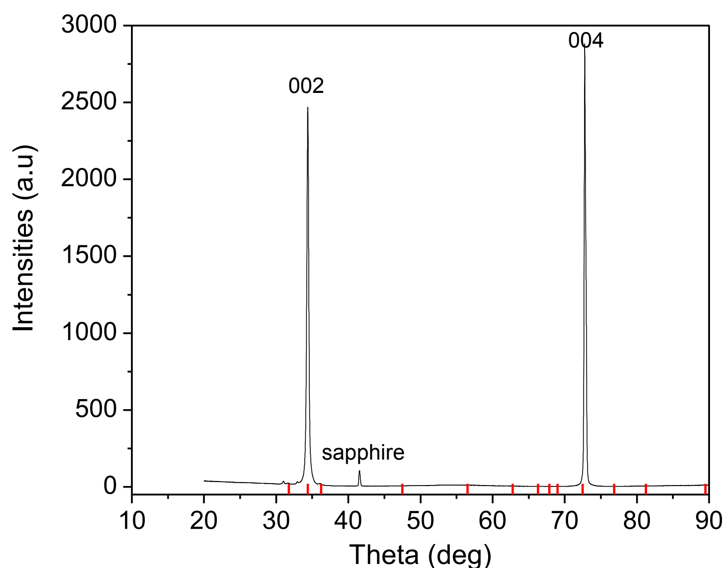

Fig 3.9 XRD of ZnO nanorods growth on GaN substrate. The growth condition is 0.01M ZnAc, 0.37 M NH_4OH. The red lines are standard position of ZnO bulk.

3.2.2 Transmission electron microscope (TEM) measurement

The lattice structure of ZnO nanorods has been studied using TEM. Fig 3.10 (a) and (b) shows the low and high resolution TEM images of ZnO nanorods respectively. In the low-resolution image, two ZnO nanorods, with lengths of about 2.7 µm, can be seen. Under high-resolution imaging, the lattice structure of ZnO can be observed very clearly. In ZnO lattice, since the oxygen (O) atom is much bigger than zinc (Zn), the oxygen atoms can be clearly observed. The lattice plane distance is about 0.51 nm. This is well within the reported figures in literature range from 5.0 to 5.2 nm [21, 109]. No obvious defects were observed, thus implying that the undoped ZnO nanorods have high crystal quality.

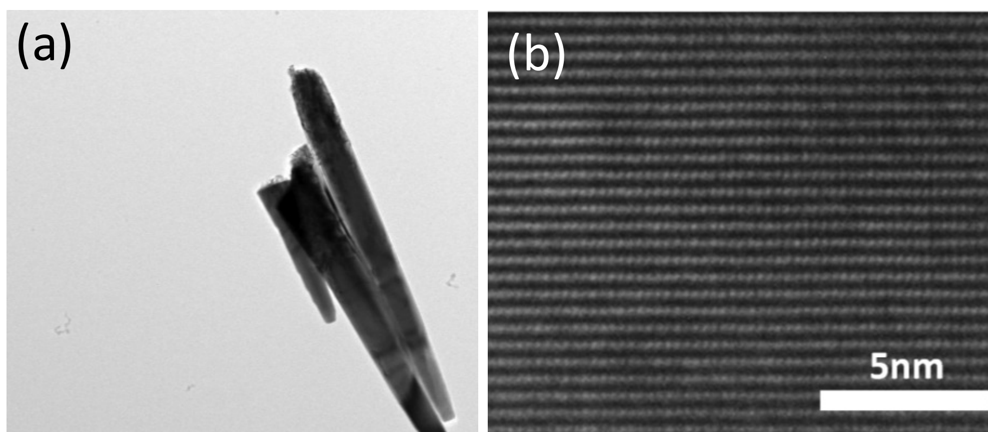

Fig 3.10 The (a) low and (b) high resolution TEM images of ZnO nanorods grown in the solution consisting of 0.01 M $ZnAc_2$, 0.37 M NH_4OH at 90℃ for 1 h.

3.2.3 SIMS analysis

The composition of ZnO nanorods was studing using ToF-SIMS. The nanorods were grown in 0.01 M $ZnAc_2$, 0.36 M NH_4OH at 90°C for 1 h. A high current Ga ion beam was employed to sputter the ZnO material while a low current Ar ion beam was used to perform analysis. Fig 3.11 shows the depth profile of Zn, O, Ga, N and K atoms in the sample. The ZnO nanorods appear to be completely removed after 900 s. During the first 900 s, the concentrations of Zn and O remain relatively constant, implying a stable Zn/O stoichiometry. In particular, the absence of impurities such as potassium shows that very pure ZnO nanostructures can be grown using the aqueous solution method.

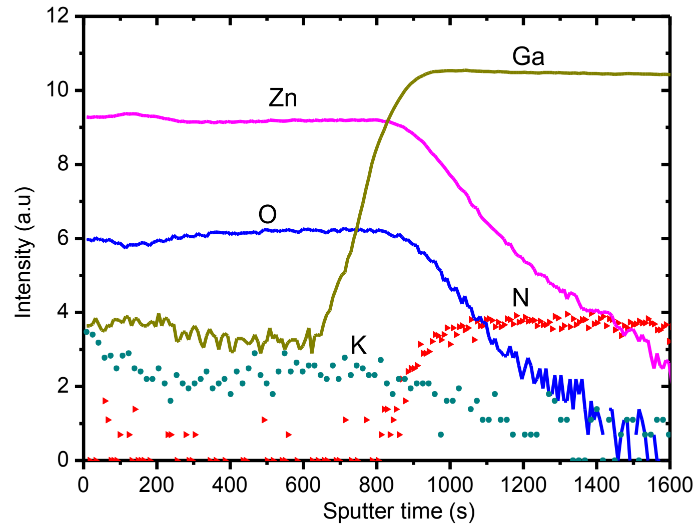

Fig 3.11. SIMS depth profile of of ZnO nanorods grown on GaN substrate using 0.01 M $ZnAc_2$ and 0.37 M NH_4OH at 90°C for 1 h.

3.2.4 Energy-dispersive X-ray spectroscopy (EDX)

The composition of the ZnO nanorods was further investigated using EDX, which allows the surface composition of the nanorods to be quantified non-destructively. Fig 3.12 shows the EDX spectrum consisting of only Zn, O and Si were detected. Si peaks originate from the substrate which are exposed in between the nanorods. The ratio of Zn/O in EDX is about 49:51, suggesting the structure is richer in oxygen.

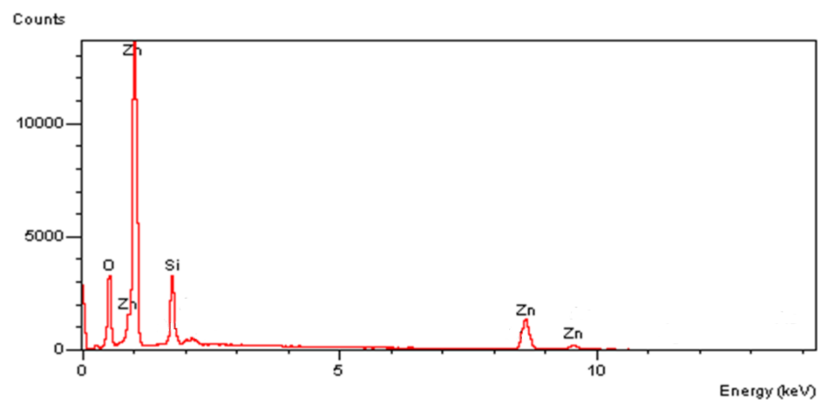

Fig 3.12 EDX spectrum of ZnO nanorods grown on Si substrate using 0.01 M $ZnAc_2$ and 0.37 M NH_4OH at 90°C for 1 h.

3.2.5 XPS analysis

Another method to quantify the composition of ZnO nanorods is X-ray photoelectron spectroscopy (XPS). As described in Chapter 2, the XPS system uses an Al-Kα source with a spot size of 700 µm. The energy steps measured at 0.1 eV intervals. The typical wide scan XPS spectrum of ZnO nanorods is shown in Fig 3.13. The peaks in the wide scan can be indexed to Zn, O, Ga and N. The corresponding peaks of these elements have been labeled in the figure.

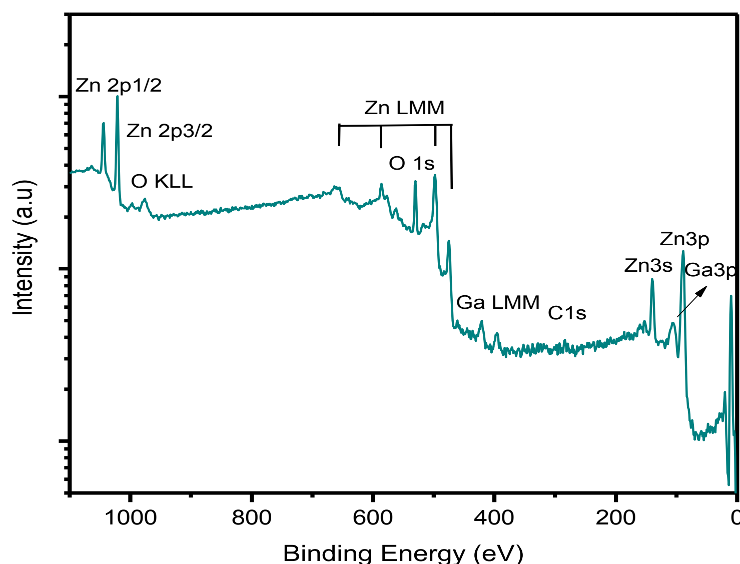

Fig 3.13. XPS spectrum of ZnO nanorods grown on GaN substrate, the growth condition is 0.2g $ZnAc_2$, 1.2ml NH_3, 1 hour and 90℃.

Fig 3.14 plots the Zn $2p_{1/2}$ and Zn $2p_{3/2}$ peaks located at 1021.7 and 1044.8 eV respectively. The magnitude of spin orbit splitting of Zn 2p levels is 23.1 eV, which is consistent with published values [110, 111]. When the measurement temperature was varied from 30°C to 600°C, the magnitude of this spin orbit splitting remained constant, suggesting that the nanorods are compositionally stable. Peak fitting gave an integrated area ratio of $2p_{3/2}$ to $2p_{1/2}$ peaks as 2:1 as expected for ZnO.

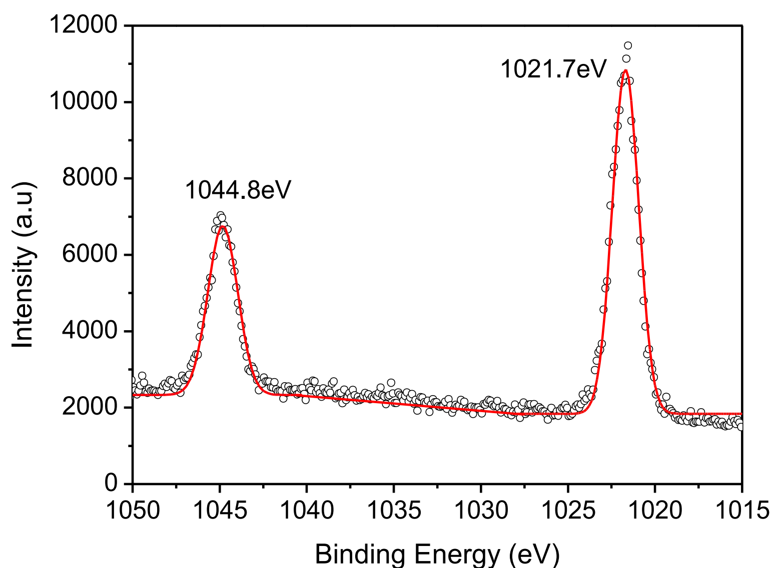

Fig 3.14. The XPS spectrum of Zn $2p_{1/2}$ and Zn $2p_{3/2}$ peaks from ZnO nanorods grown on GaN substrate in 0.02 M $ZnAc_2$ and 0.37 M NH_4OH at 90℃ for 1 h.

The O 1s peak is shown in Fig 3.15. The peak centered at 530.5 eV, consistant with values from other reports [111-113]. The presence of a single and highly symmetrical peak at 530.5 eV implies low O defects and impurities. It also suggests the absence of O-H bonding in ZnO nanorods.

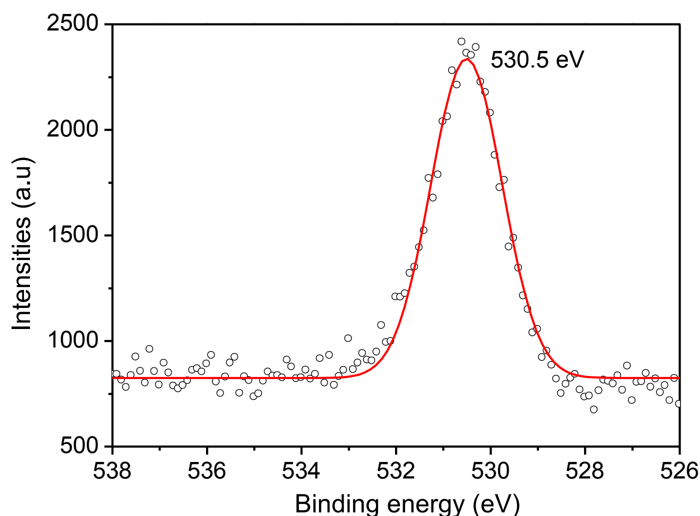

Fig3.15 The XPS spectrum of O 1s peak from ZnO nanorods grown on GaN substrate in 0.02 M $ZnAc_2$ and 0.37 M NH_4OH at 90℃ for 1 h..

3. 3 Optical properties of n-type ZnO nanorods

3.3.1 Photoluminescence of undoped ZnO nanorods

The photoluminescence (PL) was measured to study the optical quality and defects in the ZnO nanorods. Strong variations in the PL spectra were observed when ZnO nanorods were grown using different concentrations of NH_4OH ranging from 0.18 to 0.55 M NH_4OH. These spectra are shown in Fig 3.16. In general, the PL spectra of ZnO include an ultraviolet peak, centered at about 379 nm, and a broad visible band, centered at about 580 nm. The ultraviolet peak was due to band edge recombination in ZnO while the broad visible band originated from deep level recombinations, possibly created by the formation of interstitial zinc, zinc vacancies or interstitial oxygen [6] . Also apparent from Fig 3.16 is the trend of increasing visible PL intensity at the expense of UV PL intensity when the concentration of NH_4OH was increased. The ZnO nanorods grown at 0.18 M NH_4OH has a stronger band-edge recombination peak. The lower intensity of visible emission at 0.18 M NH_4OH points to a lower density of deep level defects in the nanorods. At higher concentrations of NH_4OH, the strong visible emissions can be observed. By tuning the concentration of NH_4OH, it is possible to control the intensity of orange emissions from the nanorods. This provides a promising and interesting method for controlling the UV and visible emissions in LEDs.

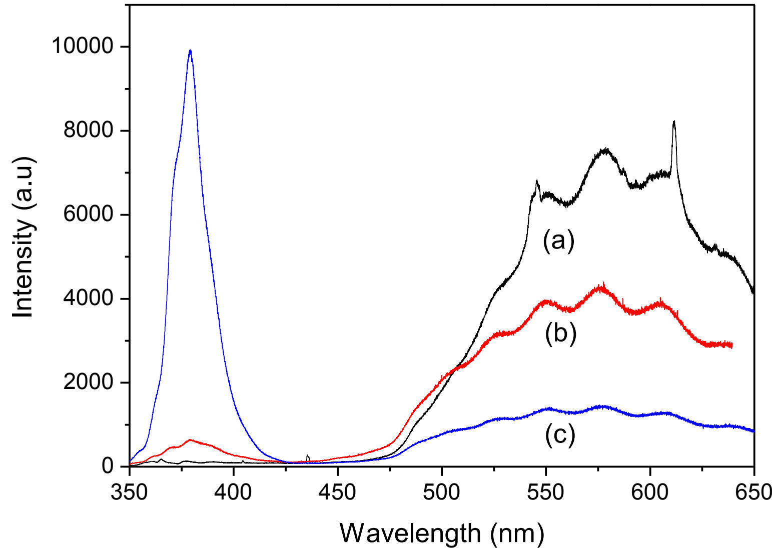

Fig 3.16. Photoluminescence of ZnO nanorods grown at (a) 0.54 M (b) 0.37 M, and (c) 0.18 M NH_4OH. The other growth parameters are concentration of $ZnAc_2$, growth temperature and duration were kept constant at 0.01 M, 90℃ and 1 h.

3.3.2 Photolumincescence of ZnO nanorods doped with Al and Ga

The doping is also having effects to photoluminescence of ZnO nanorods. Effect of doping on PL of ZnO was studied using varying doping concentration of aqueous solution. The dopant salts are 0.08 mM, 10 mM of $Ga(NO_3)_3$ and $AlCl_3$ respectively. Other growth parameters are concentration of $ZnAc_2$, NH_4OH, growth temperature and duration were kept constant at 0.01 M, 0.37M, 90°C and 1 h. The typical PL spectra of undoped and Ga, Al doped ZnO nanorods was shown in Fig 3.17. The PL of undoped ZnO nanorods is stronger in visible band. It is attributed to higher density of intrinsic donors such as zinc interstitial, oxygen vacancy or hydrogen interstitial in the nanorods. Intensity of near band-edge emission of ZnO is remaining with and without doping Ga and Al.

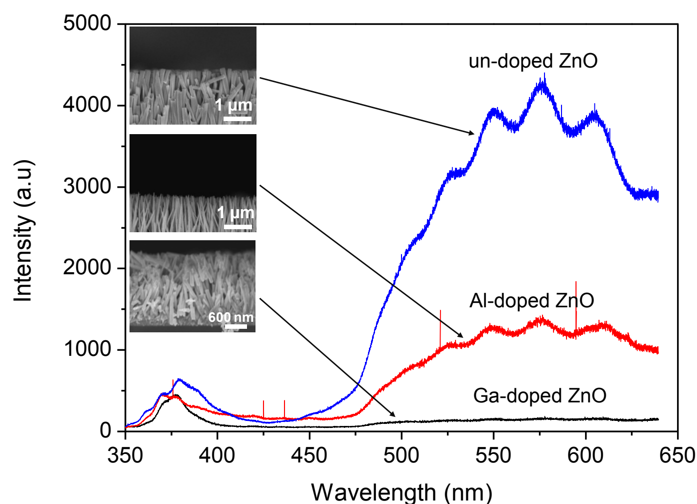

Fig 3.17 Photoluminescence of (a) un-doped, (b) 10 mM $AlCl_3$ and (c) 0.08 mM $Ga(NO_3)_3$ doped ZnO nanorods. The other growth parameters are concentration of $ZnAc_2$, NH_4OH, growth temperature and duration were kept constant at 0.01 M, 0.37M, 90℃ and 1 h.

3.3.3 Photoluminescence of undoped ZnO nanorods after annealing

In order to improve the quality of ZnO nanorods through removal of various intrinsic defects, annealing treatment can be performed. A study on effects of annealing to improve electrical and optical properties of unintentional doped ZnO had been reported by our group recently [21]. In this study, the near band-edge emission (NBE) was enhanced after annealing at temperatures from 200 to 425°C. This was attributed to the activation of hydrogen-related donors. The presence of hydrogen donors in unintentionally doped ZnO was supported by the variations in NBE of ZnO nanorods with different diameters under various annealing conditions [114]. Due to the dissociation of hydrogen donor at higher temperatures, intensity of NBE decreases after annealing temperatures above 425°C. In this section, we showed that photoluminescence of grown ZnO nanorods after annealing are in agreement with the results that were reported earlier [114]. Fig 3.18 shows that annealing can improve the NBE by three orders of magnitude. At the

same time, annealing treatments reduces the intensity of the visible peaks. Through good understanding of the underlying physics of how intrinsic defects can be removed through a combination of careful control of growth conditions and post-thermal annealing, high quality ZnO nanorods can be obtained for solid-state lighting applications.

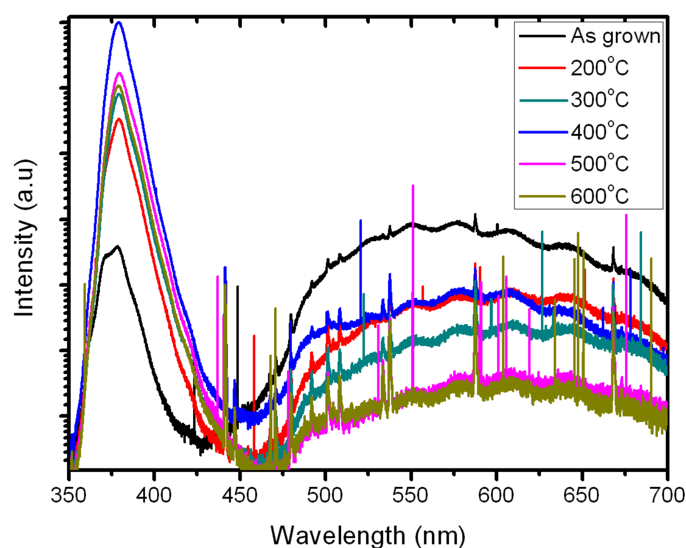

Fig 3.18 Photoluminescence of un-doped ZnO nanorods annealed at different temperatures, varying from 200℃ to 600℃. The anneal time is 30 minutes. The growth parameters are concentration of $ZnAc_2$, NH_4OH, growth temperature and duration were kept constant at 0.01 M, 0.37M, 90℃ and 1 h.

3.4 Conclusions

In this chapter, n-type ZnO nanorods obtained by unintentionally doped or doped with Ga, Al were grown using aqueous solution method. ZnO nanorods grown on GaN epi-layer substrate are well-aligned vertically and single crystalline. The morphology of n-type ZnO nanorods under effects of growth parameters and doping with Al and Ga dopants were studied. The SEM images the n-type ZnO nanorods shows that undoped ZnO nanorods have the most suitable morphology for ZnO nanorod based LED fabrication.

Chapter 4 Optimization of p-type ZnO nanorods growth by doping with potassium using aqueous solution method

In 2004, Tsukazaki et al. introduced the repeated temperature modulation epitaxial growth of p-type ZnO film [38]. After that, there more reports on successful growth of p-type ZnO by a variety methods such as MOCVD, PLD, and CVD have been observed [36, 70, 100, 115]. However, the reported hole concentrations in the p-type ZnO were either too low or unstable [4]. As such, p-type doping of ZnO remains controversial. In this work, we described our successfully growth and p-type doping of ZnO nanorods [116] with potassium using solution method. The hole concentrations that were obtained are relatively high and stable over a period of several months.

This chapter comprises of 4 sections. Section 4.1 introduces the possible dopants for p-type ZnO and reasons for the choice of potassium as a dopant. Section 4.2 describes the fabrication process of p-type ZnO and the resulting morphology of p-type ZnO nanorods. Section 4.3 reports on the characterization of the structural properties and chemical composition of p-type ZnO nanorods. Section 4.4 studies the optical properties of p-type ZnO nanorods. Finally, Section 4.5 concludes the entire chapter.

4.1 Principle of doping potassium for p-type ZnO

4.1.1 Motivation for use of potassium as p-type acceptor dopants in ZnO.

The possible p-type ZnO dopants can be Group IA elements: lithium (Li), sodium (Na) and potassium (K) or Group V elements: nitrogen (N), arsenic (As), phosphorus (P), and antimony (Sb). Substitutional p-type doping

occurs when either Group IA elements replace Zn atoms or Group V elements replace O. The Zn–O bond length is 1.93 Å [35]. Depending on the nearest-neighbor bond lengths of dopants, tensile or compressive strains are formed within the lattice. The nearest-neighbor bond lengths and the defect energy levels for negatively charged of substitutional dopants are summarized in the Table 4.1 [35]. Li and N forms the lowest defect energy level for group I and V respectively, with the former having the lowest energy level for both groups. Table 4.1 also shows that substitutional group V elements (N, P and As) are deep acceptors. N being the shallowest group V element even has a larger defect energy level compared to K, which is the highest among group I elements.

Table 4.1 Calculated nearest-neighbor bond lengths (R) and the defect energy levels for negatively charged substitution impurities. Taken from reference [35].

Group I	R(Å)	ε(eV)	Group V	R(Å)	ε(eV)
Li	2.03	0.09	N	1.88	0.40
Na	2.10	0.17	P	2.18	0.93
K	2.42	0.32	As	2.23	1.15

Although group I elements have shallower acceptor energy levels, self-compensation has been a challenge. Since Li and Na atoms are much smaller than O, and ZnO wurtzite structure is relative open, Li and Na dopant atoms are also easily incorporated interstitial sites. As interstitials, Li and Na forms a donor compensates the substitutional Li and Na acceptors, leading to a highly compensated and intrinsic ZnO. Clearly, reduction of interstitial dopant formation is a hurdle that must be addressed in order to achieve higher hole concentrations for ZnO doped with group I elements. Among the elements in group I, K has the lowest tendency to form interstitials because the large K

radius (2.42 Å) makes the formation of interstitial K energetically unfavourable, leading to either a lower incorporated concentration of interstitials during growth, or a energy barrier required to drive out interstitial K after growth.

A challenge that needs to be addressed is the low group I dopant solubility in ZnO, which limits the hole concentrations. One way to increase group I dopant solubility is by formation of stable neutral complexes between potassium and hydrogen [117-119].

Another challenge arising from the use of potassium as a dopant, is the increased formation of oxygen vacancies due to the large radius of K. Reduction of oxygen vacancies is important for high p-type conductivity because oxygen vacancies form donor defects which compensate the acceptor doping from substitutional K [120].

4.1.2 Type and Nature of Potassium Defect in ZnO

To date, numerical simulations of K doping in ZnO has yet to be reported. Most work has focused on Li and Na of group I. The work of Wardle et. al. [121] and Lee et. al. [120] have important implications for p-type doping of ZnO with Li and Na. These works will be used as a basis for understanding the mechanism of doping with K, and predicting the resulting type and nature of K defects. In general, we expect K to follow the predicted trend for Li and Na to form stable complexes with H, Li and Na interstitials in the presence of hydrogen. Extending this understanding to the case of K, the formation of stable K_{Zn}-H_i and K_{Zn}-K_i complexes is expected. The schematic diagram of these complexes in the ZnO lattice is illustrated in Fig 4.1. As these complexes are neutral, a much higher K solubility can be achieved.

Eventually, a post-growth thermal anneal can be performed to dissociate these neutral complexes, drive out H and obtain a higher p-type doping.

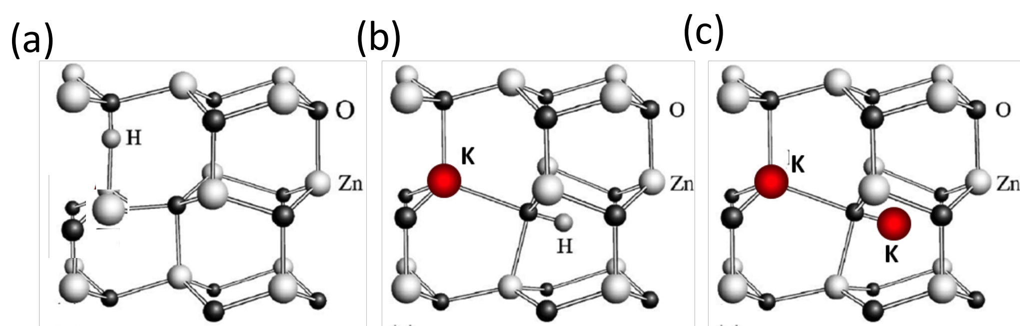

Fig 4.1 Schematic diagram showing the simulated lattice structure of ZnO (a) without any complexes, (b) with K_{Zn}-H_i and (c) K_{Zn}-K_i complexes.

One important difference between K and the other group I elements, Li and Na, is that K has a larger atomic radius compared to Zn while Li and Na have a smaller atomic radius. As a result of the larger atomic radius of K, increased oxygen vacancies have been predicted [35]. These oxygen vacancies are expected to form donor energy levels which in turn, compensate the K acceptor doping. In order to minimize the formation of oxygen vacancies, our growth process was designed to be carried out at in an environment that has a pH greater than the PZC of ZnO, which has been shown by our earlier work to have an oxygen-rich environment due to high concentrations of hydroxyl groups (O–H) [122].

4.2 Properties of p-type ZnO nanorod

4.2.1 Morphology of p-type ZnO nanorod

In this work, p-type ZnO nanorods obtained by doping potassium in aqueous solution. To study the effect of K doping on the morphology, three concentrations of KAc was used: 0, 0.07 and 0.15M. The concentrations of $ZnAc_2$ and NH_4OH, growth temperature and duration were kept constant at

0.01 M, 0.37 M, 90°C and 1 h respectively. Figs 4.2 (a-c) show the morphology of ZnO:K nanorods grown in aqueous solution with 0, 0.07 and 0.15 M KAc respectively. The nanorods are vertically aligned on GaN substrates. No significant variation in the area density, length and diameter can be observed when various KAc was added.

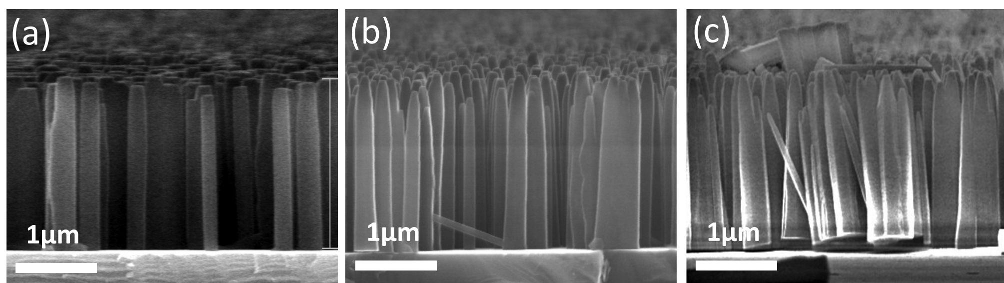

Fig 4.2 the SEM images of ZnO:K nanorods grown at (a) 0.00, (b) 0.07, and (c) 0.15 M KAc. Concentration of $ZnAc_2$, NH_4OH, growth temperature and duration are kept constant at 0.01 M, 0.37 M respectively at 90℃ for 1 h.

4.2.2 Lattice structure of p-type ZnO nanorods

a) TEM images of p-type ZnO nanorods

Fig 4.3 (a) and (b) shows the HRTEM and SAED images respectively, of a ZnO nanorod which was grown in 0.01 M $ZnAc_2$, 0.15M NH_4OH and 0.07 M KAc. From the HRTEM image, the structure is single crystalline with a separation distance of 0.504 nm between two parallel planes of oxygen atoms, which appear in Fig 4.3 (a) as white spots. This separation corresponds to the inter-planar spacing of two (0002) planes of wurtzite ZnO. The dots in the SAED image can be indexed to wurtzite ZnO.

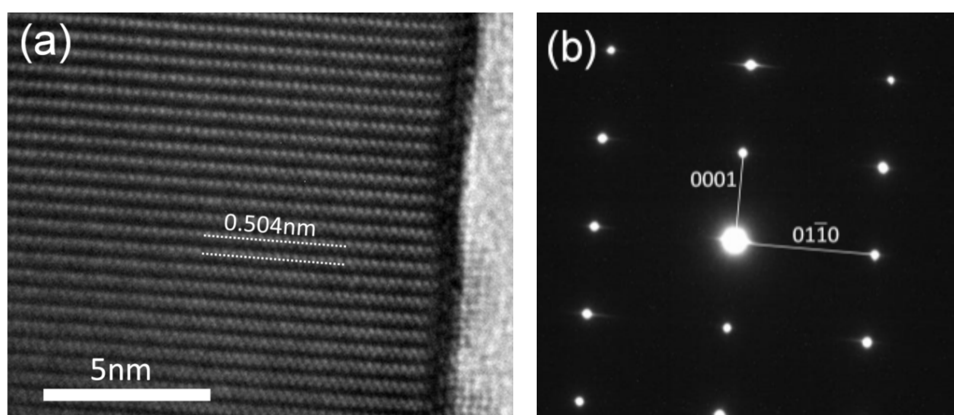

Fig 4.3 (a) HRTEM of ZnO nanorods grown in 0.01 M $ZnAc_2$, 0.15M NH_4OH and 0.07 M KAc. The white spot represent the oxygen atoms. (b) SAED image of the same ZnO nanorod.

4.2.3 Chemical composition of p-type ZnO nanorods.

SIMS and XPS were taken to investigate the incorporation of potassium in the ZnO nanorods. SIMS is the surface sensitive method. Sputtering of ZnO nanorods was performed using Ga ion source while compositional analysis was done using Ar ion source to obtain a depth profile of the ZnO nanorod. The quantitative information obtained from SIMS was complemented by the qualitative information from XPS to obtain a more complete understanding of the nature of K in ZnO.

a) Tof-SIMS study of ZnO nanorods.

The distribution of K throughout the nanorods was investigated using ToF-SIMS. Samples of ZnO nanorods were grown in solutions containing 0.01 M $ZnAc_2$, 0.37 M NH_4OH and a specific amount of KAc ranging from 0 to 0.13M. SIMS depth profiles in Fig 4.4 show that the SIMS intensity ratio of Zn and O are constant for various concentrations of KAc. The SIMS intensity for K depends on the concentration of KAc in the solution. The concentration of K incorporated in the nanorods increased with the concentration of KAc from 0 to 0.08 M. Above 0.08 M KAc, the concentration of incorporated K in

the nanorods remained constant. This is interesting because a higher KAc concentration in solution does not directly translate to higher incorporation of K in the ZnO lattice. This implies an upper limit to the amount of K that can be incorporated into the lattice by increasing the concentration of KAc.

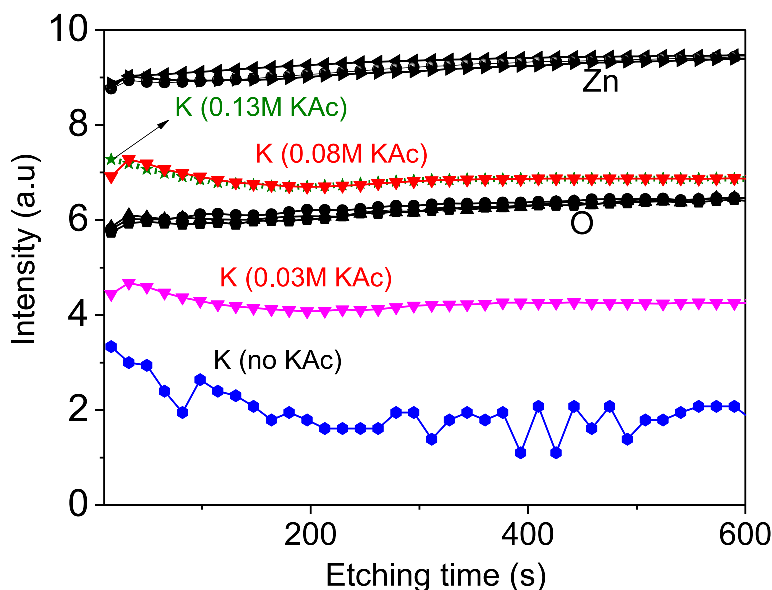

Fig 4.4 ToF-SIMS of ZnO:K nanorods on n-GaN substrate showing incorporation of K

The image map of Zn, O, K, Ga, N, Si and P in ZnO nanorods are shown in Fig 4.5. Trace concentrations of Na, Si and P impurities distributed uniformly across the entire image map without any relatioship to the Zn and O maps. Since the K map shows the same pattern dependence with the Zn and O maps, K is clearly incorporated within the ZnO nanorods.

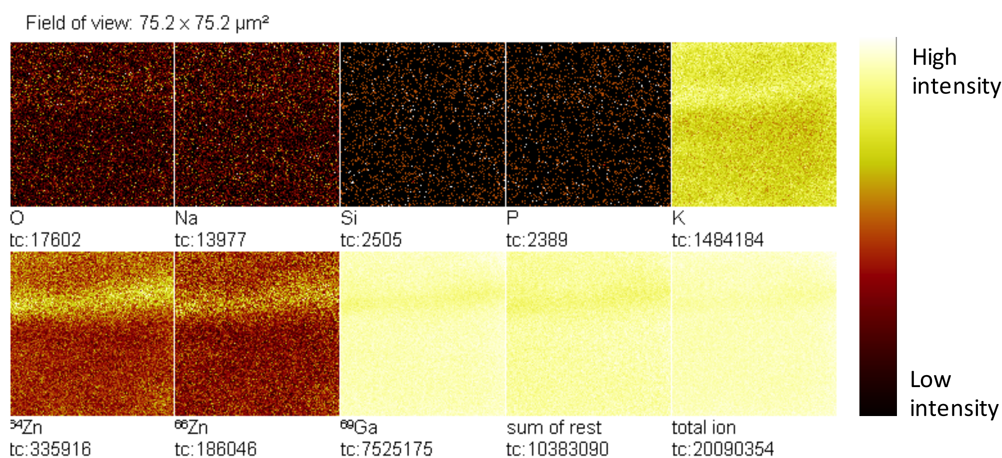

Fig 4.5 ToF-SIMS mapping image of p-type ZnO nanorods.

b) XPS analysis of p-type ZnO nanorods

Fig 4.6 shows the XPS spectra of ZnO nanorods grown in 0.01 M $ZnAc_2$, 0.07 M KAc and 0.37 M NH_4OH. The measurement was conducted at two temperatures: 25 and 500°C. From the survey scan spectra at both temperatures showed presence of Zn, O, K and C peaks.

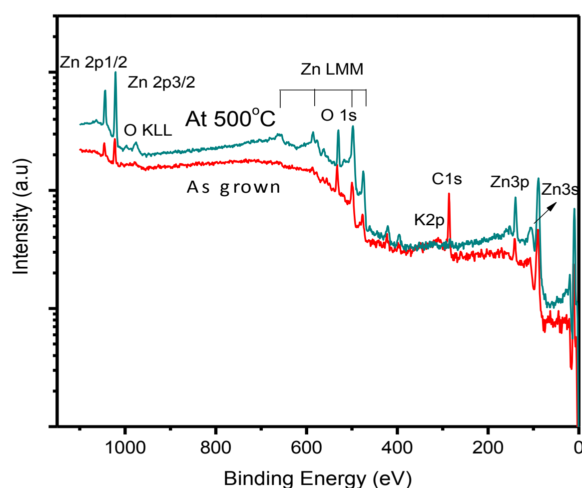

Fig 4.6 XPS spectra of the ZnO nanorods growth in aqueous solution includes: 0,01 M $ZnAc_2$, 0.07MKAc and 0.37 M NH_4OH. The measured temperatures are (a) 25 and (b) 500℃.

The detailed scans of K 2p peaks for both 25°C and 500°C are shown in Fig 4.7. The room temperature spectrum did not show a clear K 2p peak, which is expected for atomic concentrations below 1% at. At 500°C, K $2p_{1/2}$

and K $2p_{3/2}$ peaks become clearly visible. The peak positions of K $2p_{1/2}$ and K $2p_{3/2}$ are 297.6 and 294.4 eV respectively. The binding energy difference between two peak positions as well as the ratio of their integrated area of about 2:1 confirms the assignment of K 2p with spin orbit splitting [123].

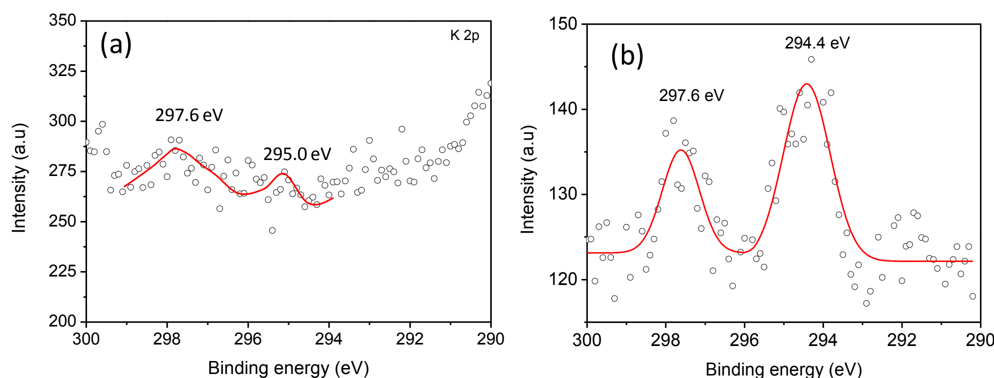

Fig 4.7 XPS spectra of the K 2p peaks of ZnO nanorods growth in aqueous solution includes: 0,01 M $ZnAc_2$, 0.07MKAc and 0.37 M NH_4OH. The measured temperatures are (a) 25 and (b) 500℃.

Quantitative analysis of Zn, O and K at 500°C, which is summarized in Table 4.2, showed that the atomic percentage of K at the surface is about 2.1%. The increase in K concentration from below 1% to 2.1% is probably due to out-diffusion of K in the rods towards the surface. Quantification results confirmed that the ZnO nanorods are oxygen rich, as a result of the growth environment.

Table 4.2 quantitative calculation of all elements in p-type ZnO nanorods at 500℃

Name	Pos.	FWHM	At%
Zn 2p	1023	3.45	46.93%
O 1s	530	3.16	50.95%
K 2p	295	3.27	2.12%

The XPS spectra of the O 1s peaks for both room temperature and 500°C are shown in Figs 4.8 (a) and (b) respectively. The peak position of O 1s peak position is 532.7 and 530.5eV for room temperature and 500°C respectively. According to Chen et. al. [124], O 1s peaks can be deconvoluted into three components. The first component centered at 530.15 eV can be attributed to fully surrounded O^{2-} ions, 531.25 eV to O^{2-} ions in oxygen deficient regions and 532.4eV to loosely bound O on surface due to adsorption of O_2 or H_2O. At room temperature, it is likely that the surface of the nanorods is covered with water moisture as a result of the solution growth and ambient humidity, thus the O 1s peak position at 352.7eV. When heated to 500°C inside the XPS chamber, water moisture is removed and the O1s peak position shows up at 530.5 eV.

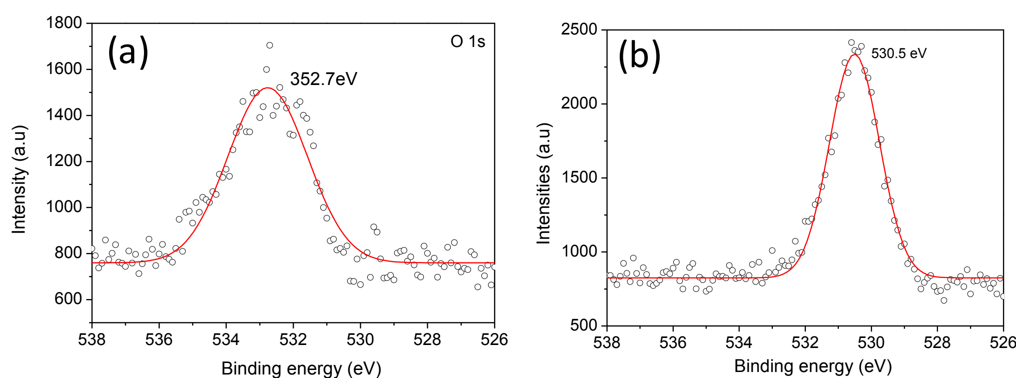

Fig 4.8 XPS spectra of the O 1s peaks of ZnO nanorods growth in aqueous solution includes: 0,01 M $ZnAc_2$, 0.07MKAc and 0.37 M NH_4OH. The measured temperatures are (a) 25 and (b) 500℃.

In contrast, Fig 4.9 (a) and (b) shows that the Zn 2p peaks, which consists of Zn $2p_{1/2}$ and Zn $2p_{3/2}$. Due to spin orbit splitting, are independent of the measurement temperature at room temperature and 500°C respectively. The binding energies of Zn $2p_{3/2}$ and Zn $2p_{1/2}$ are 1022 eV and 1044eV, respectively. The spin orbit splitting of Zn 2p levels are 23.1eV, while the area

ratio of 2p3/2 and 2p1/2 is 2:1. Both values are consistent with published values [112].

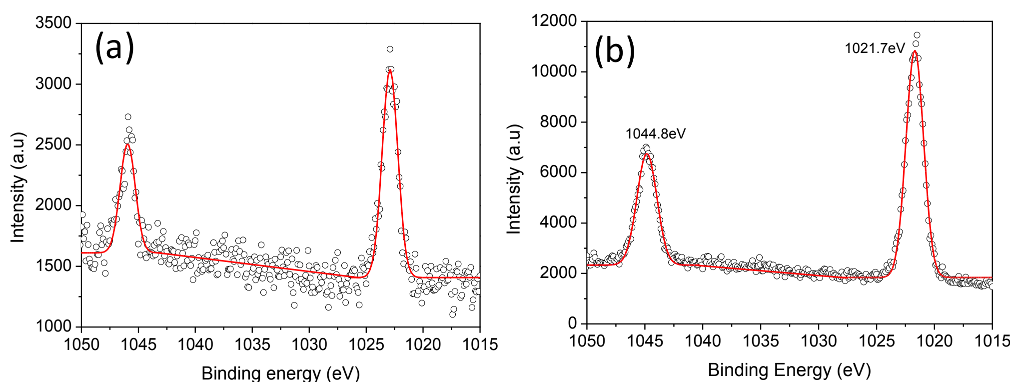

Fig 4.9 XPS spectra of the Zn 2p peaks of ZnO nanorods growth in aqueous solution includes: 0,01 M $ZnAc_2$, 0.07MKAc and 0.37 M NH_4OH. The measured temperatures are (a) 25 and (b) 500℃.

c) Raman scattering study of p-type ZnO nanorods

More evidence for substitution sites of potassium in p-type ZnO nanorods is provided by resonant Raman Scattering data of the as-grown samples as shown in Fig 4.10 (a). After removing a linear background and fitting the lower frequency shoulder with a surface mode component, the peak positions of the A_1-LO against the concentrations of K are plotted in Fig 4.10 (b). As the A_1-LO represents the vibration of the Zn-O bond along the c-axis [125], a lower wavenumber represents a longer bond length, i.e. an expansion along the c-axis. The undoped ZnO film has its A_1-LO peak at 574 cm^{-1} while the K-doped films have their A_1-LO peaks in the range 562-565 cm^{-1}. The significant decrease in frequency implies that the lattice expanded to accommodate the larger K atoms which are incorporated in the film (bond length is 0.242 nm for K-O compared to 0.193 nm for Zn-O [119]).

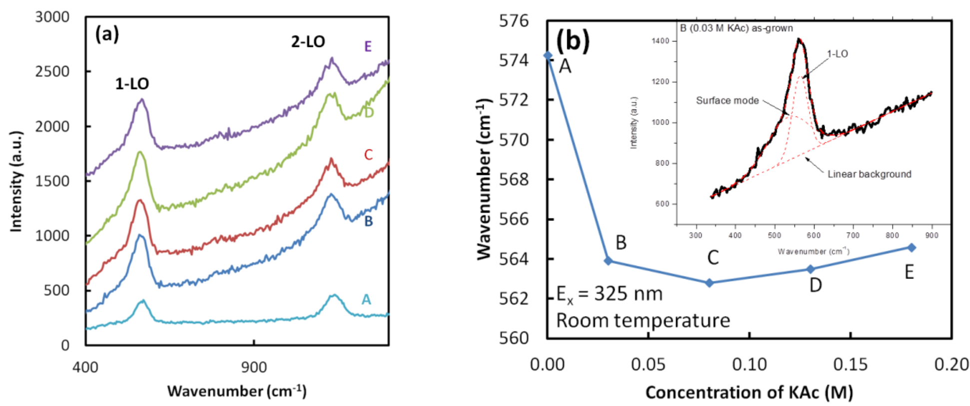

Fig 4.10 (a) Raman scattering spectra of p-type ZnO nanorods at room temperature and (b) plot of peak positions of A_1-LO against the concentration of KAc for as-grown samples A, B, C, D and E which are grown in 0, 0.03, 0.08, 0.13 and 0.18 M KAc respectively. The inset of (b) shows the fitted components consisting of the A_1-LO peak and its surface mode for sample C.

4.2.4 Electrical properties of p-type ZnO nanorods

For ZnO nanorods, traditional Hall measurement cannot be applied because of morphology limitations. In order to measure the electrical properties of ZnO nanorods, we assumed that the electrical properties of ZnO nanorods remained unchanged after multiple growth cycles. This assumption is useful because typically 2 cycles of growth results in the nanorods coalescing to form a continuous film. That film can then be conveniently characterized by Hall effect measurement to obtain the type of conductivity and its carrier concentrations. By using this indirect method, the electrical properties of the nanorods can be obtained. Further confirmation of these properties can be obtained through formation and characterization of p-n junctions, which will be discussed in Chapters 5 and 6.

Hall effect measurements were performed on ZnO films which were obtained from two successive growth cycles on sapphire substrates. Thickness of the potassium doped ZnO films were about 1.7-1.9µm. The growth solution was 0.08 M KAc, 0.01 M ZnAc and 0.18 M NH_4OH. The results of these Hall

effect measurements of ZnO films with and without doping potassium are summarized in Table 4.3. The as-grown K-doped ZnO film exhibits p-type conductivity with a hole concentration of about 10^{17} cm^{-3}. This value of hole concentration will be used later to verify the device performance in Chapter 5 and 6. In comparison, the unintentionally doped ZnO typically shows n-type conductivity, which has been attributed to formation of intrinsic defects such as interstitial hydrogen, interstitial zinc and oxygen vacancies.

Table 4.3 Summary of measured Hall effect carrier concentrations for undoped and potassium doped ZnO films. A positive and negative sign indicates hole and electron concentration per cm^{-3} respectively. Taken form reference [50]

Concentration of KAc (M)	Thickness of film (μm)	Type of major carrier	Carrier concentration (cm^{-3})
0 (undoped)	1.7	n	-1×10^{18}
0.07M	1.9	p	$+2 \times 10^{17}$

4.2.5 Optical properties of p-type ZnO nanorods: Photoluminescence

The large atomic size of potassium atoms can lead to the formation of oxygen vacancies (V_O) which in turn, provide stable sites for hydrogen atoms [21]. Interstitial oxygen acts as donors which compensates the substitutional acceptors. XPS results have earlier shown that the ZnO:K nanorods are oxygen rich which reduces the likelihood of oxygen vacancy formation, and thus compensation. One way to verify the density of oxygen vacancies is through photoluminescence (PL). A typical plot of PL spectra of ZnO:K nanorods that were grown under different doping concentrations is shown in Fig 4.11.

The PL spectra of potassium doped ZnO have an ultraviolet peak at about 378 nm and a broad peak range in yellow region which have the center is about 560 nm. The ultraviolet peak was assigned for band edge

recombination while broad peak at yellow region is issued by defect concentrations which can be interstitial zinc, zinc vacancies or interstitial oxygen [21]. In general, the room temperature PL of undoped and potassium doped ZnO have similar intensity of defect peak. Therefore, doping potassium does not affect the intensity of oxygen vacancies. This is due to oxygen rich of ZnO.

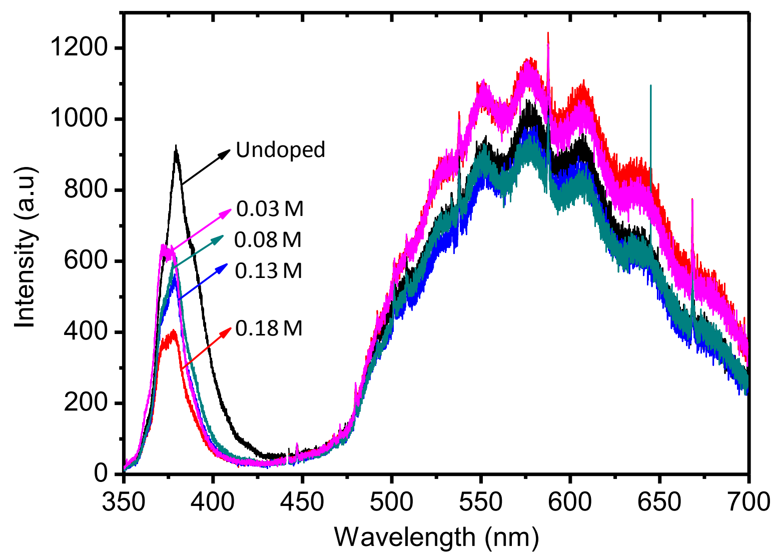

Fig 4.11 Room temperature photoluminescence of potassium doped ZnO at different doping concentration vary from 0.00 to 0.13M KAc. The other parameters are $ZnAc_2$, NH_4OH concentration; growth temperature and duration are 0.01M, 0.37M, 90℃ and 1 h, respectively.

4.3 Improving quality of p-type ZnO nanorods by of annealing.

4.3.1 Optical properties of p-type ZnO nanorods after heat-treatment in vaccum ambient

Annealing treatments can improve the near band edge emission (NBE) of unintentionally doped ZnO nanorods by three orders of magnitude. Similar improvement is expected for NBE of ZnO: K nanorods. The ZnO: K nanorods were grown in aqueous solution contain 0.01 M $ZnAc_2$, 0.07 M KAc, 0.18 M NH_4OH at 90°C for 1 h. Annealing was conducted at 200, 300, 400, 500 and 600°C in vacuum ambient for 30 minutes. The low temperature (16K)

photoluminescence of as-grown and annealled ZnO:K nanorods was shown in Figure 4.12. PL measurement in low temperature produces more information than that of room temperature. The improvement by three order of magnitude of NBE was observed after annealling ZnO:K nanorods at 400°C. Above 400°C, the NBE of the nanorods is lower. This is expected due to the activation of hydrogen which get maximum at 425°C [21].

In other hand, intensity of the visible emission reduces after annealing. The orange emission suggests the presence of oxygen interstitials (O_i) in the sample. Intensity of the orange emission is less reduction than other visible emission to show that oxygen interstitials are more difficult to remove than other defects such as hydrogen.

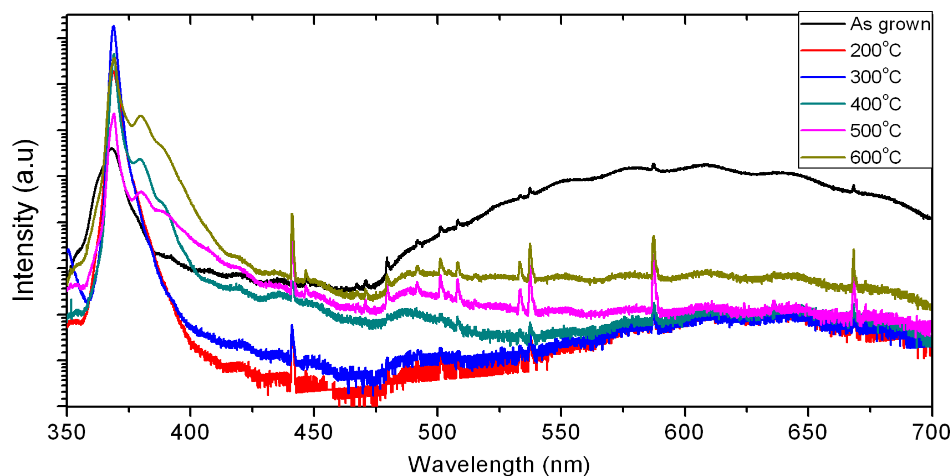

Fig 4.12 Low-temperature (16K) photoluminescence of potassium doped ZnO annealed at different temperature. The ZnO: K nanorods were grown in aqueous solution contain 0.01 M $ZnAc_2$, 0.07 M KAc, 0.18 M NH_4OH at 90°C for 1 h.

4.3.2 Energy level of defects by low temperature PL of p-type ZnO nanorods

The energy of acceptor level was calculated based on the PL spectra of ZnO:K at low temperature. Theoretically, potassium substitution have energy band at 0.32eV from the valence band of ZnO [35]. Figure 4.13 shows that the low temperature (16K) photoluminescence of potassium doped ZnO annealed

700°C for 30 minutes. After substracting the background, peak fitting was performed using Gaussian profiles to identify the peak energy levels. At 16K, taking the band-gap value of ZnO as 3.439eV [126], the acceptor peak of potassium substitution is calculated to be E_G-328meV which is in agreement with reported simulated values [35]. The energy levels of other donors and acceptors of ZnO are shown in the inset of Fig 4.13.

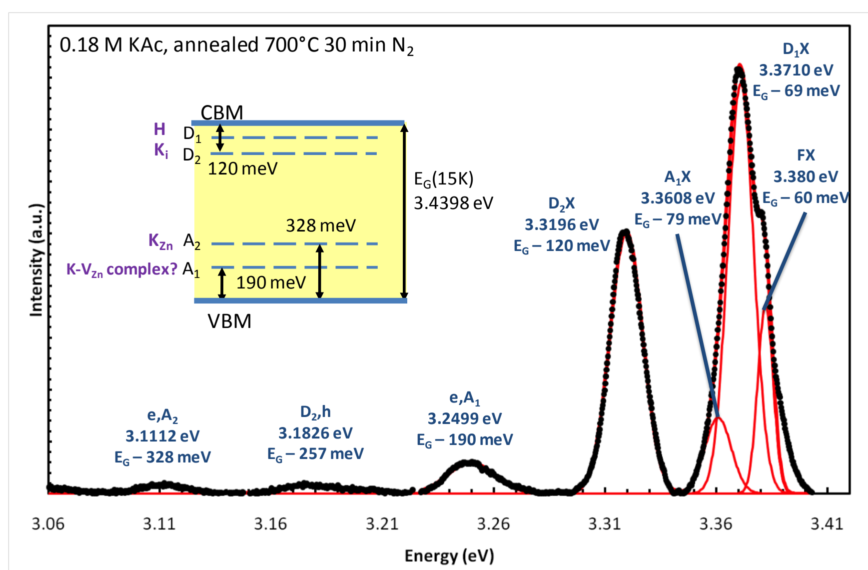

Fig 4.13 normalized low temperature (16K) photoluminescence of potassium doped ZnO annealed 700℃ for 30 minutes, inset is band diagram of potassium doped ZnO

4.4 Conclusions

In this chapter, we reported the successful fabrication p-type ZnO nanorods using solution method. SEM images showed the morphology of K-doped nanorods are similar to those that are undoped. The p-type ZnO nanorods grown on GaN substrate were vertical and single crystalline. XPS and SIMS measurement of p-type ZnO confirmed the incorporation of K within the nanorods. Raman scattering of ZnO nanorods showed the peak shifts of A_1-LO component with incorporation of K, which points to an expansion along the c-axis.

Hole concentrations and carrier mobilities of p-type ZnO nanorods were determined indirectly through Hall effect measurements of ZnO film. When grown in the presence of 0.07 M KAc, a hole concentration of about $2x10^{17}cm^{-3}$ with the hole mobility of about 117 $cm^2V^{-1}s^{-1}$. This growth recipe was used for device fabrication in following chapters.

Annealing treatment on K-doped ZnO nanorods was conducted to improve their crystal quality. Similar with undoped ZnO nanorods, annealing improved the optical properties and activated the hydrogen donors in ZnO, which unfortunately compensate the K acceptor, leading to an intrinsic or n-type conductivity.

Chapter 5 Fabrication of p- type ZnO nanorods/n-GaN film hetero-junction ultraviolet light emitting diodes by aqueous solution method

In this chapter, we report our successful growth of a p-type ZnO nanorods/n-GaN film heterojunction ultraviolet light emitting diode (LED). The heterojunction LED shows its advantages over p-ZnO/n-GaN film heterojunction. The LED demonstrates a rectifying I-V characteristic with a turn-on voltage of 2.7 V. Ideality factor is 6.5. Electroluminescence (EL) spectra of the LED consist of an ultraviolet peak at 378 nm and a broad yellow emission centered at 560nm. Fitting and comparing EL of the LED with PL of p-ZnO and n-GaN show that p-ZnO contributes more to the EL than n-GaN.

This chapter consists of 5 sections. Section 5.1 introduces the fabrication of p- type ZnO nanorods/n-GaN film hetero-junction LED. Section 5.2 shows the morphology of the p-type ZnO nanorods/n-GaN film LED. Section 5.3 investigates the electrical properties of the p-type ZnO nanorods/n-GaN film LED. Section 5.4 presents the optical properties of the p-type ZnO nanorods/n-GaN film LED. Finally, section 5.5 concludes the entire chapter.

5.1. Fabrication of p- type ZnO nanorods/n-GaN film hetero-junction LED

The p-type ZnO nanorods/n-GaN film heterojunction LED fabrication process, shown in Fig 5.1, comprised of four steps. In the first step, n-GaN film was grown on c-plane sapphire at 1020°C using an EMCORE D125 metallorganic MOCVD system. This n-GaN film layer is single crystalline and 3μm thick. Carrier concentration of this n-GaN film is $5x10^{17}cm^{-3}$. In the

second step, n-GaN film was patterned using photolithography to open window for n- contact. The n-contact comprising of Ti (15 nm)/Au (50 nm) was deposited by e-beam evaporation. Then the photo-resist was removed. Next, the samples were annealed at 500°C for 5 minutes to obtain an ohmic contact on n-GaN film. In the third step, another window was opened for growing p-type ZnO nanorods. The p-type ZnO nanorods growth process has been described in our previous study [51]. In this procedure, the solution contains 0.02 M sodium acetate, 0.07M potassium acetate and a specific amount of ammonium hydroxide. 0.07M of potassium acetate is sufficient to obtain p-type ZnO nanorods with activated carrier density of about $3x10^{17}cm^{-3}$ [50]. Varying the ammonia concentration from 0.18M to 0.54 M changes the length, diameter and area density of p-type ZnO nanorods [18]. In the fourth step, the photo-resist was removed. An In/Zn dot was applied on top of the p-ZnO nanorods to form the p-contact. The LED structure with p-n junction formed by p-ZnO nanorods and n-GaN film was thus formed.

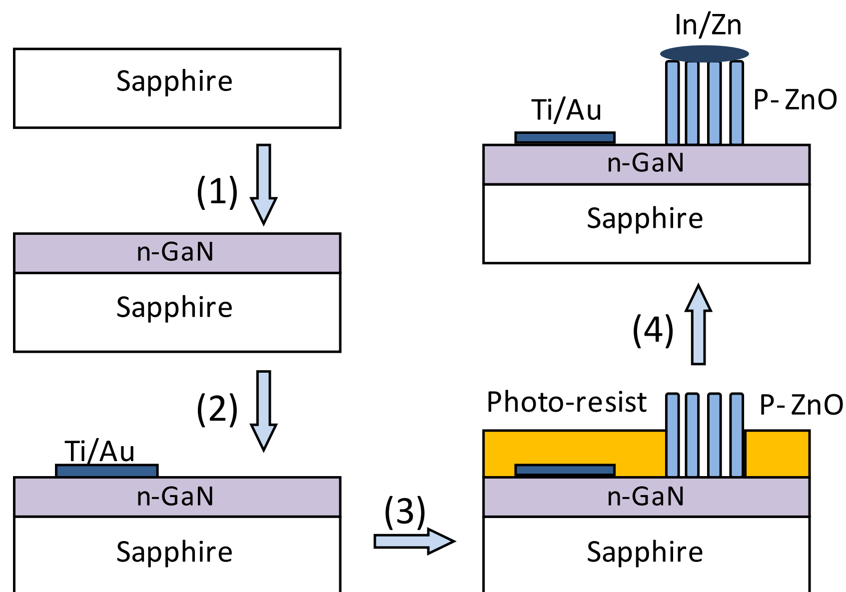

Fig 5.1 Fabrication process of p-ZnO nanorods/ n-GaN film heterojunction LED

5.2 Electrical properties of the p-type ZnO nanorods/n-GaN film LED

Fig 5.2 shows the I-V characteristic of experimental and simulated ZnO nanorods/n-GaN film heterojunction. The heterojunctions were formed in different ammonia concentrations. The simulation was carried out with the software TMA MEDICI [127] to compare against that experimental result. In the simulation, hole concentration of p-ZnO, adapted from our previous report, was $3x10^{17}cm^{-3}$ [116]. Electron concentration of n-GaN is $5x10^{17}cm^{-3}$. Inset shows the ohmic I-V characteristics of n- and p- contacts. Since the contacts are ohmic, the rectifying characteristics can be attributed to the heterojunction formed between p-ZnO nanorods and n-GaN. The reverse bias leakage current is on the order of 10^{-6} A at –5 V.

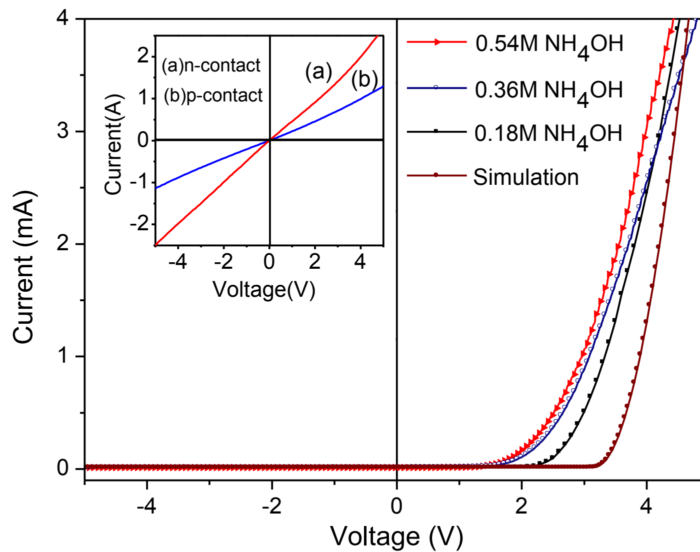

Fig5.2 comparison of the experiment and simulated I-V characteristic of p-ZnO nanorods/n-GaN films heterojunction, the simulation was performed by using TMA MEDICI software with the hole and electron concentration of 3×10^{17} and 5×10^{17} cm^{-3}, respectively. The inset shows I–V characteristic of (a) n-metal/n-GaN contact, (b) p-ZnO/p-metal contact.

From these I-V characteristics, the turn-on voltages and ideality factor were calculated and shown in Table 5.1. In the Table 5.1, the effect of pH of the solution on turn-on voltage and ideality factor is shown. Increase in the pH

of solution lead to reduction of turn-on voltage of the hererojunction. The experimental turn-on voltage is smaller than that predicted by simulation. In contrast, ideality factor of the heterojunction increases with increase in pH of the solution. Value of ideality factors is much higher than that obtained from simulation. The low turn-on voltage and anomalously high ideality factor are commonly reported in non-ideal wide band-gap hetero- and homo-junction [128-130].

Table 5.1. Turn-on voltage and ideality factor of p-ZnO nanorods/n-GaN film I-V characteristics at different ammonia concentration

p-ZnO/n-GaN heterojunction	pH of the solution	Turn-on Voltage(V)	Ideality factor
0.18M	8.5	2.7	6.2
0.36M	9.6	2.3	7.8
0.54M	10.7	2.2	9.5
Simulation	_	3.3	1

In 1996, Perlin et al. [131] explained the anomalously high ideality factor by existence of carrier tunnelling in the heterojunction. The tunnelling current contributes the total current of the p-n junction. Contribution of tunnelling current to the total current increase the ideality factor to be anomalously high value as seen in experimental result.

In the conventional diffusion-recombination model, the current at the p-n junction was calculated by:

$$I = I_{oA} \exp\left(\frac{qV}{n_A KT}\right)$$

In this equation, I is the current, V is the applied voltage, kT/q is the thermal voltage constant, IoA is diffusion-recombination current in reverse bias and nA is ideality factor. Using this model, the ideality factor ranges from 1 to 2 [132].

Under the existence of tunnelling leakage current, the total current will be as follow:

$$I = I_{oA} \exp\left(\frac{qV}{n_A KT}\right) + I_{tunnnel}$$

In this equation, I_{tunnel} is the tunneling current. The ideality factor, n_A calculated using in this equation can exceed 2.

Another factor that affect to ideality factor are the existence of interface charges in the p-ZnO nanorods/n-GaN film heterojunction. The interface charges can be H^+, Zn^{2+} and O^{2-} in the surface of ZnO due to the p-type ZnO nanorods solution growth. The interface charges also arise from defects and fixed charges incorporate at the interface due to an imperfect starting surface. The interface charges in the heterojunction are the electrically active states for surface recombination in the heterojunction under forward bias. This surface recombination current increases the ideality factor of the heterojunction [132]. The other factor contributes to the higher ideality factor of the heterojunction is series resistance. At higher apply current; the series resistance becomes more importance [132].

5.3 Optical properties of the p-type ZnO nanorods/n-GaN film LED

5.3.1 Electroluminescence of the p-type ZnO nanorods/n-GaN film LED

Fig 5.3 shows the EL spectra of p-ZnO nanorods/GaN films LED obtained by applying current in the range from 20mA to 60mA. The EL spectra shows a strong ultraviolet peak at wavelength varying from 370nm to 379nm and a broad visible region centered between 575-620nm. The ultraviolet peaks are band-edge peaks while the visible peaks are from defects. Defects in this heretojunction LED can be Zn vacancy, O interstitial, K interstitial in p-ZnO nanorods or defects in n-GaN. Increasing the applied

current causes the intensity of the EL to increase linearly till about 50mA. At applied current higher than 50mA, the intensity of the EL spectrum was reduced reaching a very low value at the applied current of 60mA. The device degradation is due to thermal heating of the device. The heating effect also caused the UV peak position of the LED to red shift.

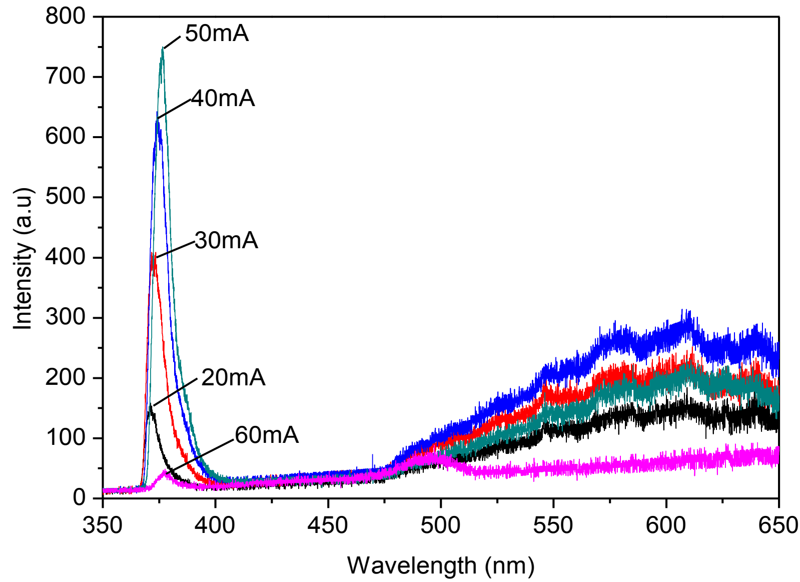

Fig5.3 Electroluminescence spectra of p-ZnO nanorods/n-GaN film LED at difference applied current.

To study the effects of heating on electroluminescence spectra of the p-ZnO nanorods/n-GaN film LED, the EL spectra at different applied current were fitted with Gaussian peaks as shown in Fig 5.4. In this Figure, temperatures of the LED were shown. The temperature associated with each operating current is deduced from the empirical relationship as followed: $E_g(T) = E_g(0) - \frac{\alpha T^2}{T+\beta}$

In this equation, E_g is band-gap of ZnO, T is temperature of the heterojunction, α = -5.5x10^{-4} [eV/K] and β = -900 [K] are constants of ZnO . Band-gap of ZnO at different operating current is calculated from the EL spectra of the heterojunction.

Gaussian fitting of the EL spectrum at 20mA applied current contains three small peaks located at 3.45, 3.32 and 3.26 eV. By fitting EL spectra of the LED at higher applied current, similar shape of the peaks are obtained. Connecting three fitting peak position accordingly, we see the trend of red shift is similar for all peaks. This is because of temperature effect on the LED. At higher temperatures, the band-gaps of ZnO and GaN become smaller. Another effect of heating on the EL spectra is the increase in FHMW of the band-edge peak. At higher temperatures, the electron or hole energy distributions broaden which increase the FHMW of the peak.

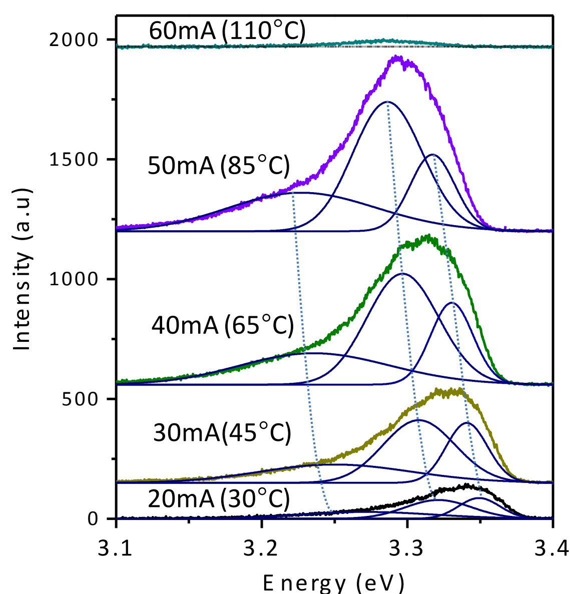

Fig 5.4 Fitting of electroluminescence spectra of p-ZnO nanorods/n-GaN film LED at different applied current to investigate the effect of thermal heating on peak position. Temperatures of the device are estimated.

The electroluminescence of the p-ZnO nanorods/n-GaN films LED can come from both sides, p-ZnO and n-GaN. To define the contribution of p-ZnO and n-GaN on the EL, band-edge peak position of the EL spectrum of p-ZnO nanorods/n-GaN films LED was compared against photoluminescence of p-ZnO and n-GaN, shown in Fig 5.5. EL spectrum of the p-ZnO nanorods/n-GaN films LED at 20mA applied current was fitted with three smaller peaks

centered at 3.35, 3.32 and 3.26 eV. The peaks centered at 3.32 and 3.26eV agree well with that of PL of p-ZnO nanorods. The peak centered at 3.35eV is contributed by both p-ZnO and n-GaN. These results show that, p-ZnO nanorods contribute more to the EL than n-GaN film. This agrees with the band diagram of the heterojunction where the n-GaN film has higher carrier concentration than p-ZnO nanorods. Since n-GaN has a higher carrier concentration, the amount of electrons injected from n-GaN to p-ZnO is higher than the amount of holes injected from p-ZnO to n-GaN; therefore, recombination which creates light occurs more in p-ZnO than in n-GaN. In addition, as GaN has a larger band-gap then ZnO so carriers are preferentially injected into the lower band-gap ZnO.

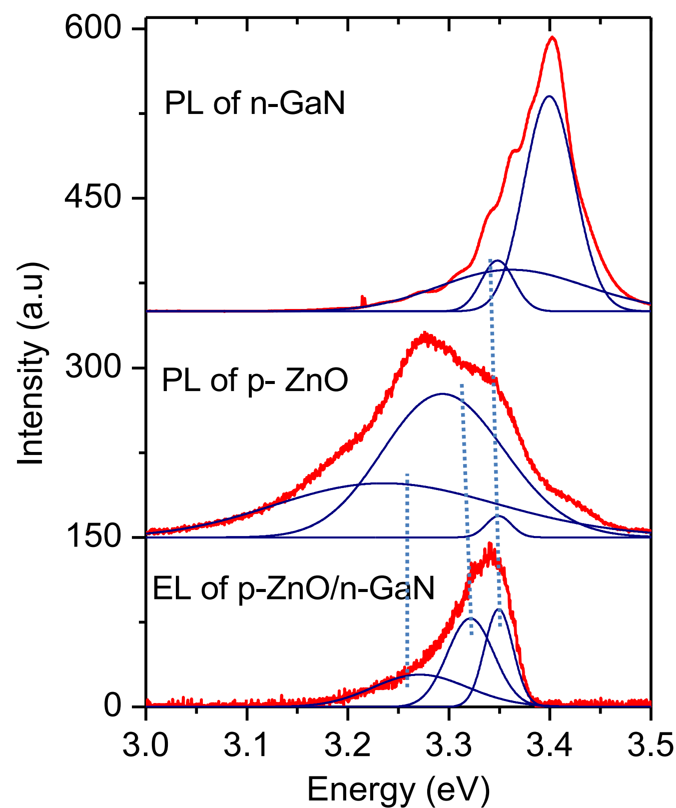

Fig 5.5 Normalized PL spectra of p-type ZnO nanorods, n-GaN film and EL spectrum of p-ZnO nanorods/n-GaN film hererojunction LED.

5.3.2 Comparison of electroluminescence of the p-type ZnO nanorods/n-GaN film LED with p-ZnO film/n-GaN film LED

A comparison of the p-ZnO nanorods/n-GaN film LED with the p-ZnO film/n-GaN film LED helps to understand the advantage of ZnO nanorods. In 2010, we reported the fabrication of a p-ZnO film/n-GaN film ultraviolet LED [50]. The growth condition of p-ZnO nanorods and n-GaN film in this paper are similar with that paper. The p-ZnO film/n-GaN film LED has a rectified I-V characteristic and an electroluminescence spectrum. In comparison with the p-ZnO film/n-GaN film LED, the p-ZnO nanorods/n-GaN film LED has higher turn-on voltage, 2.70V and 2.45V. The higher turn-on voltage shows that the leakage current is less in ZnO nanorods based LED. It is due to less dislocation and grain boundary in the ZnO nanorod LED as well as lower interface charges density in the ZnO nanorods/GaN film interface.

The EL spectra of the p-ZnO film/n-GaN film LED consist of an ultraviolet peak centered at 372 nm and broad peak centered at 500-580nm which is in the same position with the EL peak from p-ZnO nanorods/n-GaN film LED. However, The ultraviolet peak intensity of the ZnO nanorods LED is twice higher than that of ZnO film LED. This is attributed to better light extraction of ZnO nanorod. Higher EL intensity shows the advantage of ZnO nanorod over ZnO film.

5.4 Conclusions

In this chapter, we report the successful fabrication p-ZnO nanorods/n-GaN film ultraviolet LED. The LED consists of single crystalline p-ZnO nanorods grown vertically on n-GaN epi-layer. The LED demonstrates a

rectifying I-V characteristic with a turn-on voltage of 2.7V, lower than the 3.3V that obtained from simulation. Ideality factor which calculated from ln(I)-V characteristics, is 6.5. The cause for the lower turn-on voltage and higher ideality factor is attributed to interface charges in the heterojunction. The interface charges are due to high pH of the growth solution in the LED fabrication process. This reduction in turn-on voltage is confirmed by simulation using TMA MEDICI software with the presence of interface charges in the heterojunction. At room temperature, EL spectra consist of an ultraviolet peak centered at about 370-378nm and a broad visible peak. The UV peaks in the EL is observed to red shift and broaden with higher current. Finally, comparing the EL of the LED with the PL of p-ZnO nanorods and n-GaN film, it is concluded that much of the EL comes from the p-ZnO nanorods. The ZnO nanorods/GaN film EL intensity is about twice than that from a planar p-ZnO film/n-GaN film fabricated from the same solution and is attributed to the better p-ZnO crystal quality.

Chapter 6 Fabrication of ZnO core-shell nanorods homojunction on GaN substrates

In this chapter, we fabricate ZnO core-shell nanorod homojunction. In the fabrication process, un-doped ZnO nanorods grown in GaN films were covered by p-ZnO nanorods to form a core-shell nanorod homo-junction. The ZnO coaxial nanorod homo-junction demonstrates a rectifying I-V characteristic with a turn-on voltage of about 3.35 V, in agreement with device simulations using TMA MEDICI. Electroluminescence from the ZnO nanorods homo-junction LED at different forward bias currents consists of a UV peak at 372 nm and a broad visible peak centered at 560 nm. Comparison of the electroluminescence (EL) spectrum against the photoluminescence (PL) spectra of GaN substrate and ZnO nanorods, confirms that the light emission originates from the ZnO homojunction and not the GaN/ZnO junction.

The chapter comprises of 6 sections. Section 6.1 introduces the LED fabrication process. Section 6.2 shows the morphology of the LED. Section 6.3 studies the electrical properties of coaxial ZnO nanorods homojunction. Section 6.4 studies the optical properties of the homojunction. Section 6.5 describes the degradation of the ZnO homo-junction. Finally, section 6.6 concludes the chapter.

6.1 LED fabrication process.

As shown in Figure 6.1, the coaxial ZnO homojunction LED fabrication process comprises 6 steps. In the first step, the n-GaN substrate was patterned by photolithography to deposit the n-contact consisting of Ti (15 nm) / Au (50 nm) on the n-GaN epilayer, followed by a thermal anneal at

500°C for 5 minutes in nitrogen ambient to obtain an ohmic contact. The contact is then covered by a waterproof heat resistant tape to isolate it from the subsequent steps. In step 2, a layer of AZ5214 photoresist is spin-coated onto the entire surface and a window is opened for the growth of ZnO nanorods. In step 3, the substrate is immersed in the precursor solution to grow undoped ZnO nanorods in the exposed window regions. After growth, the photoresist is removed by immersion in acetone. In step 4, the undoped ZnO nanorods are covered again by photoresist followed by hard baking at 110°C for 30 min. To expose the tips of the undoped nanorods, the photoresist is dry etched with O_2 plasma in an Oxford Plasma 80 RIE system. In step 5, the sample is immersed again in a growth precursor solution containing K to grow the top K-doped ZnO nanorods over the exposed undoped ZnO tip, thus forming a coaxial structure. In step 6, the photoresist is removed by immersion in acetone. Finally, the top p-contact is formed by applying an In/Zn dot.

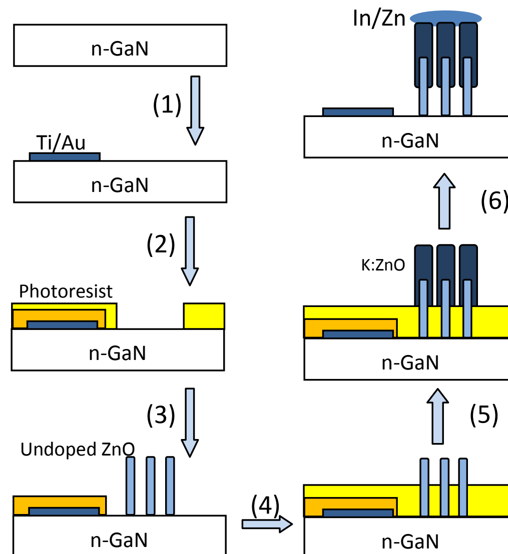

Fig 6.1 Fabrication process of coaxial ZnO nanorod homojunction LED

6.2 Morphology of the ZnO homojunctions

In the process of fabrication of ZnO coaxial homo-junction nanorods as shown in Fig 6.1, controlling the dry etching of photo-resist using O_2 plasma is a critical step because it controls the amount of surface being exposed for subsequent growth of K-doped ZnO, and thus determines the junction area and the mechanical strength of the interface. The rf-power and etching time are two parameters used to control this etching process. The power was chosen at 100 W in order to obtain an etch rate that is reasonably fast yet controllable by varying the etch duration in the range of several minutes. Fig 6.2 (a) shows the exposed tips of undoped ZnO nanorods covered in photo-resist after etching in O_2 plasma at a fixed power of 100 W for 11 min while Fig 6.2 (b) shows the corresponding morphology of the ZnO core-shell homojunction after performing the second cycle of K-doped ZnO growth on these exposed tips. The photo-resist has been removed.

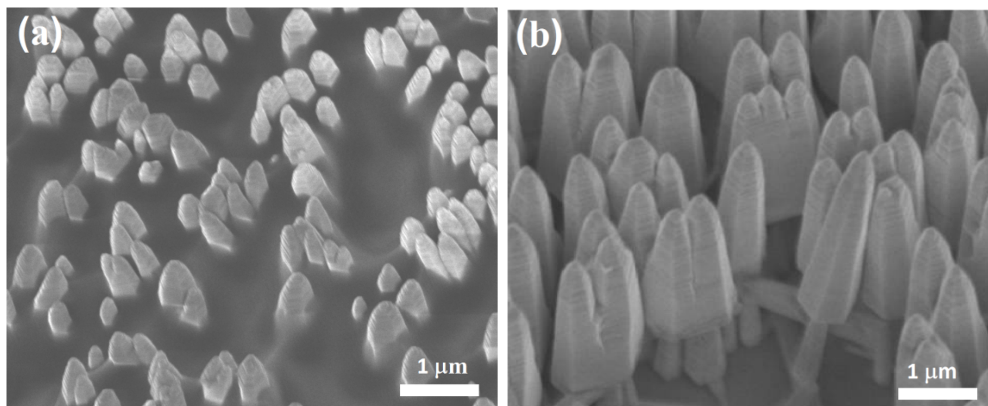

Fig 6.2 (a) SEM images showing the exposed tips of the un-doped ZnO nanorods covered in photo-resist (0.02 $ZnAc_2$ with 0.37M NH_4OH, 1h, 90^oC) after dry etching in O_2 plasma (100W) for 11 minutes and (b) corresponding ZnO core-shell homonjunction grown in solution containing 0.02 M $ZnAc_2$ and 0.37M NH_4OH for the core layer while the shell layer nanorod is grown with 0.02 M $ZnAc_2$, 0.370 M NH_4OH and 0.07 M KAc. The photoresist has been removed.

6. 3 Electrical properties of coaxial ZnO nanorods homojunction

6.3.1 Investigate the n- and p- contacts in the LED

Experimental details for I-V measurement of the n- and p- contacts of the LED were shown the Fig 6.3. They are to explain that the n-metal/n-GaN contact, n-GaN/n-ZnO junction and p-ZnO/p-metal contact are ohmic.

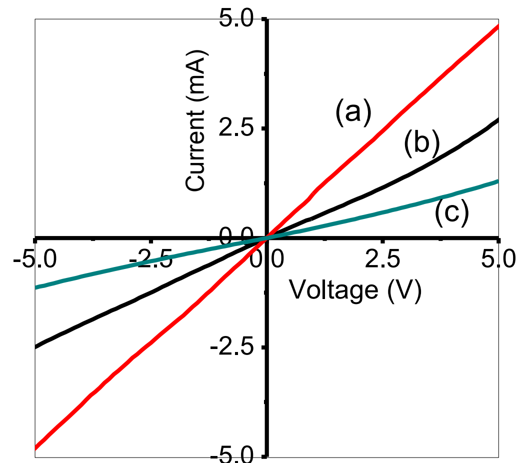

Fig 6.3 I-V characteristic of (a) n-metal/n-GaN contact, (b) n-GaN/n-ZnO junction and (c) p-ZnO/p-metal contact.

a) n-contact on n-GaN

Two circular n-contacts are formed on the n-GaN epilayer by evaporating Ti (15 nm) / Au (50 nm) through a shadow mask. I-V characteristic was measured by probing these two Ti/Au n-contacts.

b) p-contact on p-ZnO

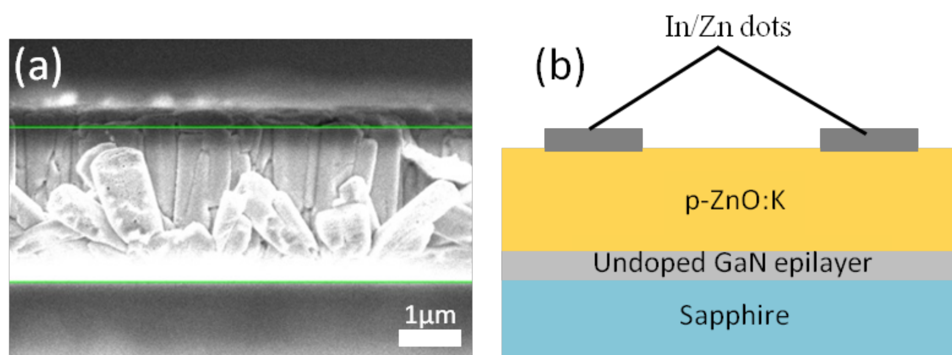

Fig 6.4 (a) SEM cross-sectional image of p-type ZnO grown on unintentionally doped GaN epi-layer. The p-ZnO was grown using two growth cycles, where each growth cycle consists of an aqueous solution of 0.02 M $ZnAc_2$, 0.37 M NH_4OH and 0.07 M KAc maintained at 90°C in a water bath for 1h. (b) Schematic of the structure to measure the I-V across the In/Zn dots for line (b) in the Fig 6.3.

A coalesced film of p-type ZnO was grown on unintentionally-doped GaN epilayer. Coalescence was achieved by using two growth cycles: each cycle consisting of an aqueous solution of 0.02 M $ZnAc_2$, 0.37 M NH_4OH and 0.07 M KAc at 90°C for 1 h. The SEM cross-sectional view is shown in Fig 6.4 (a). Two In/Zn dots were used as contacts to the p-ZnO films as schematically shown in Fig 6.4 (b), from which the I-V characteristic was obtained.

- *n-ZnO on n-GaN interface*

An array of n-ZnO nanorods were grown on n-GaN epilayer using a growth solution consisting of 0.02 M $ZnAc_2$ and 0.37 M NH_4OH at 90°C for 1 h. An ohmic contact consisting of Ti (10 nm) / Au (50 nm) was deposited on the n-GaN. For the n-ZnO nanorods, an indium dot was used. The I-V characteristic of n-ZnO/n-GaN junction was measured by probing the In dot and the Ti/Au contact as shown schematically in Fig 6.5.

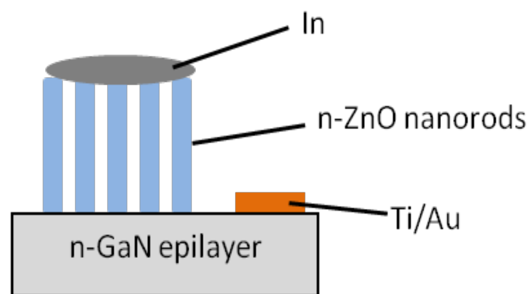

Fig 6.5 Schematic diagram of the structure to obtain the I-V characteristic between the n-ZnO nanorod and the n-GaN epilayer, Ohmic contacts to n-ZnO nanorods and n-GaN epilayer were achieved using an indium dot and Ti (10 nm) / Au (50 nm) respectively.

6.3.2 Electrical properties of coaxial ZnO nanorods homojunction

Fig 6.6 shows the rectifying I-V characteristic of a homojunction grown with 0.37 M NH_4OH and 0.07 M KAc. Since the n- and p-contacts are ohmic, the rectifying characteristics can be attributed to the formation of a p-n

junction between the K-doped ZnO shell and the unintentionally doped n-type core ZnO nanorod. The turn-on voltage is about 3.35 V and the reverse bias leakage current is 1.8 x 10^{-5} A at -5V.

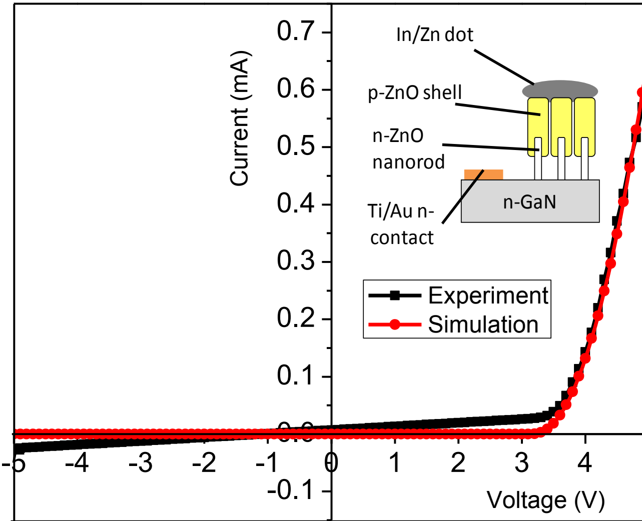

Fig 6.6 Comparison of the experiment and simulated I-V characteristic of ZnO coaxial homojunction LED. The simulated I-V was obtained using TMA MEDICI software with the hole and electron concentration of 2x10^{17} and 5x10^{17} cm^{-3}, respectively.

The electrical characteristics are simulated using a two-dimensional numerical device simulation software, MEDICI [127] by Synopsys, Inc. The hole and electron concentrations are assumed to be 2 x 10^{17} and 5 x $10^{17}$$cm^{-3}$ in the p-type shell and n-type core respectively, corresponding to as-grown carrier concentrations in ZnO films grown under similar conditions measured by Hall effect [50]. A comparison of the simulation result (red line) with the experimental result (black line) shows a good match, with the magnitude of the experimental turn-on voltage slightly smaller than the bandgap

The ideality factor of the diode can be obtained from: $n = \frac{q}{kT}\left(\frac{\partial \ln I}{\partial V}\right)^{-1}$, (6.1)

where V is the applied voltage, I is the current, kT/q is the thermal voltage constant of 25.85 meV at 300K.

The ideality factor, measured in the linear region of the plot of ln(I)-V which occurs between 3.5 to 5.0V, was found to be about 22.1. Such high ideality factors in wide bandgap semiconductors such as ZnO and GaN have been reported by various groups as summarized in Table 6.1. Possible reasons for high ideality factors are defects in the interface, imperfections in the formation of the abrupt p-n junction, deep level assisted tunneling, parasitic rectifying junctions and the space-charge limited conduction due to the low hole density and mobility. Here, we believe that the high ideality factor is contributed by the presence of defects at the interface between the n-type core and the p-type shell which were generated in between the growth of core and shell structure, when the sample was removed from the growth solution and subjected to O_2 plasma etching.

Table 6.1. Summary of reported values of turn-on voltages and ideality factors for ZnO and GaN homojunctions.

Junction	Turn-on voltage	Ideality factor	Reference
Single p-ZnO:As/undoped ZnO nanorod	1 - 2 V	3.0-3.9 for V<5 16.6-22 for 0.5<V<1.8	[132]
p-ZnO:As/n-ZnO	6 - 8 V	3-5 for V<=1 10-25 for V>1	[37]
p-ZnO: (N,Al) /n-ZnO:Al	1.4V	4.3 for V>0.7 V	[128]
AlGaN/GaN p-n junction diodes	Not shown	4.0-6.9	[130]
ZnO p–n junctions	Not shown	10.6–4.7	[133]
n-ZnO/P-doped (Zn,Mg)O junction	1 V	10 - 20	[129]

tab6. 4 Optical properties of coaxial ZnO homojunction nanorods

In Fig 6.7 (a), the electroluminesence (EL) spectra at different forward bias currents are shown. The insets show photographs of the orange EL from the LED at 20 and 30 mA. The EL spectra consist of an ultraviolet peak at 372 nm and a broad visible peak centered at about 560 nm. The UV peak originates from band-edge recombination of ZnO while the visible peak is from defect centers.

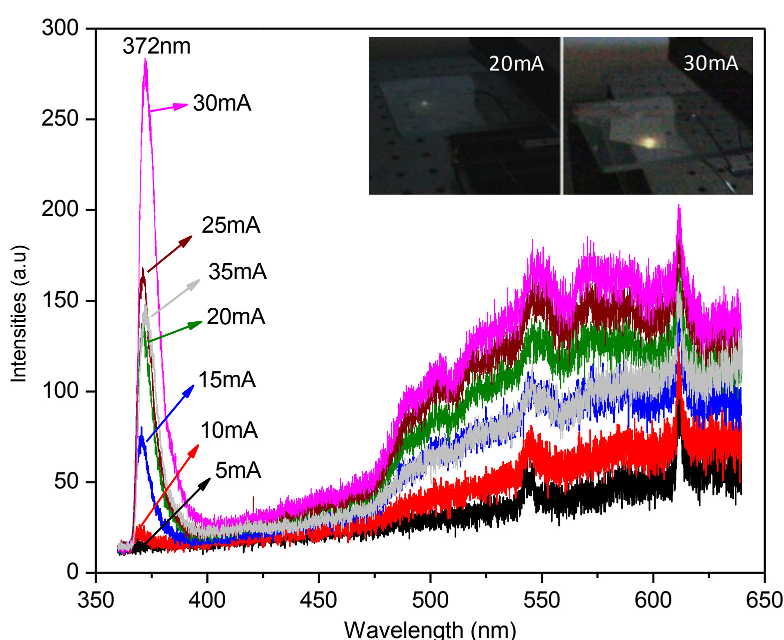

Fig 6.7 Electroluminescent spectra of ZnO coaxial homojunction LED at different applied currents; insert are photos of electroluminescence of ZnO coaxial nanorods homojunction LED at 20mA and 30mA.

As shown in Fig 6.8 (b), the peak intensity increases linearly with injection current up to 30 mA. At currents above 30 mA, the intensity drops and typically burns out at about 60-100 mA because of the limited metal contact area to the nanorods. As seen in Fig 6.8 (c), the UV peak position red shifts linearly from 369nm at 10mA applied voltage to 372nm at 30mA applied voltage. This is attributed to higher temperatures arising from resistive heating which reduces the band-gap of ZnO.

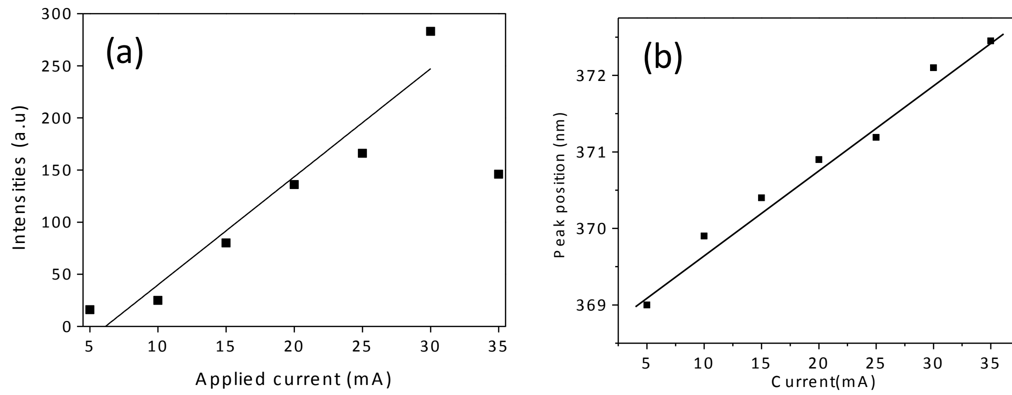

Fig 6.8 UV peak intensity increases linearly with applied current and UV peak position red shifts linearly with the applied current.

Comparison of EL spectra at 15 mA with the PL spectra of the GaN epilayer and ZnO homojunction is shown in Fig 6.9. In the ultraviolet region, the photoluminescence and electroluminescence of ZnO homojunction have the same UV peak position at 370nm which is different from the photoluminescence peak of GaN at 364nm. This confirms that electron and hole injection and recombination occurs at the ZnO homojunction and not at the junction between the ZnO and GaN. This result confirms that the I-V characteristic is that of the ZnO homojunction.

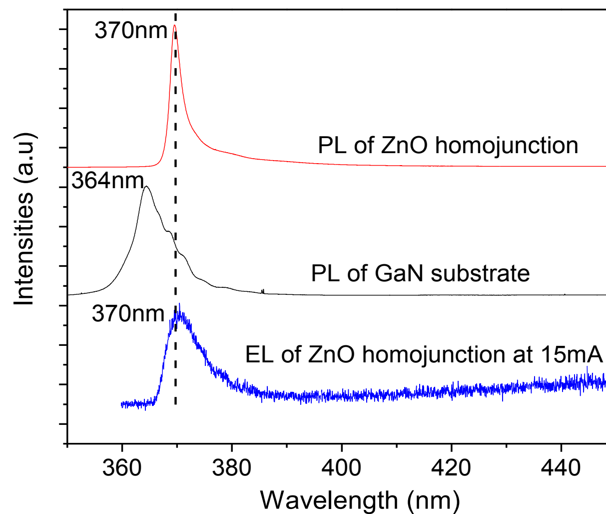

Fig 6.9 Comparison of the EL of ZnO homojunction with the PL of GaN and ZnO

6.5 Study the degradation of the ZnO homo-junction

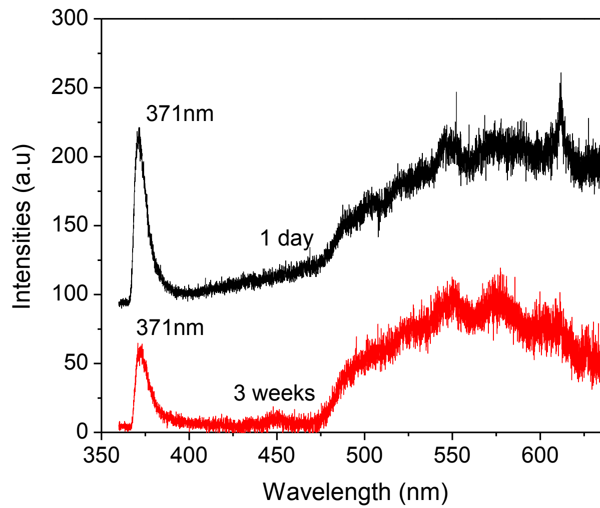

Fig 6.10 the electroluminescence of ZnO coaxial homojunction at 20 mA after 1 day and 3 weeks

The LED demonstrated long term stability over 3 weeks. Fig 6.10 compares the EL spectra at 20 mA, taken after 1 day and 3 weeks after fabrication, with the device stored in a typical sample holder inside a cleanroom. A slight reduction in the UV to visible ratio is observed although the peak positions in the UV and visible range remain unchanged. The difference in intensities could be caused by the different optical alignment between the measurements.

6.6 Conclusion

In this chapter, we report the success of fabrication ZnO coaxial homojunction UV LED. The process and morphology of the ZnO homojunction was investigated by FESEM. This ZnO homojunction demonstrates a rectifying I-V characteristic with a turn-on voltage of 3.35V which is fit well with TMA medici simulation result. Drawing in logarithm scale of ln(I)-V confirm value of turn-on voltage, this value confirm that I-V characteristic is obtained from ZnO homojunction. At room temperature, applying voltage on ZnO coaxial nanorods homojunction, electroluminescence

spectra was obtained which consist of an ultraviolet peak at about 370nm and a broad visible peak centered at 560nm. Higher applied current, this EL peak was red shifted. Comparisons of this electroluminescence with photoluminescence of ZnO homojunction and GaN substrate confirm the light emitted from ZnO. Strong photoluminescence at ultraviolet region show that ZnO is a candidate for UV LED. Repeat the measurement after three weeks, ZnO coaxial homojunction still work stable.

Chapter 7 Conclusions and recommendations

7.1 Conclusions

In this thesis, single crystalline ZnO nanorods were grown to minimize the formation of dislocations and grain boundary. n-type ZnO is annealed to reduce defects of ZnO such as zinc interstitial, oxygen interstitial and hydrogen interstitial. Difficulty in obtaining p-type ZnO was overcome by doping with potassium using solution method. The good quality of material growth was demonstrated with the succeful fabrication of p-ZnO nanorods/n-GaN film LED and ZnO nanorod core-shell homojunction LED.

Successful growth of n-type ZnO nanorods using aqueous solution method was demonstrated in this thesis. Varying growth parameters, dopants and using different types of substrates controlled the morphology of n-type ZnO nanorods. ZnO nanorods grown on GaN epi-layer substrate are vertically aligned and single crystalline. X-ray diffraction and TEM image of ZnO nanorods confirm its single crystalline structures. The high resolution TEM shows that the ZnO lattice has no line defects.

The optical property of ZnO was investigated by measuring photoluminescence. The PL spectra of all ZnO nanorods comprise of two peaks, a near band-edge emission (NBE) peak at 370nm and a broad visible peak emission from defects. Defects that can emit PL can be zinc interstitial, oxygen interstitial, oxygen vacancy or hydrogen defects. Annealing of ZnO nanorods improve optical and electrical properties of n- type ZnO nanorods. Photoluminescence of ZnO nanorods after annealing showed the improvement of NBE intensity by three orders of magnitude. Annealing also reduces the

visible peak intensity, which means defect intensity in ZnO nanorods has been reduced.

Success in fabricatiing p-type ZnO nanorods is also demonstrated in this thesis. P-type ZnO nanorods were obtained by doping with potassium using solution method. The morphology of p-type ZnO nanorods was investigated by SEM measurement. SEM images of p-type ZnO nanorods show the morphology similar to undoped ZnO nanorods grown in solution with the same pH. The p-type ZnO nanorods grown on GaN substrate are vertically aligned and single crystalline. XPS and SIMS measurement of p-type ZnO confirm the existence of potassium inside the ZnO nanorods. Raman scattering of ZnO nanorods doping with potassium show a shift in the A_1-LO component. That shift expresses the expansion along the c-axis of ZnO by doping with potassium since the radius of potassium atom is larger than that of oxygen. Hole concentration of p-type ZnO nanorods doping with 0.07 M KAc was measured to have the value of $2x10^{17}cm^{-3}$. This recipe was used for subsequent device fabrication.

The success of obtaining high quality p- and n- type ZnO with minimal dislocations and grain boundary was applied for device fabrication. In chapter 5, we report the successful fabrication of p-ZnO nanorods/n-GaN film ultraviolet LED. The LED includes a single crystalline p-ZnO nanorods layer grown vertically on a n-GaN epi-layer. The LED demonstrates a rectifying I-V characteristic with a turn-on voltage of 2.7V, lower than the 3.3V obtained from simulation. Ideality factor which is calculated from ln(I)-V characteristics, is 6.5. The reason for the lower turn-on voltage and higher ideality factor was attributed to presence of interface charges in the

heterojunction. The interface charges are due to high pH of the growth solution in the LED fabrication process. At room temperature, the EL spectrum consists of an ultraviolet peak centered 370-378nm and a broad visible peak. The UV peak was red shifted and broadened when higher current was applied. Finally, fitting and comparing EL spectrum of the LED with the PL spectrum of p-ZnO and n-GaN indicate that p-ZnO contribute for EL more than n-GaN.

Next, we are successful fabricated ZnO coaxial homojunction UV LED. The ZnO homojunction comprises of an n-type ZnO nanorod core rod and p-type ZnO shell layer. The core-shell ZnO homojunction demonstrates a rectifying I-V characteristic with a turn-on voltage of 3.35V which fitted well with that obtained from TMA medici simulation result. Plots of ln(I)-V confirm that the I-V characteristic is obtained from ZnO homojunction. At room temperature, the nanorod homojunction electroluminescence spectra consist of an ultraviolet peak at about 370nm and a broad visible peak centered at 560nm. At higher applied current, this EL peak was red shifted. Comparison of this electroluminescence with photoluminescence of ZnO homojunction and GaN substrate confirm that the light is emitted from ZnO. Three weeks of storage, the ZnO coaxial homojunction still work stable.

7.2 Recommendations

The current study can be improved by addressing several drawbacks of the growth method and device fabrication. First of all, the solution method uses a water bath can be improved by using the microwave assisted solution growth. The microwave assisted heating system offers a faster method and controllable temperature for ZnO growth. The next improvement of ZnO

based LED fabrication is optimizing the p-contact fabrication on p-type ZnO. Annealing can improve the optical properties of p-type ZnO nanorods. However, the electrical properties of ZnO are not improved by annealing. Understanding and controlling the annealing process can remove the unintentional doped hydrogen in ZnO to improve the electrical properties of p-type ZnO. Reducing hydrogen and other defects density in p-type ZnO by annealing can produce more stable p-type ZnO nanorods.

In this thesis, we only focus on using ZnO for LED application. Some other direction to use ZnO is display-related applications; transparent electronics application, sensor-related applications; and photovoltaic- related applications. ZnO can be a material for backplane transistor and electrodes. ZnO is suitable for OLED fabrication because ZnO can be fabricated at low-temperatures. Conventional polycrystalline silicon TFTs is being used for backplane for OLED. However, it is not uniform in mobility and threshold voltage over a large area; meanwhile ZnO TFTs enhances the uniformity of TFT performance and can achieve relatively high mobility.

For sensor application, ZnO can be used for ultraviolet photo detector because the wavelength of the UV light is suitable with band-gap of ZnO. Moreover, ZnO is a direct band-gap semiconductor that is more sensitive to light.

In photovoltaic - related applications, ZnO can play a role. ZnO being a transparent conductor material can be used as the top electrode in copper indium gallium selenide (CIGS) solar cell. Moreover, ZnO is usually used as a back electrode. ZnO can also be used as the electrode material for organic

photovoltaic or dye sensitive cell (DSCs). In conclusion, ZnO have a bright future in both optoelectronic and electronic applications.

Bibliography

1. Hawken, P.L., Amory; Lovins, L. Hunter *Natural Capitalism.* Back Bay Press, Time Warner Book Group, 2000. **ISBN 0-316-35300-0**.

2. Jagadish, C. and S.J. Pearton, eds. *Zinc Oxide Bulk, Thin Films and Nanostructures: processing, properties and applications*. ed. I. 0-08-044722-8 and I. 978-0-08-044722-32006, ELSEVIER.

3. Klingshirn, C., *ZnO: From basics towards applications.* physica status solidi (b), 2007. **244**(9): p. 3027-3073.

4. Look, D.C. and B. Claflin, *P-type doping and devices based on ZnO.* physica status solidi (b), 2004. **241**(3): p. 624-630.

5. Özgür, U., et al., *A comprehensive review of ZnO materials and devices.* Journal of Applied Physics, 2005. **98**(4): p. 041301.

6. Schmidt-Mende, L. and J.L. MacManus-Driscoll, *ZnO – nanostructures, defects, and devices.* Materials Today, 2007. **10**(5): p. 40-48.

7. J. G. Wen, e.a., *Self-assembly of semiconducting oxide nanowires, nanorods and nanoribbons.* Chem. Phys. Lett., 2003. **372**: p. 717.

8. Yao, B.D., Y.F. Chan, and N. Wang, *Formation of ZnO nanostructures by a simple way of thermal evaporation.* Appl. Phys. Lett., 2002. **81**(4): p. 757.

9. Huang, M.H. and e. al., *Catalytic growth of zinc oxide nanowires by vapor transport.* Adv. Materials, 2001. **13**(2): p. 113.

10. Li, J.Y. and e. al., *Fabrication of zinc oxide nanorods.* J. Cryst. Growth, 2001. **233**: p. 5.

11. Hu, J.Q. and Y. Bando, *Growth and optical properties of single crystal tubular ZnO whiskers.* Appl. Phys. Lett., 2003. **82**(9): p. 1401.

12. Muthukumar, S., IEEE Trans. Nanotechnology, 2003. **2**(1): p. 50.

13. Wu, J. and S. Liu, Adv. Mater., 2002. **14**(3): p. 215.

14. Heo, Y.W. and e. al., Appl. Phys. Lett., 2002. **81**(16): p. 3046.

15. Verges, M.A., A. Mifsud, and C.J. Serna, J. Chem. Soc., Faraday Trans., 1990. **86**: p. 959.

16. Vayssieres, L., J. Phys. Chem. B, 2001. **2001**(105): p. 3350.

17. Le, H.Q., et al., *Synthesis and optical properties of well aligned ZnO nanorods on GaN by hydrothermal synthesis.* Nanotechnol., 2006. **17**: p. 483-488.

18. Tay, C.B., et al., *Empirical Model for Density and Length Prediction of ZnO Nanorods on GaN Using Hydrothermal Synthesis.* Journal of The Electrochemical Society, 2007. **154**(9): p. K45.

19. Tay, C.B., S.J. Chua, and K.P. Loh, *Investigation of morphology and photoluminescence of hydrothermally grown ZnO nanorods on substrates pre-coated with ZnO nanoparticles.* Journal of Crystal Growth, 2009. **311**(5): p. 1278-1284.

20. Tay, C.B., *Growth of Zinc Oxide Nanostructures and Films and p-doping of Films in Aqueous Solution.* PhD thesis, National University of Singapore, 2009.

21. Huang, X.H., et al., *Universal photoluminescence evolution of solution-grown ZnO nanorods with annealing: important role of hydrogen donor.* CrystEngComm, 2011. **13**(23): p. 7032.

22. Politi, Y., et al., *Transformation mechanism of amorphous calcium carbonate into calcite in the sea urchin larval spicule.* Proc. Natl. Acad. Sci. USA, 2008. **105**(45): p. 17362.

23. Papadopoulou, E.L., et al., *Undoped and Al-doped ZnO films with tuned properties grown by pulsed laser deposition.* Thin Solid Films, 2008. **516**: p. 8141.

24. Minami, T., et al., *Conduction mechanism of highly conductive and transparent zinc oxide thin films prepared by magnetron sputtering.* J. Cryst. Growth, 1992. **117**: p. 370.

25. Ma, Y., et al., *Control of conductivity type in undoped ZnO thin films grown by metalorganic vapor phase epitaxy.* J. Appl. Phys., 2004. **95**(11): p. 6268.

26. Andeen, D., et al., *Lateral Epitaxial Overgrowth of ZnO in Water.* Adv. Funct. Mater., 2006. **16**: p. 799-804.

27. Ehrentraut, D., et al., *Solvothermal growth of ZnO.* Prog. Crystal Growth Charact. Mater., 2006. **52**: p. 280.

28. Wang, B., et al., *Hydrothermal growth and characterization of indium doped conducting ZnO crystals.* J. Cryst. Growth, 2007. **304**(1): p. 73.

29. Makino, T., et al., *Gallium concentration dependence of room temperature near-band-edge luminescence in n-type ZnO:Ga.* Appl. Phys. Lett., 2004. **85**: p. 759.

30. Kim, J.H., et al., *Effect of rapid thermal annealing on electrical and optical properties of Ga doped ZnO thin films prepared at room temperature.* J. Appl. Phys., 2006. **100**.

31. Yuen, C., et al., *Fabrication of n-ZnO: Al/p-SiC(4H) heterojunction light emitting diodes by filtered cathodic vacuum arc technique.* Appl. Phys. Lett., 2005. **86**: p. 241111.

32. Raviendra, D. and J.K. Sharma, *Electroless deposition of cadmium stannate, zinc oxide and aluminium-doped zinc oxide films.* J. Appl. Phys., 1985. **58**(2): p. 838.

33. Yu, D.Y., et al., *Structural and electrical properties of sputtered indium-zinc oxide thin films.* Thin Solid Films, 2006. **515**: p. 1364.

34. Minami, T., *Transparent and conductive multicomponent oxide films prepared by magnetron sputtering.* J. Vac. Sci. Technol. A, 1999. **17**(4): p. 1765.

35. Park, C.H., S.B. Zhang, and S.-H. Wei, *Origin of p-type doping difficulty in ZnO: The impurity perspective.* Physical Review B, 2002. **66**(7).

36. Hwang, D.-K., et al., *p-ZnO/n-GaN heterostructure ZnO light-emitting diodes.* Applied Physics Letters, 2005. **86**(22): p. 222101.

37. Ryu, Y.R., et al., *Fabrication of homostructural ZnO p–n junctions and ohmic contacts to arsenic-doped p-type ZnO.* Applied Physics Letters, 2003. **83**(19): p. 4032.

38. Tsukazaki, A., et al., *Repeated temperature modulation epitaxy for p-type doping and light-emitting diode based on ZnO.* Nature Materials, 2004. **4**(1): p. 42-46.

39. Look, D.C., *Progress in ZnO materials and devices.* J. Electron. Mater., 2006. **35**(6): p. 1299.

40. Barnes, T.M., K. Olson, and C.A. Wolden, *On the formation and stability of p-type conductivity in nitrogen doped zinc oxide.* Appl. Phys. Lett., 2005. **86**(112112).

41. Tsukazaki, A., et al., *Repeated temperature modulation epitaxy for p-type doping and light emitting diode based on ZnO.* Nat. Mater., 2005. **4**: p. 42.

42. Yu, Z.G., P. Wu, and H. Gong, *Control of p- and n-type conductivities in P doped ZnO thin films by using radio-frequency sputtering.* Appl. Phys. Lett., 2006. **88**: p. 132114.

43. Vaithianathan, V., B.-T. Lee, and S.S. Kim, *Preparation of As-doped p-type ZnO films using a Zn_3As_2/ZnO target with pulsed laser deposition.* Appl. Phys. Lett., 2005. **86**: p. 062101.

44. Mandalapu, L.J., et al., *Homojunction photodiodes based on Sb-doped p-type ZnO for ultraviolet detection.* Appl. Phys. Lett., 2006. **88**: p. 092103.

45. Yamamoto, T. and H. Katayama-Yoshida, Jpn. J. Appl. Phys. Part 2, 1999. **38**: p. L166.

46. Yuan, G.D., et al., *Control of conduction type in Al- and N-codoped ZnO thin films.* Appl. Phys. Lett., 2005. **86**: p. 202106.

47. Chen, L.L., et al., *p-type behavior in In-N codoped ZnO thin films.* Appl. Phys. Lett., 2005. **87**: p. 252106.

48. Kumar, M., et al., *Growth of epitaxial p-type ZnO thin films by codoping of Ga and N.* Appl. Phys. Lett., 2006. **89**: p. 112103.

49. Lu, J.G., et al., *Low-resistivity, stable p-type ZnO thin films realized using a Li-N dual-acceptor doping method.* Appl. Phys. Lett., 2006. **88**: p. 222114.

50. Tay, C.B., S.J. Chua, and K.P. Loh, *Stable p-Type Doping of ZnO Film in Aqueous Solution at Low Temperatures.* Journal of Physical Chemistry C, 2010. **114**: p. 9981.

51. Nguyen, X.S., et al., *ZnO Coaxial Nanorod Homojunction UV Light-Emitting Diodes Prepared by Aqueous Solution Method.* Small, 2012. **8**(8): p. 1204-1208.

52. Jeong, M.-C., et al., *ZnO-Nanowire-Inserted GaN/ZnO Heterojunction Light-Emitting Diodes.* Small, 2007. **3**(4): p. 568-572.

53. Le, H.Q., et al., *Solution epitaxy of gallium-doped ZnO on p-GaN for heterojunction light-emitting diodes.* Applied Physics B, 2010. **100**(4): p. 705-710.

54. Ohashi, T., et al., *Red Emission from ZnO-Based Double Heterojunction Diode.* Japanese Journal of Applied Physics, 2008. **47**(4): p. 2961-2964.

55. Osinsky, A., et al., *MgZnO/AlGaN heterostructure light-emitting diodes.* Applied Physics Letters, 2004. **85**(19): p. 4272.

56. Mandalapu, L.J., et al., *Ultraviolet emission from Sb-doped p-type ZnO based heterojunction light-emitting diodes.* Applied Physics Letters, 2008. **92**(12): p. 122101.

57. Choi, Y.-S., et al., *Recent Advances in ZnO-Based Light-Emitting Diodes.* EEE TRANSACTIONS ON ELECTRON DEVICES, 2010. **57**(1).

58. Rogers, D.J., et al., *Electroluminescence at 375 nm from a ZnO/GaN:Mg/c-Al[sub 2]O[sub 3] heterojunction light emitting diode.* Applied Physics Letters, 2006. **88**(14): p. 141918.

59. Yang, T.P., et al., *Room temperature electroluminescence from the n-ZnO/p-GaN heterojunction device grown by MOCVD.* Materials Research Bulletin, 2008. **43**(12): p. 3614-3620.

60. Alivov, Y.I., et al., *Fabrication and characterization of n-ZnO/p-AlGaN heterojunction light-emitting diodes on 6H-SiC substrates.* Applied Physics Letters, 2003. **83**(23): p. 4719.

61. Mares, J.W., et al., *Hybrid CdZnO/GaN quantum-well light emitting diodes.* Journal of Applied Physics, 2008. **104**(9): p. 093107.

62. Sun, J.W., et al., *Excitonic electroluminescence from ZnO-based heterojunction light emitting diodes.* JOURNAL OF PHYSICS D: APPLIED PHYSICS, 2008. **41**(15): p. 155103.

63. Ye, J.D., et al., *Electroluminescent and transport mechanisms of n-ZnO/p-Si heterojunctions.* Applied Physics Letters, 2006. **88**(18): p. 182112.

64. Choi, M.K., et al., *n-ZnO:Ga/i-ZnO/p-Si heterojunction light emitting diodes fabricated on patterned Si substrates.* Journal of Materials Science: Materials in Electronics, 2009. **20**(12): p. 1214-1218.

65. Ohta, H., et al., *Current injection emission from a transparent p–n junction composed of p-SrCu[sub 2]O[sub 2]/n-ZnO.* Applied Physics Letters, 2000. **77**(4): p. 475.

66. Ohta, H., et al., *Fabrication and characterization of ultraviolet-emitting diodes composed of transparent p-n heterojunction, p-SrCu[sub 2]O[sub 2] and n-ZnO.* Journal of Applied Physics, 2001. **89**(10): p. 5720.

67. Alivov, Y.I., et al., *Observation of 430 nm electroluminescence from ZnO/GaN heterojunction light-emitting diodes.* Applied Physics Letters, 2003. **83**(14): p. 2943.

68. Chichibu, S.F., et al., *Greenish-white electroluminescence from p-type CuGaS[sub 2] heterojunction diodes using n-type ZnO as an electron injector.* Applied Physics Letters, 2004. **85**(19): p. 4403.

69. Park, W.I. and G.-C. Yi, *Electroluminescence in n-ZnO nanorod arrays vertically grown on p-GaN.* Advanced Materials, 2004. **16**(1): p. 87.

70. Park, S.-H., S.-H. Kim, and S.-W. Han, *Growth of homoepitaxial ZnO film on ZnO nanorods and light emitting diode applications.* Nanotechnology, 2007. **18**(5): p. 055608.

71. Chang, C.-Y., et al., *Electroluminescence from ZnO nanowire/polymer composite p-n junction.* Applied Physics Letters, 2006. **88**(17): p. 173503.

72. Sun, H., Q.-F. Zhang, and J.-L. Wu, *Electroluminescence from ZnO nanorods with an n-ZnO/p-Si heterojunction structure.* Nanotechnology, 2006. **17**(9): p. 2271-2274.

73. Xi, Y.Y., et al., *NiO/ZnO light emitting diodes by solution-based growth.* Applied Physics Letters, 2008. **92**(11): p. 113505.

74. Sun, X.W., et al., *A ZnO Nanorod Inorganic Organic Heterostructure Light-Emitting Diode Emitting at 342 nm.* Nano letters, 2008. **8**(4): p. 1219-1223.

75. Nadarajah, A., et al., *Flexible Inorganic Nanowire Light-Emitting Diode.* Nano letters, 2008. **8**(2): p. 534 - 537.

76. Guo, R., et al., *Electroluminescence from ZnO nanowire-based p-GaN/n-ZnO heterojunction light-emitting diodes.* Applied Physics B, 2008. **94**(1): p. 33-38.

77. Ling, B., et al., *Electroluminescence from a n-ZnO nanorod/p-CuAlO2 heterojunction light-emitting diode.* Physica E: Low-dimensional Systems and Nanostructures, 2009. **41**(4): p. 635-639.

78. Ryu, Y., et al., *Next generation of oxide photonic devices: ZnO-based ultraviolet light emitting diodes.* Applied Physics Letters, 2006. **88**(24): p. 241108.

79. Ryu, Y.R., et al., *Excitonic ultraviolet lasing in ZnO-based light emitting devices.* Applied Physics Letters, 2007. **90**(13): p. 131115.

80. Kim, H.S., et al., *Phosphorus doped ZnO light emitting diodes fabricated via pulsed laser deposition.* Applied Physics Letters, 2008. **92**(11): p. 112108.

81. Wang, Y.-L., et al., *Dielectric passivation effects on ZnO light emitting diodes.* Applied Physics Letters, 2008. **92**(11): p. 112101.

82. Lim, J.H., et al., *UV Electroluminescence Emission from ZnO Light-Emitting Diodes Grown by High-Temperature Radiofrequency Sputtering.* Advanced Materials, 2006. **18**(20): p. 2720-2724.

83. Xu, W.Z., et al., *ZnO light-emitting diode grown by plasma-assisted metal organic chemical vapor deposition.* Applied Physics Letters, 2006. **88**(17): p. 173506.

84. Wei, Z.P., et al., *Room temperature p-n ZnO blue-violet light-emitting diodes.* Applied Physics Letters, 2007. **90**(4): p. 042113.

85. Kong, J., et al., *Dominant ultraviolet light emissions in packed ZnO columnar homojunction diodes.* Applied Physics Letters, 2008. **93**(13): p. 132113.

86. Chu, S., et al., *Sb-doped p-ZnO/Ga-doped n-ZnO homojunction ultraviolet light emitting diodes.* Applied Physics Letters, 2008. **92**(15): p. 152103.

87. Zhao, J.Z., et al., *Electroluminescence from n-ZnO/p-ZnO : Sb homojunction light emitting diode on sapphire substrate with metal–organic precursors doped p-type ZnO layer grown by MOCVD technology.* JOURNAL OF PHYSICS D: APPLIED PHYSICS, 2008. **41**(19): p. 195110.

88. Dong, X., et al., *Study on the properties of MgxZn1−xO-based homojunction light-emitting diodes fabricated by MOCVD.* Journal of Physics D: Applied Physics, 2007. **40**: p. 7298–7301.

89. Zeng, Y.J., et al., *Plasma-free nitrogen doping and homojunction light-emitting diodes based on ZnO.* JOURNAL OF PHYSICS D: APPLIED PHYSICS, 2008. **41**(16): p. 165104.

90. Aoki, T., Y. Hatanaka, and D.C. Look, *ZnO diode fabricated by excimer-laser doping.* Applied Physics Letters, 2000. **76**(22): p. 3257.

91. Guo, X.L., et al., *Fabrication and Optoelectronic Properties of a Transparent ZnO Homostructural Light-Emitting Diode.* The Japan Society of Applied Physics, 2001. **40**: p. 177.

92. Tuzemen, S., et al., *Production and properties of p–n junctions in reactively sputtered ZnO.* Physica B: Condensed Matter, 2001: p. 1197–1200.

93. Ryu, Y.R., W.J. Kim, and H.W. White, *Fabrication of homostructural ZnO p}n junctions.* Journal of Crystal Growth, 2000. **219**: p. 419 - 422.

94. Alivov, Y.I., et al., *Fabrication of ZnO-based metal–insulator–semiconductor diodes by ion implantation.* Solid-State Electronics, 2004. **48**(12): p. 2343-2346.

95. Pan, M., *ZnO based light emitting diodes growth and fabrication.* 2006. **6122**: p. 61220M-61220M-6.

96. Lee, J.M., et al., *Ohmic contact to phosphorous-doped ZnO using Pt/Ni/Au for p-n homojunction diode.* Journal of the Electrochemical Society 2006. **153**: p. 1047-1050.

97. Jiao, S.J., et al., *ZnO p-n junction light-emitting diodes fabricated on sapphire substrates.* Applied Physics Letters, 2006. **88**(3): p. 031911.

98. Zhang, Z.Z., et al., *p-Type ZnO on sapphire by using O2–N2 co-activating and fabrication of ZnO LED.* Journal of Crystal Growth, 2007. **301-302**: p. 362-365.

99. Sun, J.C., et al., *Realization of ultraviolet electroluminescence from ZnO homojunction with n-ZnO/p-ZnO:As/GaAs structure.* Applied Physics Letters, 2007. **90**(12): p. 121128.

100. Liu, W., et al., *Electroluminescence from a ZnO homojunction device grown by pulsed laser deposition.* Solid State Communications, 2007. **142**(11): p. 655-658.

101. Ye, Z.Z., et al., *ZnO light-emitting diodes fabricated on Si substrates with homobuffer layers.* Applied Physics Letters, 2007. **91**(11): p. 113503.

102. Li, W.-J., et al., *Growth mechanism and growth habit of oxide crystals.* J. Cryst. Growth, 1999. **203**: p. 186.

103. Stumm, W., ed. *Aquatic surface chemistry: chemical processes at the particle - water interface*. 1987, Wiley: New York.

104. Andeen, D., et al., *Lateral Epitaxial Overgrowth of ZnO in Water at* 90^oC*.* Adv. Funct. Mater., 2006. **16**: p. 799-804.

105. Brunelle, J.P., *Preparation of catalysts by metallic complex adsorption on mineral oxides.* Pure Appl. Chem., 1978. **50**: p. 1211-1229.

106. Vayssieres, L., et al., *Purpose-Built Anisotropic Metal Oxide Material: 3D Highly Oriented Microrod Array of ZnO.* The Journal of Physical Chemistry B, 2001. **105**: p. 3350 - 3352.

107. Quang, L.H. and C.S. Jin, *Greatly Enhanced Optical Properties of ZnO Nanorods Grown on GaN in Aqueous Solution by Using Two-Step Treatment Method.* Journal of The Electrochemical Society, 2008. **155**(7): p. K105.

108. Diakonov, I.I., et al., *Gallium speciation in aqueous solution. Experimental study and modelling: Part 1. Thermodynamic properties of Ga(OH)4− to 300°C.* Geochimica et Cosmochimica Acta, 1997. **61**(7): p. 1333-1343.

109. Hu, J.Q. and Y. Bando, *Growth and optical properties of single-crystal tubular ZnO whiskers.* Applied Physics Letters, 2003. **82**(9): p. 1401.

110. Wei, X.Q., et al., *Blue luminescent centers and microstructural evaluation by XPS and Raman in ZnO thin films annealed in vacuum, N2 and O2.* Physica B: Condensed Matter, 2007. **388**(1-2): p. 145-152.

111. Yuan, G.D., et al., *X-ray photoelectron spectroscopy study of Al- and N- co-doped p-type ZnO thin films.* Journal of Crystal Growth, 2009. **311**(8): p. 2341-2344.

112. Tabet, N., M. Faiz, and A. Al-Oteibi, *XPS study of nitrogen-implanted ZnO thin films obtained by DC-Magnetron reactive plasma.* Journal of

Electron Spectroscopy and Related Phenomena, 2008. **163**(1-3): p. 15-18.

113. Ling, C.C., et al., *Defect study in ZnO related structures—A multi-spectroscopic approach.* Applied Surface Science, 2008. **255**(1): p. 58-62.

114. Huang, X.H., et al., *Correlating the enhancement of UV luminescence from solution-grown ZnO nanorods with hydrogen doping.* CrystEngComm, 2012. **14**(16): p. 5163.

115. Zhang, J.-Y., et al., *Ultraviolet electroluminescence from controlled arsenic-doped ZnO nanowire homojunctions.* Applied Physics Letters, 2008. **93**(2): p. 021116.

116. Nguyen, X.S., et al., *ZnO Coaxial Nanorod Homojunction UV Light-Emitting Diodes Prepared by Aqueous Solution Method.* Small, 2012: p. n/a-n/a.

117. Lee, E.-C. and K.J. Chang, *Possible p-type doping with group-I elements in ZnO.* Phys. Rev. B, 2004. **70**: p. 115210.

118. Lee, E.-C. and K.J. Chang, *P-type doping with group-I elements and hydrogenation effect in ZnO.* Physica B: Condensed Matter, 2006. **376–377**(0): p. 707-710.

119. Park, C.H., S.B. Zhang, and S.-H. Wei, *Origin of p-type doping difficulty in ZnO: The impurity perspective.* Phys. Rev. B, 2002. **66**: p. 073202.

120. Lee, E.-C. and K. Chang, *Possible p-type doping with group-I elements in ZnO.* Physical Review B, 2004. **70**(11).

121. Wardle, M.G., J.P. Goss, and P.R. Briddon, *Theory of Li in ZnO: A limitation for Li-based p -type doping.* Physical Review B, 2005. **71**(15).

122. Tay, C.B., S.J. Chua, and K.P. Loh, *Investigation of morphology and photoluminescence of hydrothermally grown ZnO nanorods on substrates pre-coated with ZnO nanoparticles.* J. Cryst. Growth, 2009. **311**: p. 1278-1284.

123. S Lia, et al., *In situ XPS studies of thermally deposited potassium on poly(p-phenylene vinylene) and its ring-substituted derivatives.* Applied Surface Science, 2001. **181**(3-4): p. 201–210.

124. Chen, M., et al., *X-ray photoelectron spectroscopy and auger electron spectroscopy studies of Al-doped ZnO films.* Applied Surface Science, 2000. **158**(1-2): p. 134-140.

125. Morkoç, H. and Ü. Özgür, *General Properties of ZnO*, in *Zinc Oxide*2009, Wiley-VCH Verlag GmbH & Co. KGaA. p. 1-76.

126. Lin, S., et al., *Temperature-dependent photoluminescence and photoluminescence excitation of aluminum monodoped and aluminum-indium dual-doped ZnO nanorods.* Journal of Applied Physics, 2008. **104**(11): p. 114307.

127. manual, T.M.U.s., *Technolygy Modeling Associates.* 2009.

128. Lu, J.G., et al., *Electrical characterization of ZnO-based homojunctions.* Applied Physics Letters, 2006. **89**(5): p. 053501.

129. Heo, Y.W., et al., *p-type behavior in phosphorus-doped (Zn,Mg)O device structures.* Applied Physics Letters, 2004. **84**(18): p. 3474.

130. Shah, J.M., et al., *Experimental analysis and theoretical model for anomalously high ideality factors (n≫2.0) in AlGaN/GaN p-n junction diodes.* Journal of Applied Physics, 2003. **94**(4): p. 2627.

131. Perlin, P., et al., *Low-temperature study of current and electroluminescence in InGaN/AlGaN/GaN double-heterostructure blue light-emitting diodes.* Applied Physics Letters, 1996. **69**(12): p. 1680.

132. Yang, Y., et al., *A p-n homojunction ZnO nanorod light-emitting diode formed by As ion implantation.* Applied Physics Letters, 2008. **93**(25): p. 253107.

133. Hazra, S. and S. Basu, *ZnO p–n junctions produced by a new route.* Solid-State Electronics, 2005. **49**(7): p. 1158-1162.

Biography

07/2008-08/2012: PhD candidate in Advanced Materials in Micro- & Nano-Systems" program, Singapore- MIT Alliance

09/2006- 06/2008: Lecturer at Hanoi University of Technology, Vietnam

09/2001- 06/2006: B. Eng. in engineering physics, Hanoi University of Technology, Vietnam

Publication list

Journal Papers

[1] **X. S. Nguyen**, C. B. Tay, E. A. Fitzgerald, S. J. Chua, *ZnO coaxial nanorods homojunction UV LED prepared by aqueous solution method*, Small, vol. 8, p. 1204, **2012**. (Impact factor 7.3)

[2] Tay C.B.; Tang J.; **Nguyen X.S**.; Huang X.H.; Chai J.W.; Venkatesan T.; Chua S.J., *optimized route to reliable p-type doping in ZnO with K by low temperature aqueous solution growth method*, submitted to the Journal of Physical Chemistry C

[3] **X. S. Nguyen**, C. B. Tay, J. Tang, E. A. Fitzgerald, S. J. Chua, *Fabrication of p- type ZnO nanorods/n-GaN film hetero-junction ultraviolet light emitting diodes by aqueous solution method*, submitted revised version to Physica Status Solidi (a)

Conferences and Workshops

18 oral and poster presentations in MRS, E-MRS, ICMAT 2011, ICYRAM 2012 and other conferences and workshops

Awards & Honors

1. Best poster awards at the MRS-S trilateral conference on Advances in nanoscience: Energy, Water and healthcare, August 2010

2. Co-author of Best poster awards at ICMAT 2011 - International Conference on Materials for Advanced Technologies, Singapore, June 2011

3. Co-author of First poster prize at Institute of Material Research and Engineering (IMRE) post-graduate poster competition, July 2011

4. Co-author of Best poster awards at ICYRAM 2012 - International Conference of Young Researchers on Advanced Materials, Singapore, July 2012.